NOAA Technical Report NESDIS 142-2

Regional Climate Trends and Scenarios for the U.S. National Climate Assessment

Part 2. Climate of the Southeast U.S.

Washington, D.C.
January 2013

U.S. DEPARTMENT OF COMMERCE
National Oceanic and Atmospheric Administration
National Environmental Satellite, Data, and Information Service

NOAA TECHNICAL REPORTS

National Environmental Satellite, Data, and Information Service

The National Environmental Satellite, Data, and Information Service (NESDIS) manages the Nation's civil Earth-observing satellite systems, as well as global national data bases for meteorology, oceanography, geophysics, and solar-terrestrial sciences. From these sources, it develops and disseminates environmental data and information products critical to the protection of life and property, national defense, the national economy, energy development and distribution, global food supplies, and the development of natural resources.

Publication in the NOAA Technical Report series does not preclude later publication in scientific journals in expanded or modified form. The NESDIS series of NOAA Technical Reports is a continuation of the former NESS and EDIS series of NOAA Technical Reports and the NESC and EDS series of Environmental Science Services Administration (ESSA) Technical Reports.

Copies of earlier reports may be available by contacting NESDIS Chief of Staff, NOAA/ NESDIS, 1335 East-West Highway, SSMC1, Silver Spring, MD 20910, (301) 713-3578.

NOAA Technical Report NESDIS 142-2

Regional Climate Trends and Scenarios for the U.S. National Climate Assessment

Part 2. Climate of the Southeast U.S.

Kenneth E. Kunkel, Laura E. Stevens, Scott E. Stevens, and Liqiang Sun
Cooperative Institute for Climate and Satellites (CICS), North Carolina State University and NOAA's National Climatic Data Center (NCDC)
Asheville, NC

Emily Janssen and Donald Wuebbles
University of Illinois at Urbana-Champaign
Champaign, IL

Charles E. Konrad II and Christopher M. Fuhrman
Southeast Regional Climate Center
University of North Carolina at Chapel Hill
Chapel Hill, NC

Barry D. Keim
Louisiana State Climate Office
Louisiana State University and Southern Climate Impacts Planning Program
Baton Rouge, LA

Michael C. Kruk
ERT Inc., NOAA's National Climatic Data Center (NCDC)
Asheville, NC

Amanda Billot
Louisiana State Climate Office
Louisiana State University
Baton Rouge, LA

Hal Needham
Louisiana State University and Southern Climate Impacts Planning Program
Baton Rouge, LA

Mark Shafer
Oklahoma Climatological Survey and Southern Climate Impacts Planning Program**,**
Norman, OK

J. Greg Dobson
National Environmental Modeling and Analysis Center
University of North Carolina at Asheville
Asheville, NC

U.S. DEPARTMENT OF COMMERCE
Rebecca Blank, Acting Secretary

National Oceanic and Atmospheric Administration
Dr. Jane Lubchenco, Under Secretary of Commerce for Oceans and Atmosphere
and NOAA Administrator

National Environmental Satellite, Data, and Information Service
Mary Kicza, Assistant Administrator

PREFACE

This document is one of series of regional climate descriptions designed to provide input that can be used in the development of the National Climate Assessment (NCA). As part of a sustained assessment approach, it is intended that these documents will be updated as new and well-vetted model results are available and as new climate scenario needs become clear. It is also hoped that these documents (and associated data and resources) are of direct benefit to decision makers and communities seeking to use this information in developing adaptation plans.

There are nine reports in this series, one each for eight regions defined by the NCA, and one for the contiguous U.S. The eight NCA regions are the Northeast, Southeast, Midwest, Great Plains, Northwest, Southwest, Alaska, and Hawai‘i/Pacific Islands.

These documents include a description of the observed historical climate conditions for each region and a set of climate scenarios as plausible futures – these components are described in more detail below.

While the datasets and simulations in these regional climate documents are not, by themselves, new, (they have been previously published in various sources), these documents represent a more complete and targeted synthesis of historical and plausible future climate conditions around the specific regions of the NCA.

There are two components of these descriptions. One component is a description of the historical climate conditions in the region. The other component is a description of the climate conditions associated with two future pathways of greenhouse gas emissions.

Historical Climate

The description of the historical climate conditions was based on an analysis of core climate data (the data sources are available and described in each document). However, to help understand, prioritize, and describe the importance and significance of different climate conditions, additional input was derived from climate experts in each region, some of whom are authors on these reports. In particular, input was sought from the NOAA Regional Climate Centers and from the American Association of State Climatologists. The historical climate conditions are meant to provide a perspective on what has been happening in each region and what types of extreme events have historically been noteworthy, to provide a context for assessment of future impacts.

Future Scenarios

The future climate scenarios are intended to provide an internally consistent set of climate conditions that can serve as inputs to analyses of potential impacts of climate change. The scenarios are not intended as projections as there are no established probabilities for their future realization. They simply represent an internally consistent climate picture using certain assumptions about the future pathway of greenhouse gas emissions. By “consistent” we mean that the relationships among different climate variables and the spatial patterns of these variables are derived directly from the same set of climate model simulations and are therefore physically plausible.

These future climate scenarios are based on well-established sources of information. No new climate model simulations or downscaled data sets were produced for use in these regional climate reports.

The use of the climate scenario information should take into account the following considerations:

1. All of the maps of climate variables contain information related to statistical significance of changes and model agreement. This information is crucial to appropriate application of the information. Three types of conditions are illustrated in these maps:
    a. The first condition is where most or all of the models simulate statistically significant changes and agree on the direction (whether increasing or decreasing) of the change. If this condition is present, then analyses of future impacts and vulnerabilities can more confidently incorporate this direction of change. It should be noted that the models may still produce a significant range of magnitude associated with the change, so the manner of incorporating these results into decision models will still depend to a large degree on the risk tolerance of the impacted system.
    b. The second condition is where the most or all of the models simulate changes that are too small to be statistically significant. If this condition is present, then assessment of impacts should be conducted on the basis that the future conditions could represent a small change from present or could be similar to current conditions and that the normal year-to-year fluctuations in climate dominate over any underlying long-term changes.
    c. The third condition is where most or all of the models simulate statistically significant changes but do not agree on the direction of the change, i.e. a sizeable fraction of the models simulate increases while another sizeable fraction simulate decreases. If this condition is present, there is little basis for a definitive assessment of impacts, and, separate assessments of potential impacts under an increasing scenario and under a decreasing scenario would be most prudent.
2. The range of conditions produced in climate model simulations is quite large. Several figures and tables provide quantification for this range. Impacts assessments should consider not only the mean changes, but also the range of these changes.
3. Several graphics compare historical observed mean temperature and total precipitation with model simulations for the same historical period. These should be examined since they provide one basis for assessing confidence in the model simulated future changes in climate.
    a. Temperature Changes: Magnitude. In most regions, the model simulations of the past century simulate the magnitude of change in temperature from observations; the southeast region being an exception where the lack of century-scale observed warming is not simulated in any model.
    b. Temperature Changes: Rate. The *rate* of warming over the last 40 years is well simulated in all regions.
    c. Precipitation Changes: Magnitude. Model simulations of precipitation generally simulate the overall observed trend but the observed decade-to-decade variations are greater than the model observations.

In general, for impacts assessments, this information suggests that the model simulations of temperature conditions for these scenarios are likely reliable, but users of precipitation simulations may want to consider the likelihood of decadal-scale variations larger than simulated by the models. It should also be noted that accompanying these documents will be a web-based resource with downloadable graphics, metadata about each, and more information and links to the datasets and overall descriptions of the process.

1. INTRODUCTION 5

2. REGIONAL CLIMATE TRENDS AND IMPORTANT CLIMATE FACTORS 10

2.1. DESCRIPTION OF DATA SOURCES 10

2.2. GENERAL DESCRIPTION OF SOUTHEAST CLIMATE 11

2.3. IMPORTANT CLIMATE FACTORS 15

2.3.1. Heavy Rainfall and Floods 15

2.3.2. Drought 17

2.3.3. Extreme Heat and Cold 17

2.3.4. Winter Storms 20

2.3.5. Severe Thunderstorms and Tornadoes 20

2.3.6. Tropical Cyclones 22

2.4. CLIMATIC TRENDS 22

2.4.1. Temperature 24

2.4.2. Precipitation 28

2.4.3. Extreme Heat and Cold 32

2.4.4. Extreme Precipitation and Floods 36

2.4.5. Freeze-Free Season 37

2.4.6. Winter Storms 37

2.4.7. Severe Thunderstorms and Tornadoes 37

2.4.8. Hurricanes 39

2.4.9. Sea Level Rise and Sea-Surface Temperature 40

3. FUTURE REGIONAL CLIMATE SCENARIOS 42

3.1. DESCRIPTION OF DATA SOURCES 42

3.2. ANALYSES 44

3.3. MEAN TEMPERATURE 45

3.4. EXTREME TEMPERATURE 52

3.5. OTHER TEMPERATURE VARIABLES 58

3.6. TABULAR SUMMARY OF SELECTED TEMPERATURE VARIABLES 62

3.7. MEAN PRECIPITATION 63

3.8. EXTREME PRECIPITATION 70

3.9. TABULAR SUMMARY OF SELECTED PRECIPITATION VARIABLES 70

3.10. COMPARISON BETWEEN MODEL SIMULATIONS AND OBSERVATIONS 73

4. SUMMARY 83

5. REFERENCES 86

6. ACKNOWLEDGEMENTS 94

6.1. REGIONAL CLIMATE TRENDS AND IMPORTANT CLIMATE FACTORS 94

6.2. FUTURE REGIONAL CLIMATE SCENARIOS 94

1. INTRODUCTION

The Global Change Research Act of 1990[1] mandated that national assessments of climate change be prepared not less frequently than every four years. The last national assessment was published in 2009 (Karl et al. 2009). To meet the requirements of the act, the Third National Climate Assessment (NCA) report is now being prepared. The National Climate Assessment Development and Advisory Committee (NCADAC), a federal advisory committee established in the spring of 2011, will produce the report. The NCADAC Scenarios Working Group (SWG) developed a set of specifications with regard to scenarios to provide a uniform framework for the chapter authors of the NCA report.

This climate document was prepared to provide a resource for authors of the Third National Climate Assessment report, pertinent to the states of Kentucky, Virginia, Tennessee, North Carolina, South Carolina, Arkansas, Louisiana, Mississippi, Alabama, Georgia, and Florida; hereafter referred to collectively as the Southeast. The specifications of the NCADAC SWG, along with anticipated needs for historical information, guided the choices of information included in this description of Southeast climate. While guided by these specifications, the material herein is solely the responsibility of the authors, and usage of this material is at the discretion of the 2013 NCA report authors.

This document has two main sections: one on historical conditions and trends, and the other on future conditions as simulated by climate models. The historical section concentrates on temperature and precipitation, primarily based on analyses of data from the National Weather Service's (NWS) Cooperative Observer Network, which has been in operation since the late 19th century. Additional climate features are discussed based on the availability of information. The future simulations section is exclusively focused on temperature and precipitation.

With regard to the future, the NCADAC, at its May 20, 2011 meeting, decided that scenarios should be prepared to provide an overall context for assessment of impacts, adaptation, and mitigation, and to coordinate any additional modeling used in synthesizing or analyzing the literature. Scenario information for climate, sea-level change, changes in other environmental factors (such as land cover), and changes in socioeconomic conditions (such as population growth and migration) have been prepared. This document provides an overall description of the climate information.

In order to complete this document in time for use by the NCA report authors, it was necessary to restrict its scope in the following ways. Firstly, this document does not include a comprehensive description of all climate aspects of relevance and interest to a national assessment. We restricted our discussion to climate conditions for which data were readily available. Secondly, the choice of climate model simulations was also restricted to readily available sources. Lastly, the document does not provide a comprehensive analysis of climate model performance for historical climate conditions, although a few selected analyses are included.

The NCADAC directed the "use of simulations forced by the A2 emissions scenario as the primary basis for the high climate future and by the B1 emissions scenario as the primary basis for the low climate future for the 2013 report" for climate scenarios. These emissions scenarios were generated by the Intergovernmental Panel on Climate Change (IPCC) and are described in the IPCC Special

[1] http://thomas.loc.gov/cgi-bin/bdquery/z?d101:SN00169:|TOM:/bss/d101query.html

Report on Emissions Scenarios (SRES) (IPCC 2000). These scenarios were selected because they incorporate much of the range of potential future human impacts on the climate system and because there is a large body of literature that uses climate and other scenarios based on them to evaluate potential impacts and adaptation options. These scenarios represent different narrative storylines about possible future social, economic, technological, and demographic developments. These SRES scenarios have internally consistent relationships that were used to describe future pathways of greenhouse gas emissions. The A2 scenario "describes a very heterogeneous world. The underlying theme is self-reliance and preservation of local identities. Fertility patterns across regions converge very slowly, which results in continuously increasing global population. Economic development is primarily regionally oriented and per capita economic growth and technological change are more fragmented and slower than in the other storylines" (IPCC 2000). The B1 scenario describes "a convergent world with…global population that peaks in mid-century and declines thereafter…but with rapid changes in economic structures toward a service and information economy, with reductions in material intensity, and the introduction of clean and resource-efficient technologies. The emphasis is on global solutions to economic, social, and environmental sustainability, including improved equity, but without additional climate initiatives" (IPCC 2000).

The temporal changes of emissions under these two scenarios are illustrated in Fig. 1 (left panel). Emissions under the A2 scenario continually rise during the 21st century from about 40 gigatons (Gt) CO_2-equivalent per year in the year 2000 to about 140 Gt CO_2-equivalent per year by 2100. By contrast, under the B1 scenario, emissions rise from about 40 Gt CO_2-equivalent per year in the year 2000 to a maximum of slightly more than 50 Gt CO_2-equivalent per year by mid-century, then falling to less than 30 Gt CO_2-equivalent per year by 2100. Under both scenarios, CO_2 concentrations rise throughout the 21st century. However, under the A2 scenario, there is an acceleration in concentration trends, and by 2100 the estimated concentration is above 800 ppm. Under the B1 scenario, the rate of increase gradually slows and concentrations level off at about 500 ppm by 2100. An increase of 1 ppm is equivalent to about 8 Gt of CO_2. The increase in concentration is considerably smaller than the rate of emissions because a sizeable fraction of the emitted CO_2 is absorbed by the oceans.

The projected CO_2 concentrations are used to estimate the effects on the earth's radiative energy budget, and this is the key forcing input used in global climate model simulations of the future. These simulations provide the primary source of information about how the future climate could evolve in response to the changing composition of the earth's atmosphere. A large number of modeling groups performed simulations of the 21st century in support of the IPCC's Fourth Assessment Report (AR4), using these two scenarios. The associated changes in global mean temperature by the year 2100 (relative to the average temperature during the late 20th century) are about +6.5°F (3.6°C) under the A2 scenario and +3.2°F (1.8°C) under the B1 scenario with considerable variations among models (Fig. 1, right panel).

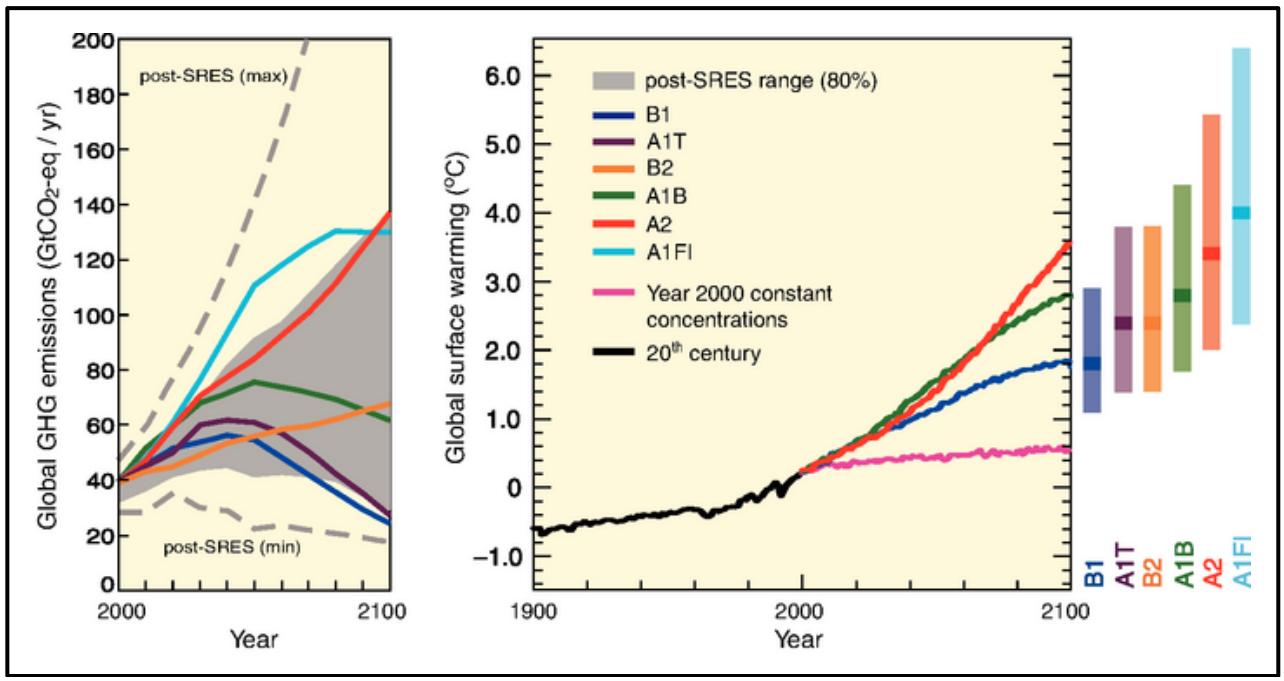

Figure 1. Left Panel: Global GHG emissions (in $GtCO_2$-eq) in the absence of climate policies: six illustrative SRES marker scenarios (colored lines) and the 80th percentile range of recent scenarios published since SRES (post-SRES) (gray shaded area). Dashed lines show the full range of post-SRES scenarios. The emissions include CO_2, CH_4, N_2O and F-gases. Right Panel: Solid lines are multi-model global averages of surface warming for scenarios A2, A1B and B1, shown as continuations of the 20th-century simulations. These projections also take into account emissions of short-lived GHGs and aerosols. The pink line is not a scenario, but is for Atmosphere-Ocean General Circulation Model (AOGCM) simulations where atmospheric concentrations are held constant at year 2000 values. The bars at the right of the figure indicate the best estimate (solid line within each bar) and the likely range assessed for the six SRES marker scenarios at 2090-2099. All temperatures are relative to the period 1980-1999. From IPCC AR4, Sections 3.1 and 3.2, Figures 3.1 and 3.2, IPCC (2007b).

In addition to the direct output of the global climate model simulations, the NCADAC approved "the use of both statistically- and dynamically-downscaled data sets". "Downscaling" refers to the process of producing higher-resolution simulations of climate from the low-resolution outputs of the global models. The motivation for use of these types of data sets is the spatial resolution of global climate models. While the spatial resolution of available global climate model simulations varies widely, many models have resolutions in the range of 100-200 km (~60-120 miles). Such scales are very large compared to local and regional features important to many applications. For example, at these scales mountain ranges are not resolved sufficiently to provide a reasonably accurate representation of the sharp gradients in temperature, precipitation, and wind that typically exist in these areas.

Statistical downscaling achieves higher-resolution simulations through the development of statistical relationships between large-scale atmospheric features that are well-resolved by global models and the local climate conditions that are not well-resolved. The statistical relationships are developed by comparing observed local climate data with model simulations of the recent historical climate. These relationships are then applied to the simulations of the future to obtain local high-

resolution projections. Statistical downscaling approaches are relatively economical from a computational perspective, and thus they can be easily applied to many global climate model simulations. One underlying assumption is that the relationships between large-scale features and local climate conditions in the present climate will not change in the future (Wilby and Wigley 1997). Careful consideration must also be given when deciding how to choose the appropriate predictors because statistical downscaling is extremely sensitive to the choice of predictors (Norton et al. 2011).

Dynamical downscaling is much more computationally intensive but avoids assumptions about constant relationships between present and future. Dynamical downscaling uses a climate model, similar in most respects to the global climate models. However, the climate model is run at a much higher resolution but only for a small region of the earth (such as North America) and is termed a "regional climate model (RCM)". A global climate model simulation is needed to provide the boundary conditions (e.g., temperature, wind, pressure, and humidity) on the lateral boundaries of the region. Typically, the spatial resolution of an RCM is 3 or more times higher than the global model used to provide the boundary conditions. With this higher resolution, topographic features and smaller-scale weather phenomena are better represented. The major downside of dynamical downscaling is that a simulation for a region can take as much computer time as a global climate model simulation for the entire globe. As a result, the availability of such simulations is limited, both in terms of global models used for boundary conditions and time periods of the simulations (Hayhoe 2010).

Section 3 of this document (Future Regional Climate Scenarios) responds to the NCADAC directives by incorporating analyses from multiple sources. The core source is the set of global climate model simulations performed for the IPCC AR4, also referred to as the Climate Model Intercomparison Project phase 3 (CMIP3) suite. These have undergone extensive evaluation and analysis by many research groups. A second source is a set of statistically-downscaled data sets based on the CMIP3 simulations. A third source is a set of dynamically-downscaled simulations, driven by CMIP3 models. A new set of global climate model simulations is being generated for the IPCC Fifth Assessment Report (AR5). This new set of simulations is referred to as the Climate Model Intercomparison Project phase 5 (CMIP5). These scenarios do not incorporate any CMIP5 simulations as relatively few were available at the time the data analyses were initiated.
As noted earlier, the information included in this document is primarily concentrated around analyses of temperature and precipitation. This is explicitly the case for the future scenarios sections; due in large part to the short time frame and limited resources, we capitalized on the work of other groups on future climate simulations, and these groups have devoted a greater effort to the analysis of temperature and precipitation than other surface climate variables.

Climate models have generally exhibited a high level of ability to simulate the large-scale circulation patterns of the atmosphere. These include the seasonal progression of the position of the jet stream and associated storm tracks, the overall patterns of temperature and precipitation, the occasional occurrence of droughts and extreme temperature events, and the influence of geography on climatic patterns. There are also important processes that are less successfully simulated by models, as noted by the following selected examples.

Climate model simulation of clouds is problematic. Probably the greatest uncertainty in model simulations arises from clouds and their interactions with radiative energy fluxes (Dufresne and Bony 2008). Uncertainties related to clouds are largely responsible for the substantial range of

global temperature change in response to specified greenhouse gas forcing (Randall et al. 2007). Climate model simulation of precipitation shows considerable sensitivities to cloud parameterization schemes (Arakawa 2004). Cloud parameterizations remain inadequate in current GCMs. Consequently, climate models have large biases in simulating precipitation, particularly in the tropics. Models typically simulate too much light precipitation and too little heavy precipitation in both the tropics and middle latitudes, creating potential biases when studying extreme events (Bader et al. 2008).

Climate models also have biases in simulation of some important climate modes of variability. The El Niño-Southern Oscillation (ENSO) is a prominent example. In some parts of the U.S., El Niño and La Niña events make important contributions to year-to-year variations in conditions. Climate models have difficulty capturing the correct phase locking between the annual cycle and ENSO (AchutaRao and Sperber 2002). Some climate models also fail to represent the spatial and temporal structure of the El Niño - La Niña asymmetry (Monahan and Dai 2004). Climate simulations over the U.S. are affected adversely by these deficiencies in ENSO simulations.

The model biases listed above add additional layers of uncertainty to the information presented herein and should be kept in mind when using the climate information in this document.

The representation of the results of the suite of climate model simulations has been a subject of active discussion in the scientific literature. In many recent assessments, including AR4, the results of climate model simulations have been shown as multi-model mean maps (e.g., Figs. 10.8 and 10.9 in Meehl et al. 2007). Such maps give equal weight to all models, which is thought to better represent the present-day climate than any single model (Overland et al. 2011). However, models do not represent the current climate with equal fidelity. Knutti (2010) raises several issues about the multi-model mean approach. These include: (a) some model parameterizations may be tuned to observations, which reduces the spread of the results and may lead to underestimation of the true uncertainty; (b) many models share code and expertise and thus are not independent, leading to a reduction in the true number of independent simulations of the future climate; (c) all models have some processes that are not accurately simulated, and thus a greater number of models does not necessarily lead to a better projection of the future; and (d) there is no consensus on how to define a metric of model fidelity, and this is likely to depend on the application. Despite these issues, there is no clear superior alternative to the multi-model mean map presentation for general use. Tebaldi et al. (2011) propose a method for incorporating information about model variability and consensus. This method is adopted here where data availability make it possible. In this method, multi-model mean values at a grid point are put into one of three categories: (1) models agree on the statistical significance of changes and the sign of the changes; (2) models agree that the changes are not statistically significant; and (3) models agree that the changes are statistically significant but disagree on the sign of the changes. The details on specifying the categories are included in Section 3.

2. REGIONAL CLIMATE TRENDS AND IMPORTANT CLIMATE FACTORS

2.1. Description of Data Sources

One of the core data sets used in the United States for climate analysis is the National Weather Service's Cooperative Observer Network (COOP), which has been in operation since the late 19th century. The resulting data can be used to examine long-term trends. The typical COOP observer takes daily observations of various climate elements that might include precipitation, maximum temperature, minimum temperature, snowfall, and snow depth. While most observers are volunteers, standard equipment is provided by the National Weather Service (NWS), as well as training in standard observational practices. Diligent efforts are made by the NWS to find replacement volunteers when needed to ensure the continuity of stations whenever possible. Over a thousand of these stations have been in operation continuously for many decades (NOAA 2012a).

For examination of U.S. long-term trends in temperature and precipitation, the COOP data is the best available resource. Its central purpose is climate description (although it has many other applications as well); the number of stations is large, there have been relatively few changes in instrumentation and procedures, and it has been in existence for over 100 years. However, there are some sources of temporal inhomogeneities in station records, described as follows:

- One instrumental change is important. For much of the COOP history, the standard temperature system was a pair of liquid-in-glass (LIG) thermometers placed in a radiation shield known as the Cotton Region Shelter (CRS). In the 1980s, the NWS began replacing this system with an electronic maximum-minimum temperature system (MMTS). Inter-comparison experiments indicated that there is a systematic difference between these two instrument systems, with the newer electronic system recording lower daily maximum temperatures (T_{max}) and higher daily minimum temperatures (T_{min}) (Quayle et al. 1991; Hubbard and Lin 2006; Menne et al. 2009). Menne et al. (2009) estimate that the mean shift (going from CRS/LIG to MMTS) is -0.52K for T_{max} and +0.37K for T_{min}. Adjustments for these differences can be applied to monthly mean temperature to create homogeneous time series.
- Changes in the characteristics and/or locations of sites can introduce artificial shifts or trends in the data. In the COOP network, a station is generally not given a new name or identifier unless it moves at least 5 miles and/or changes elevation by at least 100 feet (NWS 1993). Site characteristics can change over time and affect a station's record, even if no move is involved (and even small moves << 5 miles can have substantial impacts). A common source of such changes is urbanization around the station, which will generally cause artificial warming, primarily in T_{min} (Karl et al. 1988), the magnitude of which can be several degrees in the largest urban areas. Most research suggests that the overall effect on national and global temperature trends is rather small because of the large number of rural stations included in such analyses (Karl et al. 1988; Jones et al. 1990) and because homogenization procedures reduce the urban signal (Menne et al. 2009).
- Station siting can cause biases. Recent research by Menne et al. (2010) and Fall et al. (2011) examined this issue in great detail. The effects on mean trends was found to be small in both studies, but Fall et al. (2011) found that stations with poor siting overestimate (underestimate) minimum (maximum) temperature trends.

- Changes in the time that observations are taken can also introduce artificial shifts or trends in the data (Karl et al. 1986; Vose et al. 2003). In the COOP network, typical observation times are early morning or late afternoon, near the usual times of the daily minimum and maximum temperatures. Because observations occur near the times of the daily extremes, a change in observation time can have a measurable effect on averages, irrespective of real changes. The study by Karl et al. (1986) indicates that the difference in monthly mean temperatures between early morning and late afternoon observers can be in excess of 2°C. There has, in fact, been a major shift from a preponderance of afternoon observers in the early and middle part of the 20th century to a preponderance of morning observers at the present time. In the 1930s, nearly 80% of the COOP stations were afternoon observers (Karl et al. 1986). By the early 2000s, the number of early morning observers was more than double the number of late afternoon observers (Menne et al. 2009). This shift tends to introduce an artificial cooling trend in the data.

A recent study by Williams et al. (2011) found that correction of known and estimated inhomogeneities lead to a larger warming trend in average temperature, principally arising from correction of the biases introduced by the changeover to the MMTS and from the biases introduced by the shift from mostly afternoon observers to mostly morning observers.

Much of the following analysis on temperature, precipitation, and snow is based on COOP data. For some of these analyses, a subset of COOP stations with long periods of record was used, specifically less than 10% missing data for the period of 1895-2011. The use of a consistent network is important when examining trends in order to minimize artificial shifts arising from a changing mix of stations.

2.2. General Description of Southeast Climate

The climate of the Southeast is quite variable and influenced by a number of factors, including latitude, topography, and proximity to large bodies of water. The topography of the region is diverse. In the southern and eastern portions of the region, extensive coastal plains stretch from Louisiana eastward to southeastern Virginia, while rolling low plateaus, known as the Piedmont, are present from eastern Alabama to Central Virginia. North and west of these areas, mountain ridges are found, including the Ozarks in Arkansas (1500-3000 feet) and the Appalachians, which stretch from Alabama to Virginia (2000-6600 feet). Finally, elevated, dissected plateaus lie from northern Alabama to Kentucky. Temperatures generally decrease with increasing latitude and elevation while precipitation decreases away from the Gulf-Atlantic coasts, although it is locally greater over portions of the Appalachian Mountains. Overall, the climate of the Southeast is generally mild and pleasant, which makes it a popular region for relocation and tourism.

A semi-permanent high pressure system, known as the Bermuda High, is typically situated off of the Atlantic Coast. Depending on its position, it commonly draws moisture northward or westward from the Atlantic and Gulf of Mexico, especially during the warm season. As a result, summers across the Southeast are characteristically warm and moist with frequent thundershower activity in the afternoon and early evening hours. Day-to-day and week-to-week variations in the positioning of the Bermuda High can have a strong influence on precipitation patterns. When the Bermuda High builds west over the region, hot and dry weather occurs, although humidities often remain relatively high. This pattern can cause heat waves and poor air quality, both of which negatively affect human

health. When the westward extension of the Bermuda High persists over or immediately south of the area for extended periods, drought conditions typically develop. This places stress on water supplies, agricultural crops, and can reduce hydroelectric energy production. Variations in the positioning of the Bermuda High also affect the tracking of hurricanes across the region.

During the cooler months of the year, the Bermuda High shifts southeastward as the jet stream expands southward. Accompanying the jet stream are extratropical cyclones and fronts that cause much day-to-day variability in the weather. When the jet stream dives southward, continental air can overspread the Southeast behind these cyclones, leading to cold-air outbreaks. Sometimes sub-freezing air reaches as far south as central Florida, causing major damage to citrus crops. Extratropical cyclones also draw warm and humid air from the Atlantic Ocean and Gulf of Mexico northward over frontal boundaries, and this can lead to potentially dangerous snowstorms or ice storms. These winter storms are generally confined to the northern tier of the region, where temperatures are cold enough for frozen precipitation. In the spring, the sharp contrast in temperature and humidity in the vicinity of the jet stream can promote the development of severe thunderstorms that produce damaging winds, large hail, and tornadoes.

Temperature contrasts are especially great across the region in the wintertime. Average daily minimum temperatures in January range from 60°F in South Florida to 20°F across the Southern Appalachians and northern Kentucky (Fig. 2). In contrast, average daily maximum temperatures in July range from 95°F across the lower Mississippi River Valley and southeast Georgia to 75°F across the higher elevations of the Southern Appalachians (Fig. 3). Seasonal variations in temperature are relatively modest across the Caribbean due to its tropical climate. In Puerto Rico, these variations relate to both elevation and soil wetness. For example, minimum winter temperatures drop to as low as 50°F in the Cordillera Central mountain range (above 4,000 feet) while maximum summer temperatures reach 95°F across the drier southwestern part of the island.

Average annual precipitation across the region shows variations that relate both to the proximity to moisture sources (e.g., Gulf of Mexico and Atlantic Ocean) and the influences of topography, such as orographic lifting and rain shadows (Fig. 4). The Gulf Coast regions of Louisiana, Mississippi, Alabama, and the Florida Panhandle receive over 60 inches of precipitation, while much of Virginia, northern Kentucky, and central sections of the Carolinas and Georgia receive between 40-50 inches of precipitation annually. Higher amounts of precipitation are found along the Atlantic coast and across the Florida Peninsula, due in part to the lifting of the air associated with the sea breeze circulation. Tropical cyclones can also contribute significantly to annual precipitation totals in the region, especially over the Southeast Atlantic coast (Knight and Davis 2009).

The wettest locations in the Southeast are found in southwestern North Carolina and across the eastern (i.e. windward) slope of Puerto Rico, where average annual totals exceed 100 inches. Across the northern tier of the region, average annual snowfall ranges from 5 to 25 inches, except at the higher elevations of the southern Appalachians in North Carolina and Tennessee (Fig. 5). These locations can receive up to 100 inches of snowfall annually, which is comparable to annual snowfall amounts experienced across portions of New England (Perry et al. 2010). The southern tier of the region experiences very little snowfall (i.e. less than 1 inch per year) and can go several years without recording any measurable snowfall.

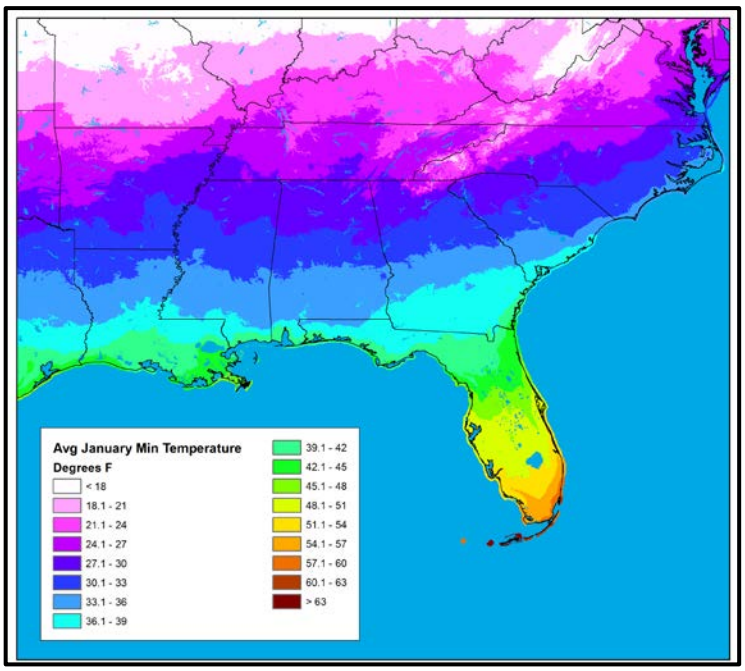

Figure 2. Average daily January minimum temperature for the Southeast region using the Parameter-elevation Regressions on Independent Slopes Model (PRISM) [PRISM Climate Group, Oregon State University, http://www.prism.oregonstate.edu/, created 21 Aug 2012]. This illustrates the large north-south differences in temperature and the generally mild winter temperatures along the Gulf Coast and Florida.

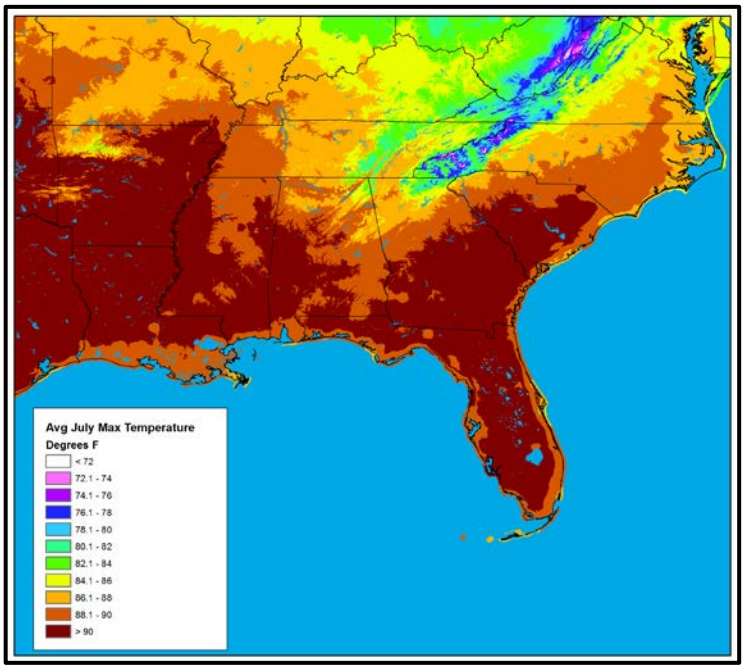

Figure 3. Same as Fig. 2, but for average daily July maximum temperature. Very warm mid-summer conditions are characteristic of most of this region. The coolest areas during mid-summer are the higher elevation areas of the southern Appalachians.

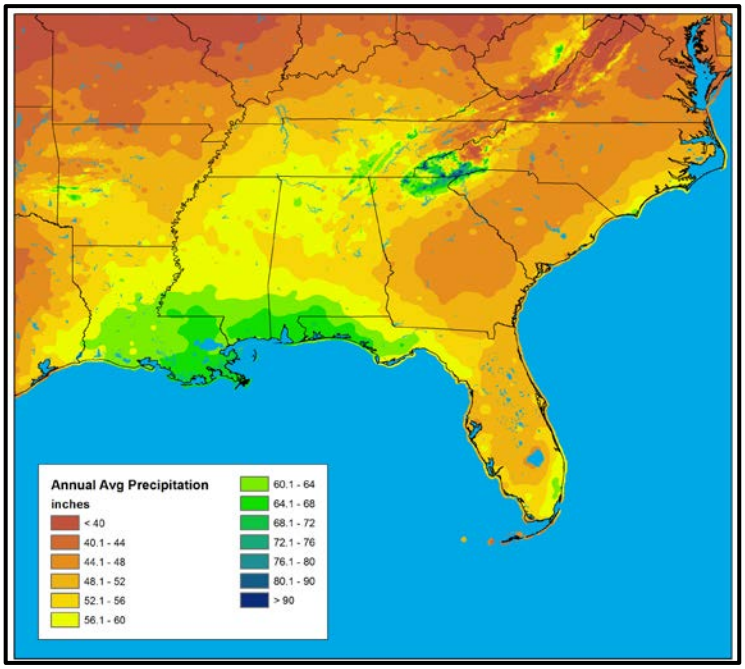

Figure 4. Annual average precipitation for the Southeast region using the Parameter-elevation Regressions on Independent Slopes Model (PRISM) [PRISM Climate Group, Oregon State University, http://www.prism.oregonstate.edu/, created 21 Aug 2012]. Precipitation is abundant throughout the region. Highest precipitation values are found along the central Gulf Coast and some higher elevation areas of the southern Appalachians.

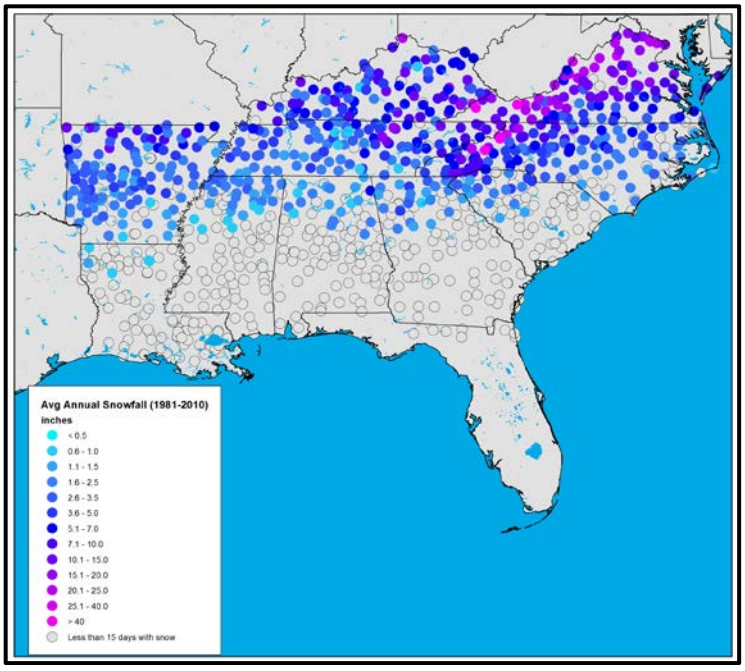

Figure 5. Annual average snowfall from 1981 to 2010 for the Southeast region using data from the Global Historical Climatology Network (GHCN) [http://www.ncdc.noaa.gov/oa/climate/ghcn-daily/]. Snow is a regular occurrence only in the northern half of the region. The southern half of the region receives snow less than once every two years.

Although the Southeast is mostly in a humid subtropical climate type, the seasonality of precipitation varies considerably across the region (Fig. 6). Along the coast, as well as some areas in the interior, a summer precipitation maximum is found, especially across the Florida Peninsula. This can be related to the daytime thunderstorm activity that is associated with the heating of the land surface and lifting of air along the sea breeze front. Many locations in the interior Southeast have nearly the same amount of precipitation in the cool season as in the warm season. In the cool season, extratropical cyclones and associated fronts frequently traverse much of the region and bring with them precipitation. Cool season precipitation totals, however, show much regional scale variability. The northern Gulf coast is especially wet as mid-latitude cyclones frequently advect high levels of moisture northward from the Gulf of Mexico along frontal systems (Keim 1996). In contrast, the Florida Peninsula is often positioned south and east of cyclones and fronts and therefore displays a winter precipitation minimum (Trewartha 1981). Locations along the Atlantic Coast are situated in the path of extratropical cyclones in winter and spring. However, the fast motion of these systems frequently limits the deep transport of moisture and the duration of the associated precipitation (Keim 1996). Precipitation in the Caribbean is influenced primarily by the Bermuda High. In the winter (summer), as the Bermuda High shifts southward (northward), easterly trade winds increase (decrease) while sea-surface temperatures (SSTs) and humidities decrease (increase) across the Caribbean, resulting in a winter (summer) precipitation minimum (maximum) (Taylor and Alfaro 2005). A reduction in precipitation in July, known as the Caribbean mid-summer drought, occurs when the Bermuda High temporarily expands southwestward across the Caribbean (Gamble et al. 2008). Tropical cyclones also contribute significantly to precipitation totals across the Caribbean in the summer and fall seasons.

The Southeast includes 28 of the top 100 metropolitan statistical areas by population and is the second most urbanized assessment region (after the Northeast), with 131 persons per square mile. Major urban centers in the region, ranked in the top 30 (U.S. Census Bureau 2011), include Miami (rank #8), Atlanta (#9), Tampa (#18), and Orlando (#26).

2.3. Important Climate Factors

The Southeast region experiences a wide range of extreme weather and climate events that affect human society, ecosystems, and infrastructure. Since 1980, the Southeast has experienced more billion-dollar weather disasters than any other region in the U.S. Most of these were associated with hurricanes, floods, and tornadoes (NOAA 2011). This discussion is meant to provide general information about these types of weather and climate phenomena. These include:

2.3.1. Heavy Rainfall and Floods

Heavy rainfall can produce short-lived flash floods and long-duration river floods that have enormous impacts on property and human life. These events result from a variety of weather systems that show much seasonality in their occurrence. In the winter and spring, slow-moving extratropical cyclones can produce large areas of very heavy rainfall, and during the late spring and summer, slow-moving or training thunderstorms can generate excessive rainfalls over local areas. Finally, during the later summer and fall, tropical cyclones can produce extremely heavy rainfall, both locally and regionally, especially when they interact with frontal systems (Konrad and Perry 2010).

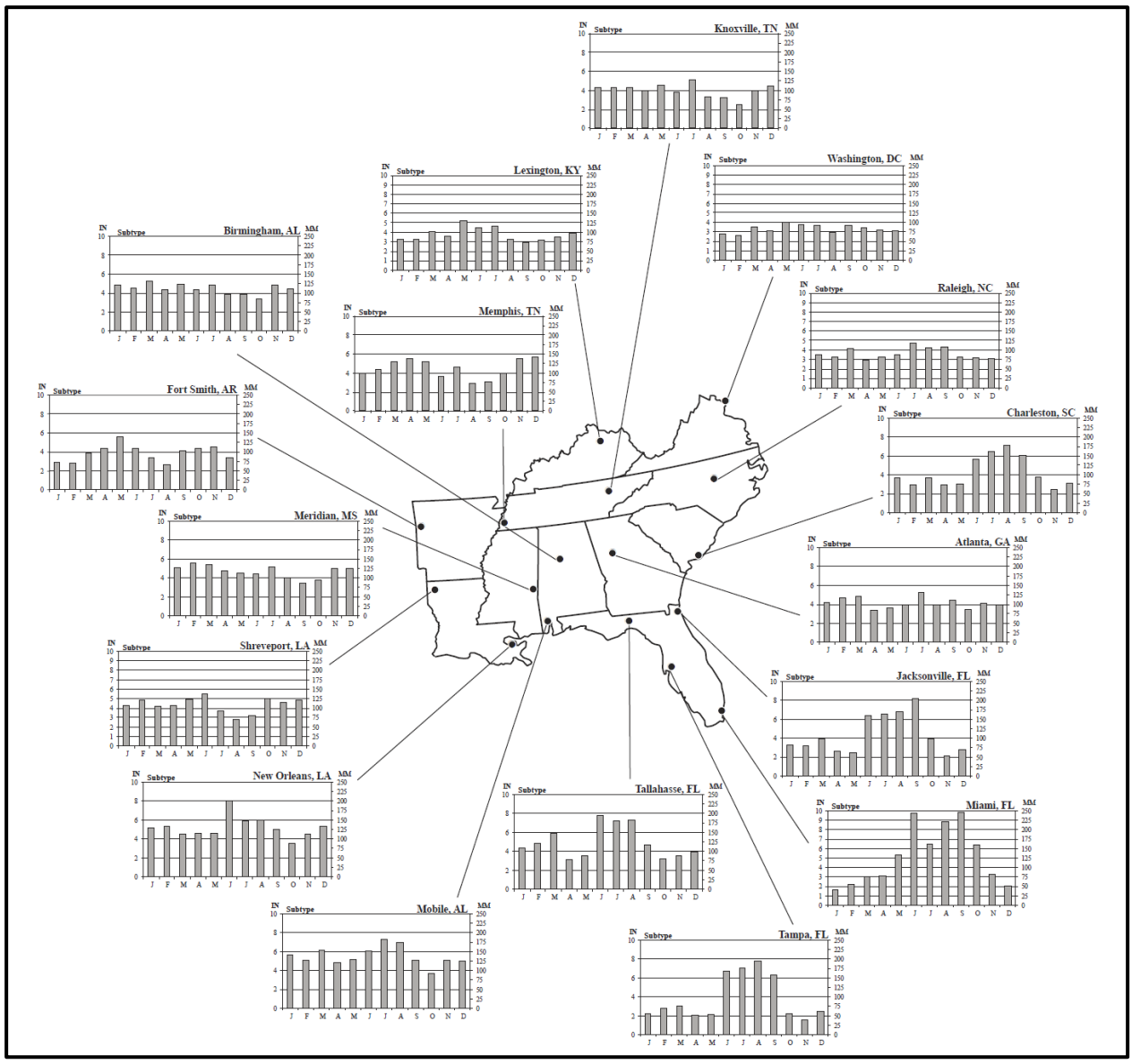

Figure 6. Monthly precipitation normals (1981-2010) for 17 geographically distributed stations in the Southeast region. These stations are located in mostly medium to large urban areas. At most locations precipitation is rather evenly distributed throughout the year. Coastal regions experience a summer maximum, most prominent in southern Florida.

Major rivers in the Southeast region are susceptible to flooding, which can have a big impact on transportation, utility and industrial plants, as well as population interests along the major river basins (e.g., Mississippi and Ohio Rivers). Additional impacts include the increased incidence of waterborne disease, contamination of water supplies, as well as property and agricultural losses. Most flood-related deaths result from flash floods associated with extratropical cyclones and tropical cyclones (Ashley and Ashley 2008). Of those deaths associated with tropical cyclones from 1970 to 1999, nearly 60 percent resulted from inland freshwater floods (Rappaport 2000). The orographic lifting of very moist air in tropical cyclones can produce extraordinary precipitation totals, resulting in flash and river flooding as well as landslides on the steeper slopes of the Southern Appalachians (Fuhrmann et al. 2008).

2.3.2. Drought

Despite the abundance of moisture, the Southeast region is prone to drought as deficits of precipitation lead to a shortage of freshwater supplies. Rapid population growth and development has greatly increased the region's demand for water and vulnerability to drought. In the Southeast, droughts typically display a relatively shorter duration (i.e. one to three years) as compared to the multi-decadal droughts sometimes experienced in the western and central parts of the U.S. (Seager et al. 2009). This may be due in part to the periodic occurrence of tropical cyclones, which can ameliorate the effects of drought during the peak water demand months of the late summer and fall (Maxwell et al. 2011). In contrast, the absence of tropical cyclones, combined with high variability in warm season rainfall, increased evapotranspiration, and increased water usage can lead to the rapid development of drought conditions across the Southeast. Recent examples include the 1998-2002 drought, which resulted in record low lake, reservoir, and groundwater levels across parts of the Carolinas (Carbone et al. 2008), and the 2007-2008 drought, which resulted in over $1 billion in losses in Georgia alone and led to federal lawsuits over control of water releases from Lake Lanier in northern Georgia (Manuel 2008). In some cases, flooding and drought can occur simultaneously, as was the case in early summer of 2011 (see Box 1).

2.3.3. Extreme Heat and Cold

Due to its mid-latitude location, the Southeast region often experiences extreme heat during the summer months and is occasionally prone to extreme cold during the winter months (Figs. 7 and 8). Periods of extreme heat, particularly when combined with high humidity, can cause heat-related illness among vulnerable individuals as well as place stress on agriculture, water supplies, and energy production. Periods of extreme heat across the interior of the Southeast region have been tied to an upper-level ridge of high pressure centered over the Mississippi River Valley (Fuhrmann et al. 2011). There are significant local-scale variations in extreme heat and humidity related to adiabatic warming associated with downsloping winds off of the Appalachian Mountains, daytime mixing and draw-down of dry air from aloft, and the presence and strength of the sea-breeze circulation (Fuhrmann et al. 2011).

Box 1: Extreme Drought amongst a Record Flood

The complexities of climate variability may combine to produce a paradoxical mix of climate-related conditions. In the early summer of 2011, the lower Mississippi Valley experienced something very unusual, the simultaneous occurrence of both flooding and drought. People were piling sandbags to hold back the floodwaters, and the Morganza Spillway in Louisiana was opened for the first time since 1973 to relieve pressure on the swollen river downstream in Baton Rouge and New Orleans. (Fig. A). As the swollen river meandered across this region, however, much of the south Louisiana landscape was in extreme drought according to the U.S. Drought Monitor (http://www.drought.gov). As such, the region was experiencing both flood and drought at the same time.

Interestingly, both the flood and the drought were tied to La Niña conditions in the equatorial Pacific Ocean. Las Niñas tend to dry out the Gulf Coast region by shifting storm tracks to the north across the Ohio River Valley. As storms tracked across the Central portion of the United States, they bypassed Texas, Oklahoma, Louisiana, and Mississippi, leaving them high and dry and producing drought conditions. However, excessive rainfall in the Midwest associated with the northward-displaced storm track, compounded by a large volume of spring snowmelt, produced a flood wave that moved downstream into drought stricken Tennessee, Arkansas, Mississippi and Louisiana.

Figure A. On May 14, 2011, the U.S. Army of Corps of Engineers opened the first gate on the Morganza Floodway in Louisiana to relieve flooding on the Mississippi River. Photo Credit: U.S. Army Corps of Engineers. Available at: http://www.flickr.com/photos/30539067@N04/5722952407.

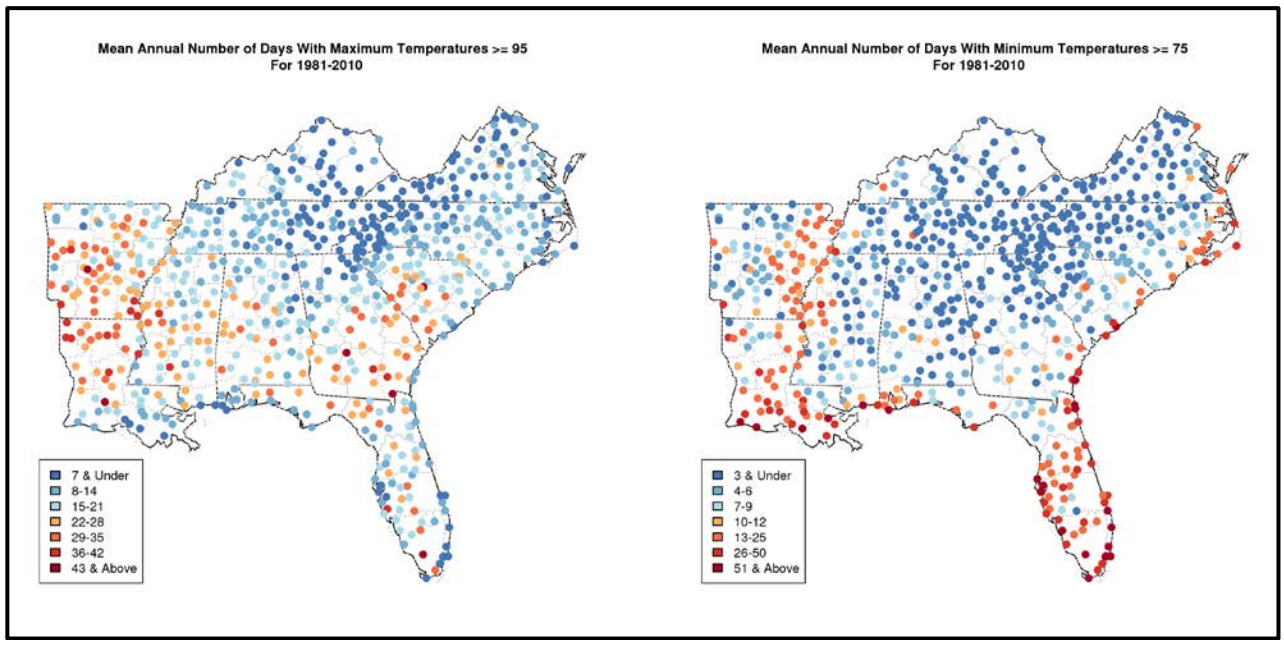

Figure 7. Mean annual number of days with a maximum temperature ≥95°F (left) and a minimum temperature ≥75°F (right) for the Southeast region. Variability from one station to the next is associated with local effects, including topography and land cover. The highest number of 95°F days occurs in western and interior southern parts of the region. Hot nights are most frequent in Florida, along the coasts, and along the Mississippi River valley.

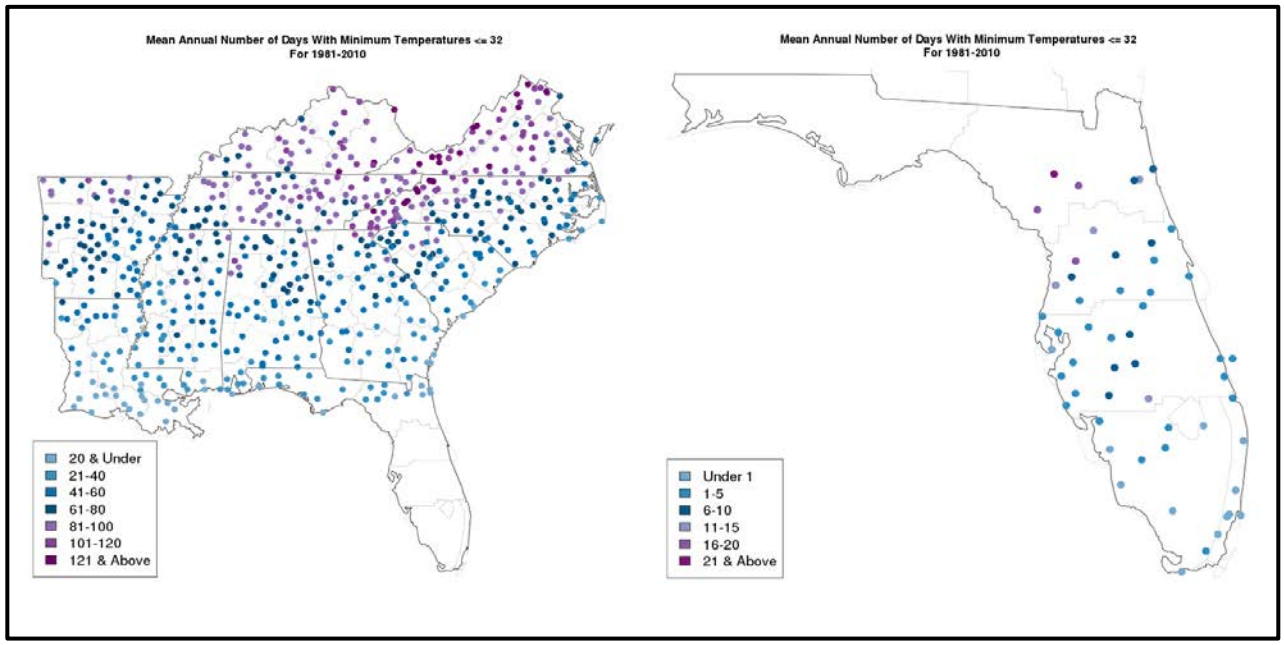

Figure 8. Mean annual number of days with a minimum temperature ≤32°F for the Southeast region (left) and Florida (right, with a different scale). The number of freezing days exhibits a smooth north-south gradient with a very large range from greater than 100 days in the far north to less than 1 day in southern Florida.

Outbreaks of extreme cold can have devastating effects on agriculture, particularly in the southern tier of the region. For example, a severe cold outbreak lasting over a week in January 2010 resulted in more than $200 million in losses to the Florida citrus crop industry. Periods of extreme cold can also lead to cold water anomalies that result in coral mortality. The cold outbreak of January 2010 resulted in the death of nearly 12 percent of corals along the Florida Reef Tract in the lower Keys, marking the worst coral mortality on record for the region (Lirman et al. 2011). Outbreaks of extreme cold (e.g., deep freezes) in the Southeast are generally associated with a strong anticyclone moving southward from the Great Plains (Rogers and Rohli 1991). The most severe freezes occur when the anticyclone tracks into the Gulf coast region, transporting cold polar air and promoting strong radiational cooling at night.

2.3.4. Winter Storms

Winter storms, including snowstorms and ice storms, occur most frequently across the northern tier of the Southeast region. These storms have significant impacts on society, including property damage, disruption to utilities and transportation, power outages, school and business closings, injury, and loss of life. Snowstorms exceeding 6 inches occur one to two times per year on average across Tennessee, Kentucky, and northern Virginia, and two to three times per year on average across the Southern Appalachians (Changnon et al. 2006). In contrast, snowstorms exceeding 6 inches occur only once every 100 years on average across the Gulf coast region (Changnon et al. 2006).

Ice storms occur when a shallow dome of sub-freezing air near the ground causes rain to freeze on surfaces. The resulting glaze of ice can bring down tree limbs and power lines and cause widespread power outages. These events are most common across west-central portions of Virginia and North Carolina, which experience three to four days with freezing rain per year on average, and least common along the Gulf Coast (i.e. one day with freezing rain every 10 years on average) (Changnon and Karl 2003).

Damaging ice storms can also occur across the Mid-South from Arkansas to South Carolina. In February 1994, a major ice storm struck much of the southern tier of the U.S., resulting in over $3 billion in damage and power outages exceeding one month in parts of Mississippi. A major ice storm in December 2002 produced over one inch of ice accretion across parts of the Carolinas. Though monetary losses from this event were lower than the 1994 storm, over 1.8 million customers lost power, eclipsing the previous record for power outages in the region from a single storm set by Hurricane Hugo in 1989 (Jones et al. 2004).

2.3.5. Severe Thunderstorms and Tornadoes

Thunderstorms are a frequent occurrence across the region during the warmer months of the year. Severe thunderstorms, which are defined by the occurrence of winds in excess of 58 mph, hail at least 1 inch in diameter, or a tornado, occur most frequently in the late winter and spring months. Damaging winds and large hail occur most frequently across Alabama, Mississippi, Arkansas, western Tennessee, and northern Louisiana. This region also sees the highest number of strong tornadoes (F2 and greater) and experiences more killer tornadoes than the notorious “Tornado Alley” of the Great Plains (Ashley 2007) (Fig. 9).

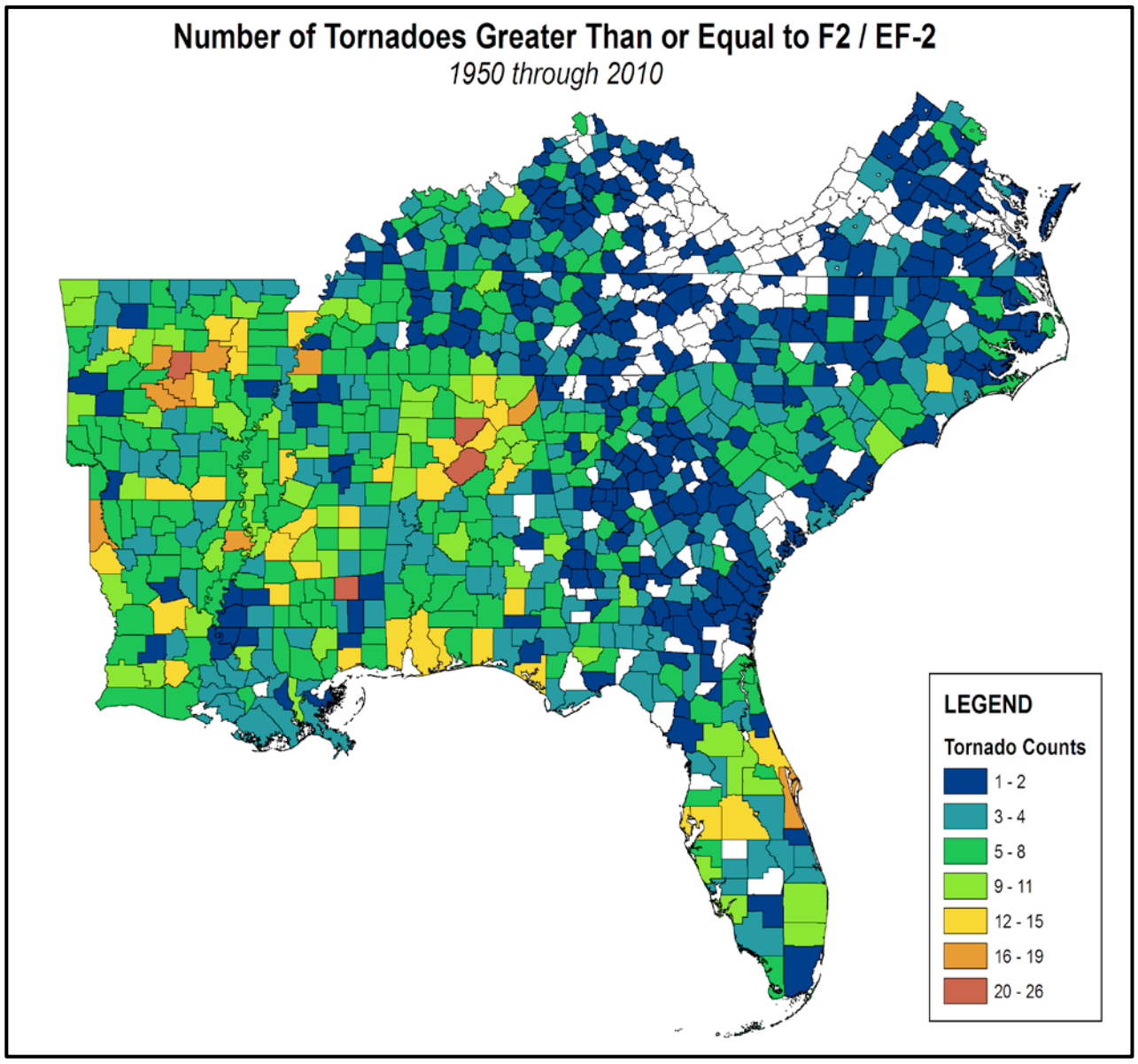

Figure 9. Number of tornadoes of F2/EF-2 intensity and greater by county from 1950 to 2010 for the Southeast region. Variations from one county to the next are affected by track length and county size. Higher numbers are seen in the west. Data from NOAA National Weather Service Storm Prediction Center [http://www.spc.noaa.gov/wcm/#data].

The high death tolls can be attributed to increased mobile home density, longer path lengths, poor visibility, and a greater number of cool season and nocturnal tornadoes (Brooks et al. 2003; Ashley 2007; Ashley and Ashley 2008; Dixon et al. 2011). Cloud-to-ground lightning is also a significant hazard. The greatest frequencies of lightning strikes in the U.S. are found across the Gulf Coast and the Florida Peninsula. Moreover, eight of the eleven Southeast states rank in the top 20 for lightning-related fatalities from 1959 to 2006 (Ashley and Gilson 2009).

2.3.6. Tropical Cyclones

Tropical cyclones (tropical storms and hurricanes) have contributed to more billion-dollar weather disasters in the region than any other hazard since 1980 (NOAA 2011). The Atlantic hurricane seasons of 2004 and 2005 were especially active and included seven of the top 10 costliest hurricanes to affect the U.S. since 1900 (Blake et al. 2011). Tropical cyclones produce a wide variety of impacts, including damaging winds, inland flooding, tornadoes, and storm surge (see Box 2). While their impacts are the greatest along the coast, significant effects are often observed well inland. Wind gusts exceeding 75 mph occur every five to 10 years across portions of the coastal plain of the region and every 50 to 75 years across portions of the Carolina Piedmont, central Alabama, Mississippi, and northern Louisiana (Kruk et al. 2010). They also contribute significantly to the rainfall climatology of the Southeast (Knight and Davis 2007), and relieve short-term droughts by providing a replenishing supply of soil moisture and rainfall for water supplies across the region. However, the heavy rainfall periodically results in deadly inland flooding, especially when the tropical cyclone is large or interacts with a stalled-out front (Konrad and Perry 2010).

Tropical cyclones make landfall most frequently along the Outer Banks of North Carolina (i.e. once every two years), southern Florida, and southeast Louisiana (i.e. once every three years) (Keim et al. 2007). They are least frequent along concave portions of the coastline, including the western bend of Florida and the Georgia coast (Keim et al. 2007). Major hurricane landfalls (i.e. categories 3-5) are most frequent in South Florida (i.e. once every 15 years) and along the northern Gulf Coast (i.e. once every 20 years) (Keim et al. 2007).

2.4. Climatic Trends

The temperature and precipitation data sets used to examine trends were obtained from NOAA's National Climatic Data Center (NCDC). The NCDC data is based on NWS Cooperative Observer Network (COOP) observations, as descibed in Section 2.1. Some analyses use daily observations for selected stations from the COOP network. Other analyses use a new national gridded monthly data set at a resolution of 5 x 5 km, for the time period of 1895-2011. This gridded data set is derived from bias-corrected monthly station data and is named the "Climate Division Database version 2 beta" (CDDv2) and is scheduled for public release in January 2013 (R. Vose, NCDC, personal communication, July 27, 2012).

The COOP data were processed using 1901-1960 as the reference period to calculate anomalies. In Section 3, this period is used for comparing net warming between model simulations and observations. There were two considerations in choosing this period for this purpose. Firstly, while some gradually-increasing anthropogenic forcing was present in the early and middle part of the 20th century, there is a pronounced acceleration of the forcing after 1960 (Meehl et al. 2003). Thus, there is an expectation that the effects of that forcing on surface climate conditions should accelerate after 1960. This year was therefore chosen as the ending year of the reference period. Secondly, in order to average out the natural fluctuations in climate as much as possible, it is desirable to use the longest practical reference period. Both observational and climate model data are generally available starting around the turn of the 20th century, thus motivating the use of 1901 as the beginning year of the reference period. We use this period as the reference for historical time series appearing in this section in order to be consistent with related figures in Section 3.

Box 2: Gulf Coast Storm Surge Database

SURGEDAT provides the world's most comprehensive archive of maximum observed storm surge data. This dataset has identified the magnitude and location of peak storm surge for more than 500 tropical cyclone-generated surge events around the world since 1880. Prior to the creation of this dataset, such information was not archived in one central location.

Spatial analysis along the U.S. Gulf Coast reveals that the greatest storm surge activity, in terms of both surge magnitudes and frequencies, generally occurs along the northern and western Gulf Coast, as well as the Florida Keys. Florida's West Coast, from the Eastern Panhandle to the Everglades, has generally observed less storm surge activity (Fig. B). Although storm tracks may help determine this pattern, bathymetry, or the offshore water depth, storm size, and duration of maximum sustained winds also play important roles (Chen et al. 2008; Irish et al. 2008).

The complete dataset and map are hosted by the Southern Regional Climate Center at http://surge.srcc.lsu.edu. Points on the map are interactive, enabling users to click on a peak surge location and obtain information about that surge event. These data are supported by robust metadata files that provide documentation of all surge observations. This website also hosts a blog, which compares active and historic cyclones, incorporating historic surge observations into a discussion about surge potential in an active cyclone. Such discourse brings storm surge history to life, potentially enhancing surge forecasts, hurricane research, and public awareness.

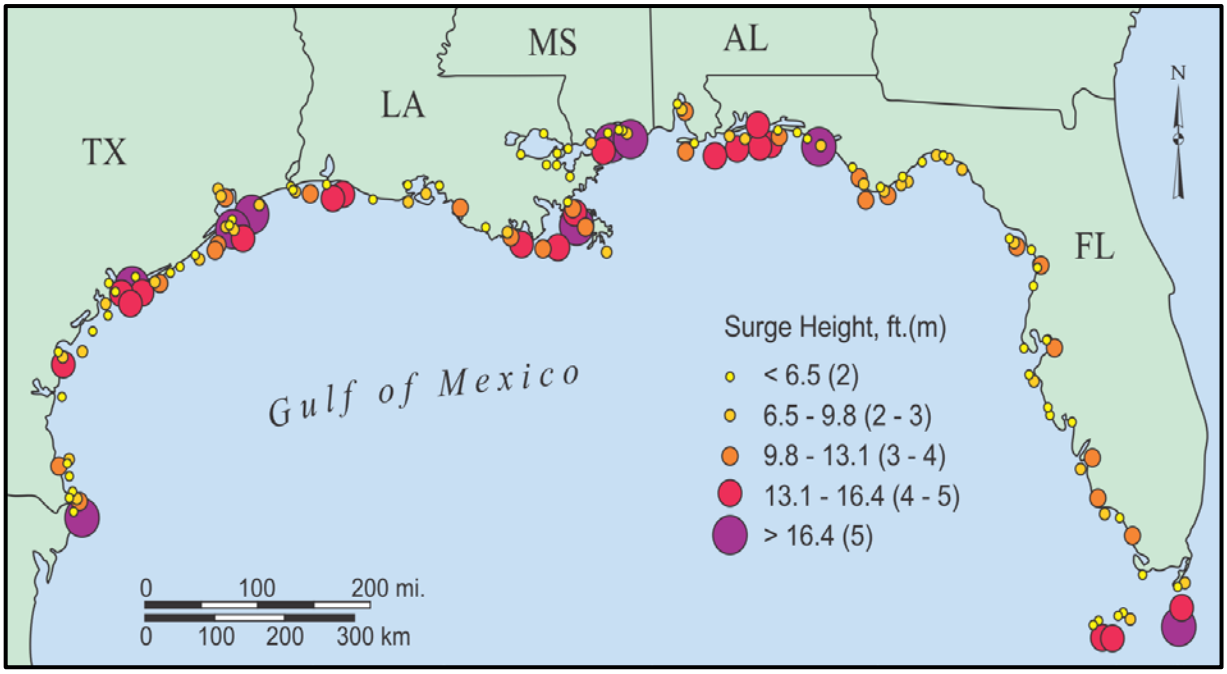

Figure B. The location and height of the 195 peak storm surges along the U.S. Gulf Coast identified in SURGEDAT (Adapted from Needham and Keim 2011).

2.4.1. Temperature

Figure 10 shows annual and seasonal time series of temperature anomalies for the period of 1895-2011. The Southeast U.S. is one of the few regions globally not to exhibit an overall warming trend in surface temperature over the 20th century (IPCC 2007a). Annual and seasonal temperatures across the region exhibited much variability over the first half of the 20th century, though most years were above the long-term average. This was followed by a cool period in the 1960s and 1970s. Since then, temperatures have steadily increased, with the most recent decade (2001 to 2010) being the warmest on record. The recent increase in temperature is most pronounced during the summer season, particularly along the Gulf and Atlantic coasts, while winter season temperatures have generally cooled over the same areas (Figs. 11 and 12).

Table 1 shows temperature trends for the period of 1895-2011, calculated using the CDDv2 data set. Values are only displayed for trends that are statistically significant at the 95% confidence level. Temperature trends are not statistically significant for any season. The nominal upward trends seen in Fig. 10 are not statistically significant.

Table 1. 1895-2011 trends in temperature anomaly (°F/decade) and precipitation anomaly (inches/decade) for the Southeast U.S., for each season as well as the year as a whole. Based on a new gridded version of COOP data from the National Climatic Data Center, the CDDv2 data set (R. Vose, personal communication, July 27, 2012). Only values statistically significant at the 95% confidence level are displayed. Statistical significance of trends was assessed using Kendall's tau coefficient. The test using tau is a non-parametric hypothesis test.

Season	Temperature (°F/decade)	Precipitation (inches/decade)
Winter	—	—
Spring	—	—
Summer	—	−0.10
Fall	—	+0.27
Annual	—	—

The observed lack of warming during the 20th century (i.e. "warming hole"; Pan et al. 2004) also includes parts of the Great Plains and Midwest regions, and several hypotheses have been put forward to explain it, including increased cloud cover and precipitation (Pan et al. 2004), increased aerosols and biogenic production from forest re-growth (Portmann et al. 2009), decreased sensible heat flux due to irrigation (Puma and Cook 2010), and multi-decadal variability in both North Atlantic SSTs (Kunkel et al. 2006) and tropical Pacific SSTs (Robinson et al. 2002). In the Caribbean, no long-term trend has been identified in temperatures from the mid-18th to the mid-20th centuries (Kilbourne et al. 2008) but significant multi-decadal variability is evident in the time series. Since then, a significant warming trend has occurred, which is consistent with the overall global trend (Campbell et al. 2011) and is positively correlated with both the AMO and ENSO (i.e. warmer Atlantic SSTs, more El Niño events) (Malmgren et al. 1998).

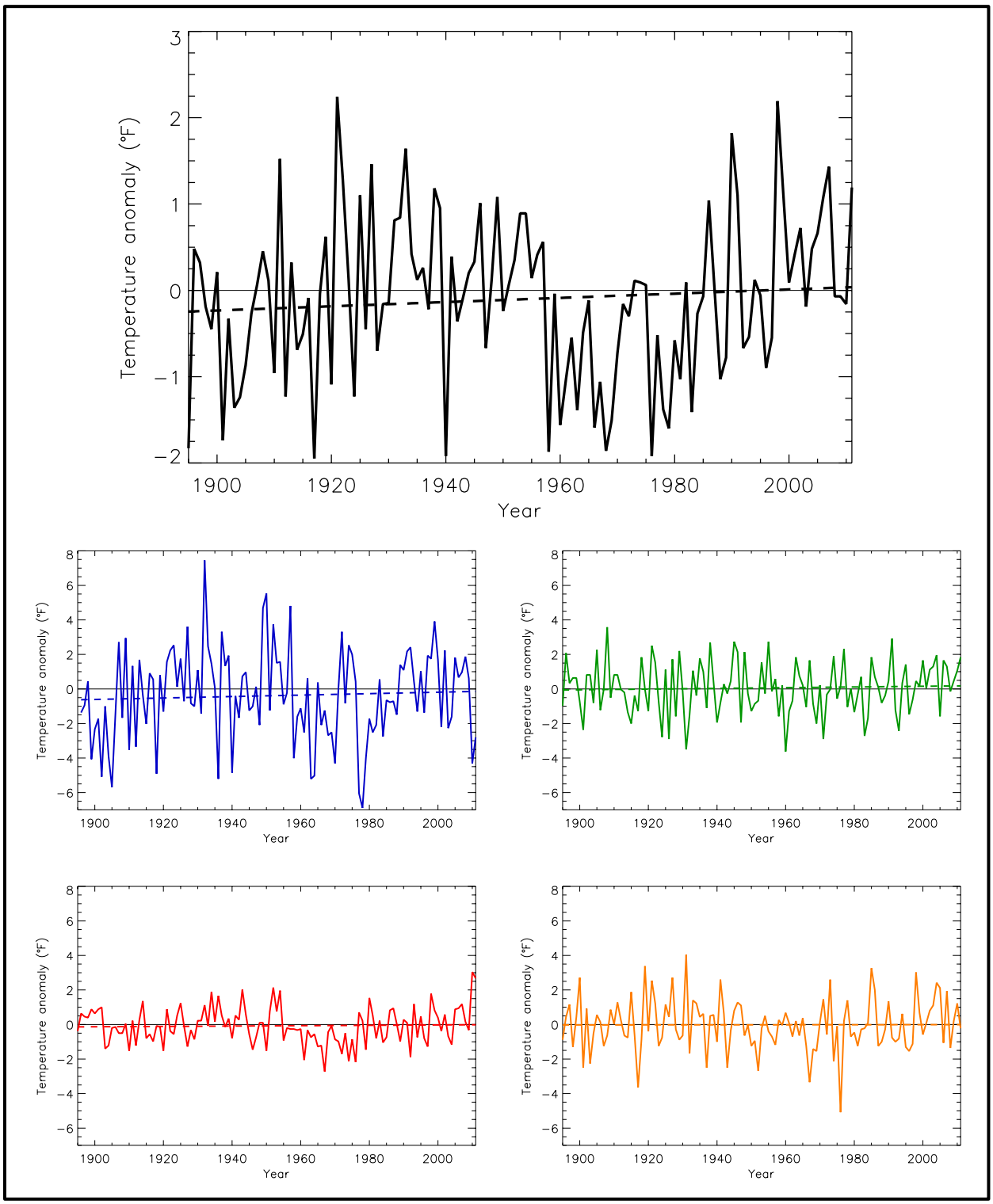

Figure 10. Temperature anomaly (deviations from the 1901-1960 average, °F) for annual (black), winter (blue), spring (green), summer (red), and fall (orange), for the Southeast U.S. Dashed lines indicate the best fit by minimizing the chi-square error statistic. Based on a new gridded version of COOP data from the National Climatic Data Center, the CDDv2 data set (R. Vose, personal communication, July 27, 2012). Note that the annual time series is on a unique scale. Trends are not statistically significant for any season.

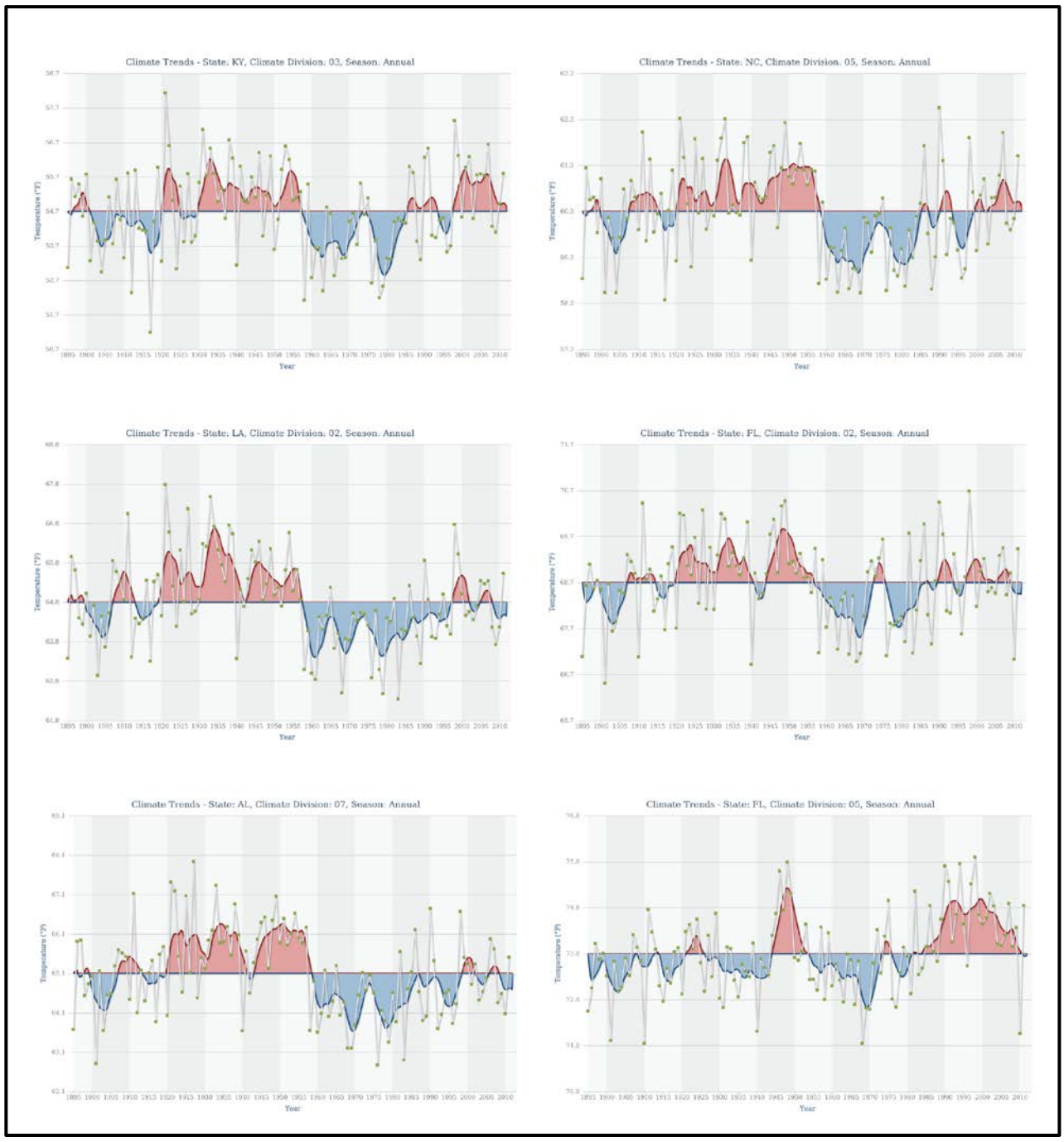

Figure 11. Annual temperature trends at six climate divisions (CDs) in the Southeast region (clockwise from top-left): Kentucky Blue Grass CD; North Carolina Southern Piedmont CD; Florida North CD; Florida Everglades and Southwest Coast CD; Alabama Coastal Plain CD; Louisiana North-Central CD. Decadal variability is the dominant characteristic.

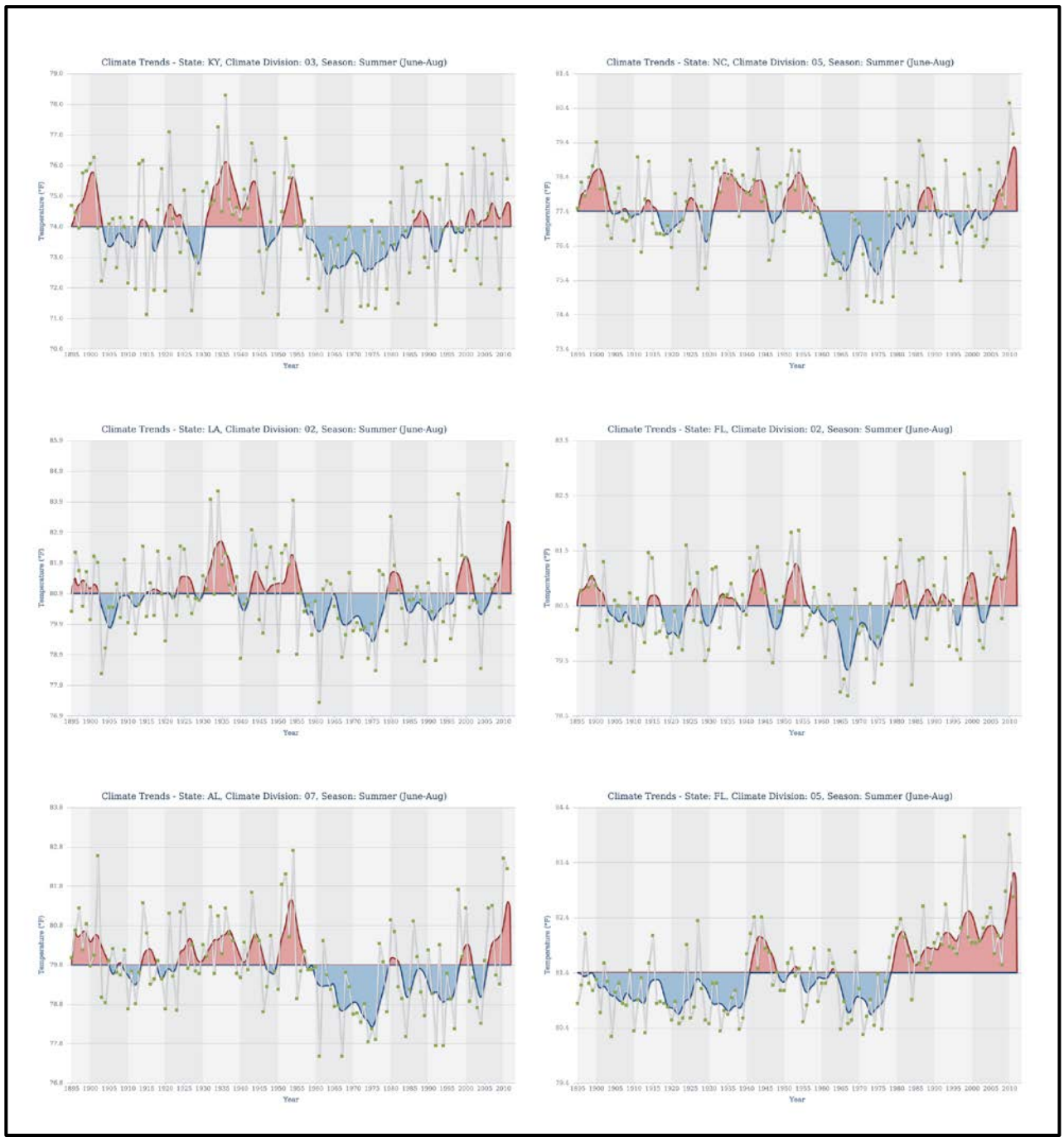

Figure 12. Same as Figure 11, but for summer temperature trends. All of these climate divisions have seen warm conditions in the 2000s.

2.4.2. Precipitation

Figure 13 shows annual and seasonal time series of precipitation anomalies for the period of 1895-2011, again calculated using the CDDv2 data set. Trends in precipitation for this time period can be seen in Table 1. While a slight upward trend is evident in the annual time series, it is not statistically significant. At selected individual stations, precipitation over the last 100 years does not exhibit trends, except along the northern Gulf Coast where precipitation has increased annually and in summer (Figs. 14, and 15). The seasonal time series (Fig. 13) exhibit statistically significant long-term trends in fall, which shows an upward trend, and summer, which shows a downward trend.

Inter-annual variability in precipitation has increased over the last several decades across much of the region with more exceptionally wet and dry summers observed as compared to the middle part of the 20th century (Groisman and Knight 2008; Wang et al. 2010). This precipitation variability is related at least partly to the mean positioning of the Bermuda High. For example, when the western ridge of the Bermuda High shifts to the southwest (northwest), precipitation tends to increase (decrease) in the Southeast region (Li et al. 2011). This broad scale relationship, however, is modulated in coastal areas by precipitation variations that relate to the strength of the sea breeze circulation. An intensification and westward expansion of the Bermuda High, for example, has been shown to correspond to a stronger sea breeze circulation and increased precipitation along the Florida Panhandle (Misra et al. 2011). Similar increases in precipitation are noted along much of the northern Gulf Coast (Keim et al. 2011). In addition, anthropogenic land cover change may also be influencing the pattern and intensity of sea breeze forced precipitation along the Florida Peninsula (Marshall et al. 2004b).

The strength and position of the Bermuda High has been tied to SST anomalies in the North Pacific (i.e. the Pacific Decadal Oscillation; Li et al. 2011) and the subtropical western North Atlantic (i.e. Atlantic warm pool; Misra et al. 2011). Summer precipitation variability in the Southeast also shows some relationship with Atlantic SST anomalies and the Atlantic Multidecadal Oscillation (AMO). In general, warmer than average SSTs in the North Atlantic lead to increased warm-season precipitation across the Southeast (Curtis 2008) as well as the Caribbean (Winter et al. 2011).

Sea-surface temperature anomalies in the equatorial Pacific (i.e. El Niño-Southern Oscillation, or ENSO) are correlated with precipitation totals across all seasons in South Florida and the Caribbean (Jury et al. 2007; Mo et al. 2009). This influence extends across much of the rest of the Southeast during the winter and spring months. Specifically, a warm anomaly in the equatorial Pacific (El Niño) is associated with wetter and cooler than normal conditions across most of the region, while a cold anomaly (La Niña) is tied to unseasonably dry and warm conditions (New et al. 2001). The influence of ENSO on precipitation diminishes during the warmer months and is restricted to southern portions of the region (e.g., Florida) where El Niño conditions typically lead to a dry weather pattern. The persistence of El Niño conditions can lead to significant impacts, as was the case during the unusually strong El Niño event of 1997-1998. For instance, numerous wildfires broke out across Florida in June 1998, which were fueled by a dense growth of vegetation caused by heavy winter rainfall (Changnon 1999).

See http://charts.srcc.lsu.edu/trends/ (LSU 2012a) for a comparative seasonal or annual climate trend analysis of a specified state from the Southeast region, using National Climate Data Center (NCDC) monthly and annual temperature and precipitation datasets.

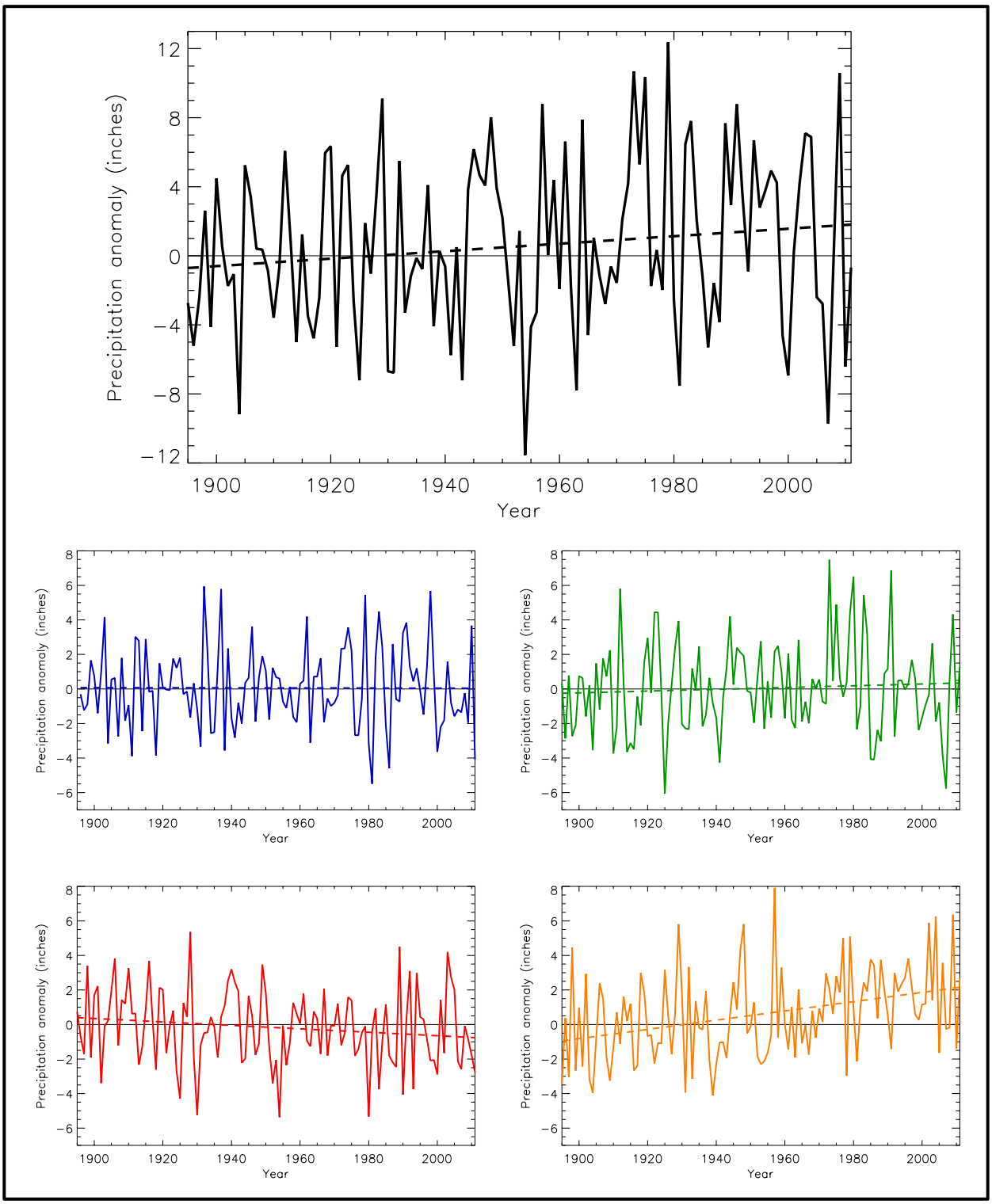

Figure 13. Precipitation anomaly (deviations from the 1901-1960 average, inches) for annual (black), winter (blue), spring (green), summer (red), and fall (orange), for the Southeast U.S. Dashed lines indicate the best fit by minimizing the chi-square error statistic. Based on a new gridded version of COOP data from the National Climatic Data Center, the CDDv2 data set (R. Vose, personal communication, July 27, 2012). Note that the annual time series is on a unique scale. Trends are statistically significant for the summer and fall seasons.

Figure 14. Annual precipitation trends at six climate divisions in the Southeast region (clockwise from top-left): Kentucky Blue Grass CD; North Carolina Southern Piedmont CD; Florida North CD; Florida Everglades and Southwest Coast CD; Alabama Coastal Plain CD; Louisiana North-Central CD. Time series are dominated by decadal scale variability.

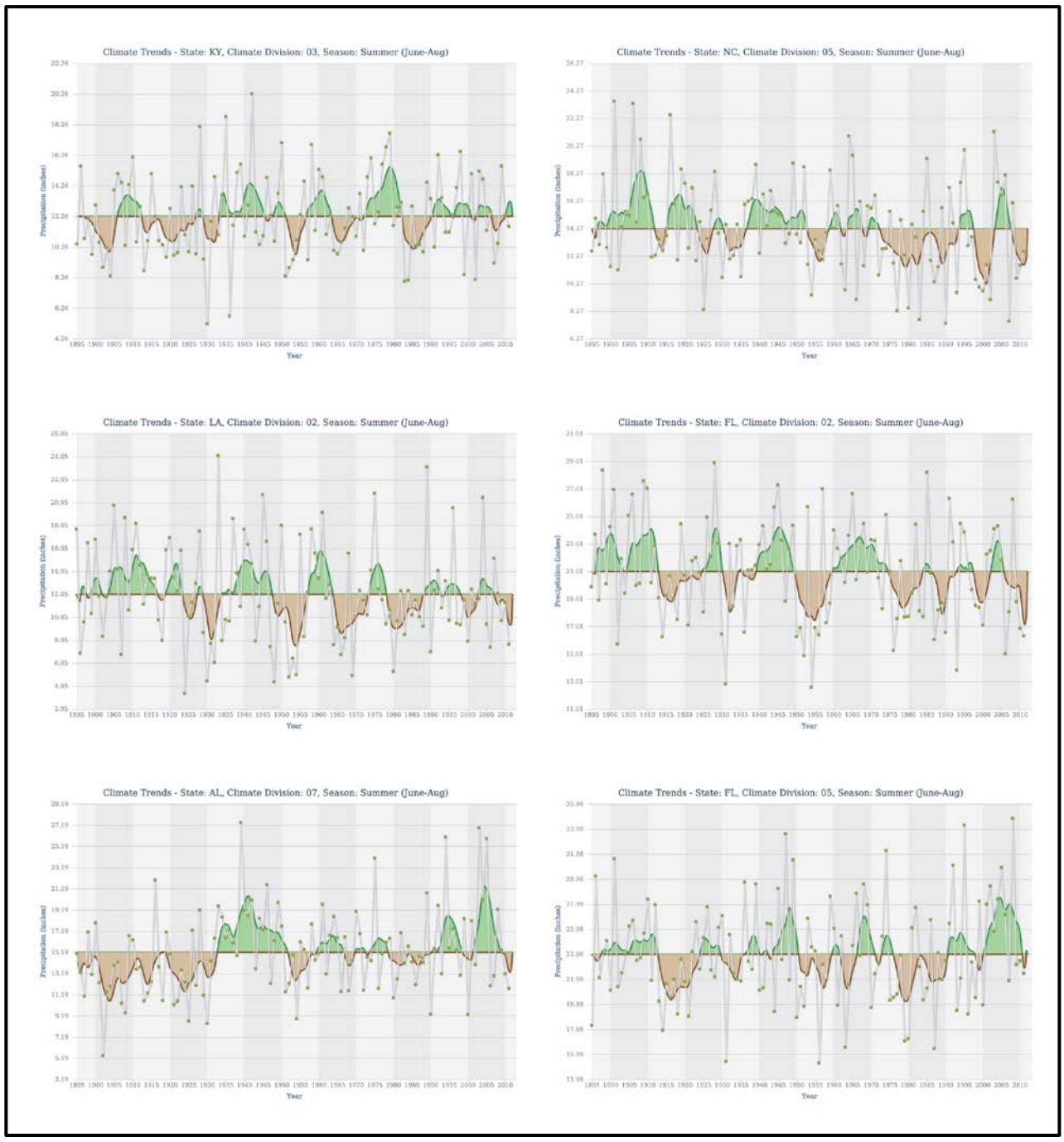

Figure 15. Same as Fig. 14, but for summer precipitation trends. These time series are dominated by decadal scale variability.

2.4.3. Extreme Heat and Cold

The frequency of maximum temperatures exceeding 95°F has been declining across much of the Southeast region since the early 20th century, particularly across the lower Mississippi River Valley (Fig. 16). Higher frequencies of extreme maximum temperatures are noted in the 1930s and 1950s and correspond to periods of exceptionally dry weather. Following a period of relatively few extreme maximum temperatures in the 1960s and 1970s, there has been an upward trend over the last three decades, particularly across the northern Gulf Coast, Florida Peninsula, and northern Virginia. The frequency of minimum temperatures exceeding 75°F has generally been increasing across most of the Southeast region. This increase is most pronounced over the past few decades (Fig. 17) and one study attributed this to urbanization (DeGaetano and Allen 2002). Long-term trends of such climate extremes, using Global Historical Climatology Network (GHCN) data from NCDC, can be seen at http://charts.srcc.lsu.edu/ghcn/ (LSU 2012b).

Large spatial variations in the temperature climatology of this region result in analogous spatial variations in the definition of "extreme temperature". We define here extremes as relative to a location's overall temperature climatology, in terms of local frequency of occurrence.

Figure 18 shows time series of an index intended to represent heat and cold wave events. This index specifically reflects the number of 4-day duration episodes with extreme hot and cold temperatures, exceeding a threshold for a 1 in 5-year recurrence interval, calculated using daily COOP data from long-term stations. Extreme events are first identified for each individual climate observing station. Then, annual values of the index are gridding the station values and averaging the grid box values.

There is a large amount of interannual variability in extreme cold periods and extreme hot periods, reflecting the fact that, when they occur, such events affect large areas and thus large numbers of stations in the region simultaneously experience an extreme event exceeding the 1 in 5-year threshold.

The highest number of heat waves (Fig. 18, top), by far, occurred in 1930, followed by 1952 and 1936. More recently, three of the top ten heat index values occurred within the last 5 years, however, there is no statistically significant trend.

There is no overall trend in the frequency of cold wave events (Fig. 18, bottom). However, the number of days with extreme cold has generally been declining across most locations in the Southeast, though there is much decadal and intra-regional variability (Figs. 19 and 20). For example, major Florida freezes tend to be clustered in time, particularly in the late 19th and early 20th century and from the late 1970s to the late 1980s (Rogers and Rohli 1991). These clusters are tied to decadal-scale periods in which the PNA (NAO) pattern was predominantly positive (negative) (Downton and Miller 1993) and ENSO neutral conditions prevailed across the equatorial Pacific (Goto-Maeda et al. 2008). Recent cold winters across the eastern U.S. have also been associated with a persistent negative phase of the NAO (Seager et al. 2010).

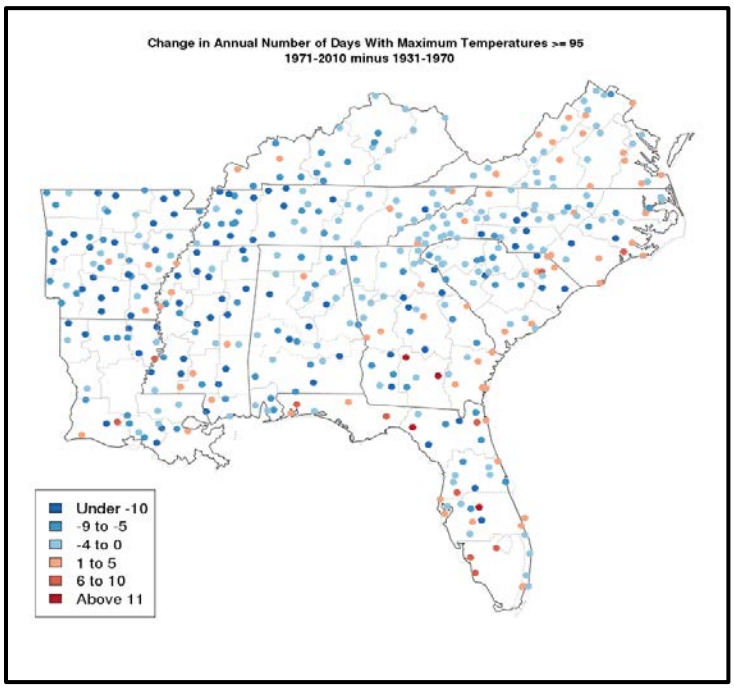

Figure 16. Difference in cumulative number of days with a maximum temperature ≥95°F between 1971-2010 and 1931-1970 for the Southeast region using data from the GHCN. Most stations have experienced little change or decreases. The overall field of differences is statistically significant at the 95% confidence level.

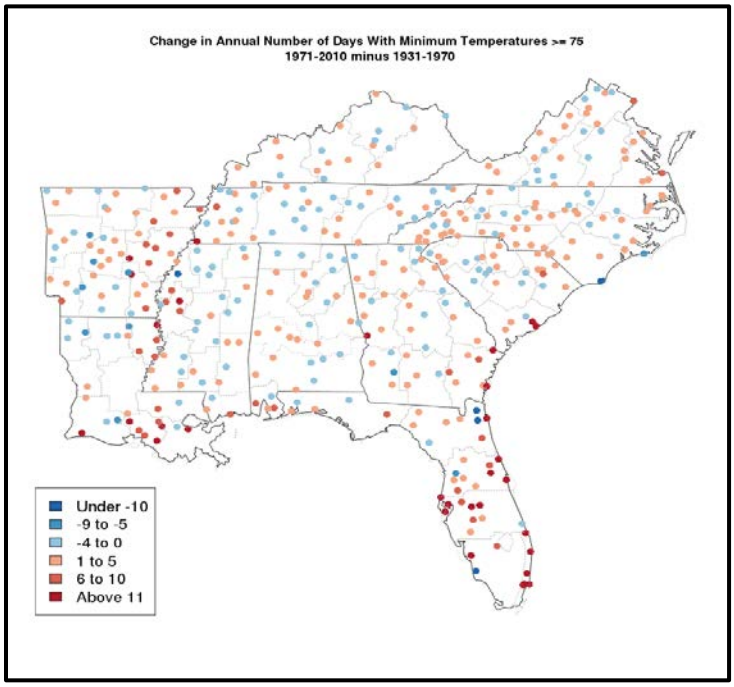

Figure 17. Same as Fig. 16, but for number of days with a minimum temperature ≥75°F for the Southeast region. Most stations have experienced little change or increases. The overall field of differences is not statistically significant at the 95% confidence level.

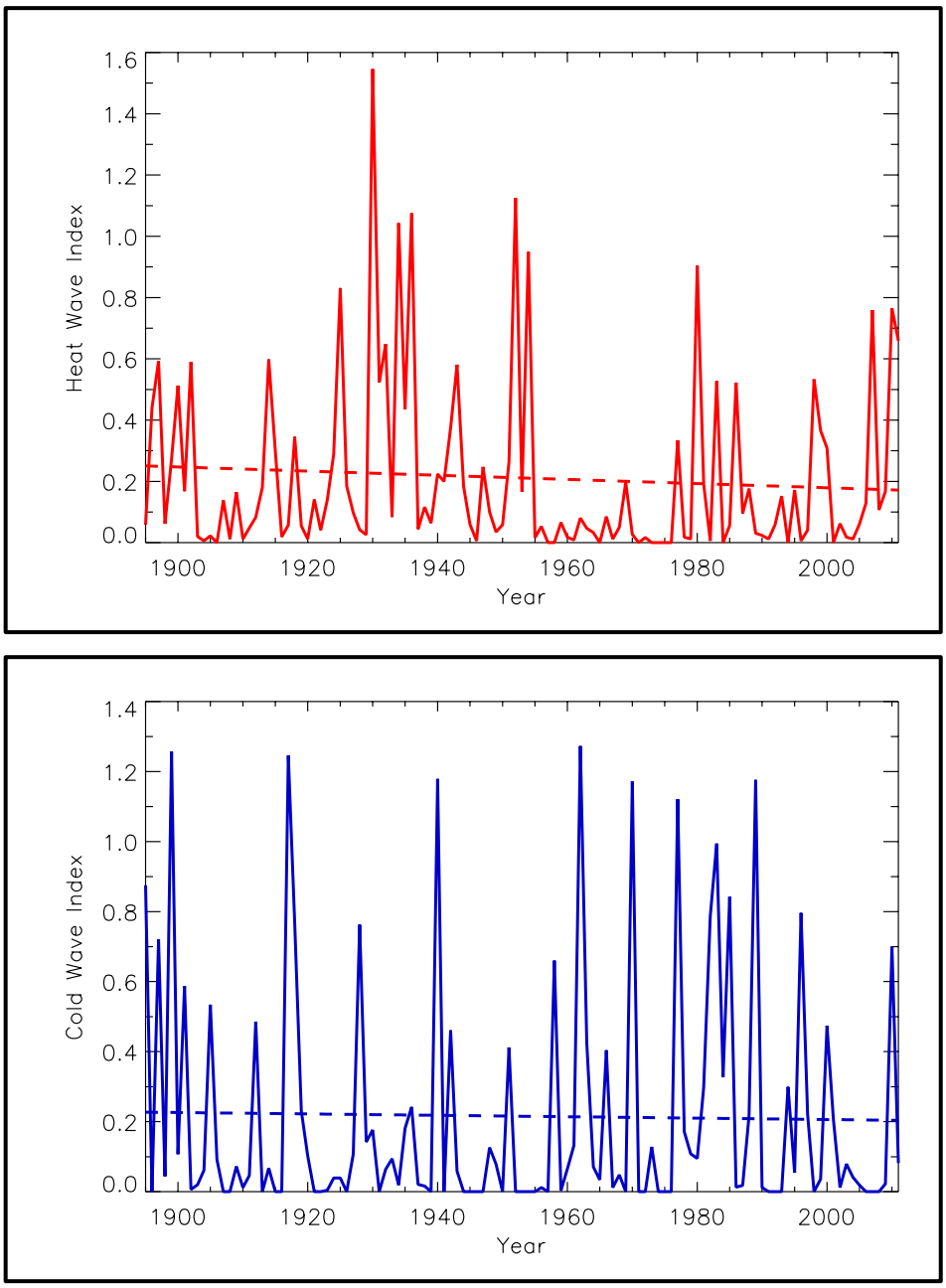

Figure 18. Time series of an index for the occurrence of heat waves (top) and cold waves (bottom), defined as 4-day periods that are hotter and colder, respectively, than the threshold for a 1 in 5-year recurrence, for the Southeast region. The dashed line is a linear fit. Based on daily COOP data from long-term stations in the National Climatic Data Center's Global Historical Climate Network data set. Only stations with less than 10% missing daily temperature data for the period 1895-2011 are used in this analysis. Events are first identified for each individual station by ranking all 4-day period mean temperature values and choosing the highest (heat waves) and lowest (cold waves) non-overlapping N/5 events, where N is the number of years of data for that particular station. Then, event numbers for each year are averaged for all stations in each 1x1° grid box. Finally, a regional average is determined by averaging the values for the individual grid boxes. This regional average is the index. The most frequent intense heat waves occurred during the 1930s and 50s, however, there is no overall trend. There is also no significant overall trend in the number of intense cold wave events.

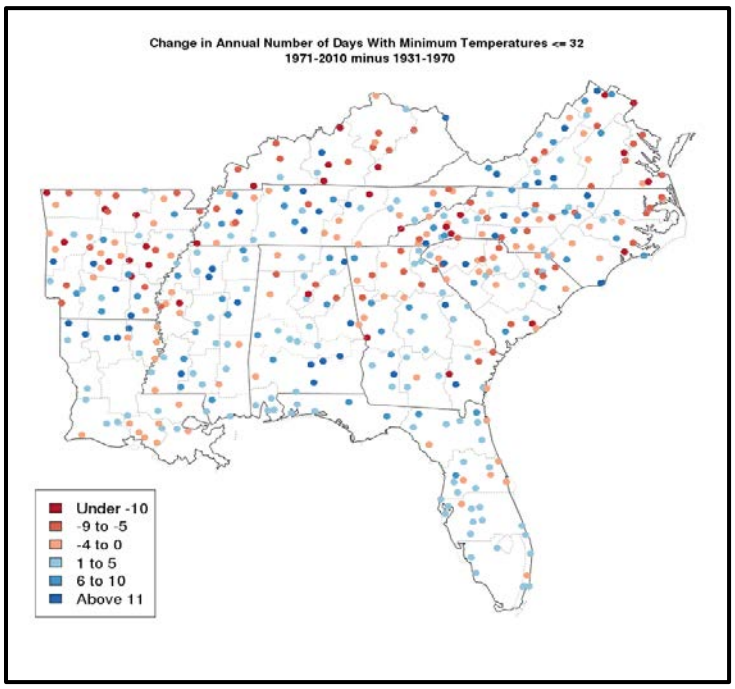

Figure 19. Same as Fig. 16, but for number of days with a minimum temperature ≤32°F for the Southeast region. Most stations have experienced small changes or decreases. Decreases are most common in the north. The overall field of differences is not statistically significant at the 95% confidence level.

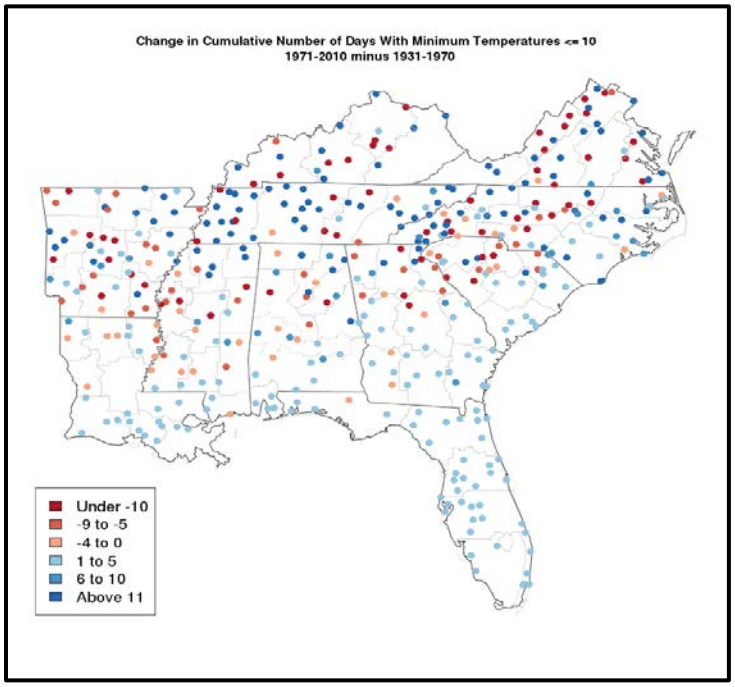

Figure 20. Same as Fig. 16, but for number of days with a minimum temperature ≤10°F for the Southeast region. Most stations have experienced decreases in the north. The overall field of differences is not statistically significant at the 95% confidence level.

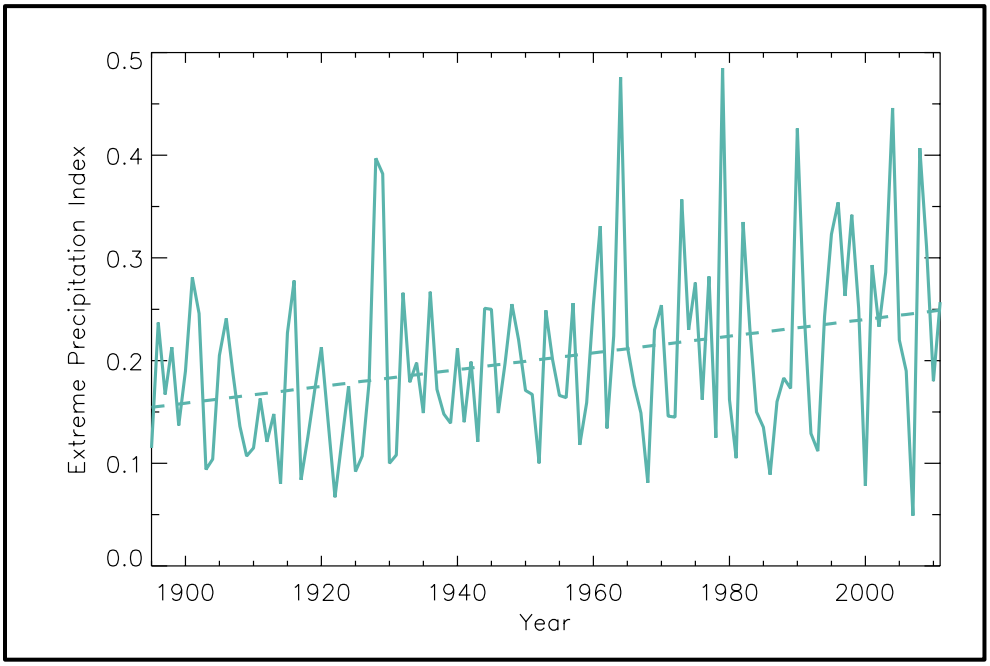

Figure 21. Time series of the extreme precipitation index for the Southeast region for the occurrence of 1-day, 1 in 5-year extreme precipitation events. The dashed line indicates the best fit by minimizing the chi-square error statistic. The dashed line is a linear fit. Based daily COOP data from long-term stations in the National Climatic Data Center's Global Historical Climate Network data set. Only stations with less than 10% missing daily precipitation data for the period 1895-2011 are used in this analysis. Events are first identified for each individual station by ranking all daily precipitation values and choosing the top N/5 events, where N is the number of years of data for that particular station. Then, event numbers for each year are averaged for all stations in each 1x1° grid box. Finally, a regional average is determined by averaging the values for the individual grid boxes. This regional average is the extreme precipitation index. There is a statistically significant upward trend.

The occurrence of several strong freezes beginning in the 19th century have gradually forced the citrus industry and other industries (e.g., winter vegetables and sugarcane), to migrate from northern Florida into South Florida. To accommodate this shift, substantial areas of wetlands were drained and converted to agricultural land, reducing the upward moisture flux from the surface and therefore increasing the risk of a freeze (Marshall et al. 2004a).

2.4.4. Extreme Precipitation and Floods

There are many different metrics that have been used in research studies to examine temporal changes in extreme precipitation. Here, we define the threshold for an extreme event based on a recurrence interval. This type of definition is commonly used for design applications, for example, in the design of runoff control structures. The analysis was performed using daily COOP data from long-term stations for a range of recurrence intervals, from one to twenty years. The results were not very sensitive to the exact choice. Results are presented for the five-year threshold, as an intermediate value. The duration of the extreme event is another choice for a metric. A range of durations was analyzed, from one to ten days, but the results were also not very sensitive to the choice. Results are presented (Fig. 21) for 1-day duration events, which is the shortest duration possible because of the daily time resolution of the COOP data.

It can be seen that the frequency of extreme precipitation events has been increasing across the Southeast region, particularly over the past two decades. Five of the top ten annual values of this extreme precipitation index have occurred since 1990. Increases in extreme precipitation events are most pronounced across the lower Mississippi River Valley and along the northern Gulf Coast (see Figs. 22 and 23). This trend in more intense precipitation events is seen in many other places around the world (IPCC 2007a) and may be tied to a warming atmosphere, which has a greater capacity to hold water vapor and therefore has the potential to produce higher rates of precipitation. Despite a long-term increase in extreme precipitation events, there is no discernible trend in the magnitude of floods along non-urbanized, unregulated streams across the region (Hirsch and Ryberg 2012). The increase in extreme precipitation, coupled with increased runoff due to the expansion of impervious surfaces and urbanization, has led to an increased risk of flooding in urban areas of the region (e.g., the record-breaking Atlanta, GA flood in 2009; Shepherd et al. 2011).

2.4.5. Freeze-Free Season

Figure 24 shows time series of freeze-free season length, calculated using daily COOP data from long-term stations. Over the entire time period of 1895-2011 there is no statistically significant trend in freeze-free season length.

2.4.6. Winter Storms

Average annual snowfall totals across the Southeast have declined at a rate of approximately 1 percent per year since the late 1930s (Kunkel et al. 2009). Additionally, snowstorms exceeding 6 inches have been declining in frequency since the start of the 20th century (Changnon et al. 2006). This trend, however, is punctuated by an increase in frequency of snowstorms in the 1960s (Changnon et al. 2006). The decline in snowfall and snowstorms corresponds to low-frequency variability in the NAO, which reveals a positive trend (i.e. warmer winters) over the latter half of the 20th century (Durkee et al. 2008). It is worth noting that this decline stands in contrast to a positive trend in snowfall and snowstorms over much of the 20th century (Changnon et al. 2006; Kunkel et al. 2009) across the northeastern U.S. and Midwest. The frequency of days with freezing rain has shown little overall change since the middle of the 20th century but more inter-decadal variability relative to snowstorms (Changnon and Karl 2003).

2.4.7. Severe Thunderstorms and Tornadoes

There has been a marked increase in the number of severe thunderstorm reports, including tornadoes, over the last 50 years; however, this increase is associated with a much-improved ability to identify and record storm damage (e.g., large increase in storm spotters). In the case of tornadoes, improving radar technology (Doppler radars) has allowed meteorologists to resolve storm circulations and thus identify where to look for storm damage (Verbout et al. 2006). The annual frequencies of stronger tornadoes (F1 and greater) have remained relatively constant nationally over the last 50 years (Brooks and Doswell 2001). The 2011 storm season was one of the most active and deadliest on record. Due to increased public awareness as well as improved weather forecasting and technology, tornado fatalities have declined dramatically since the 1930s (Ashley 2007) in spite of the fact that the population has increased in tornado-prone areas.

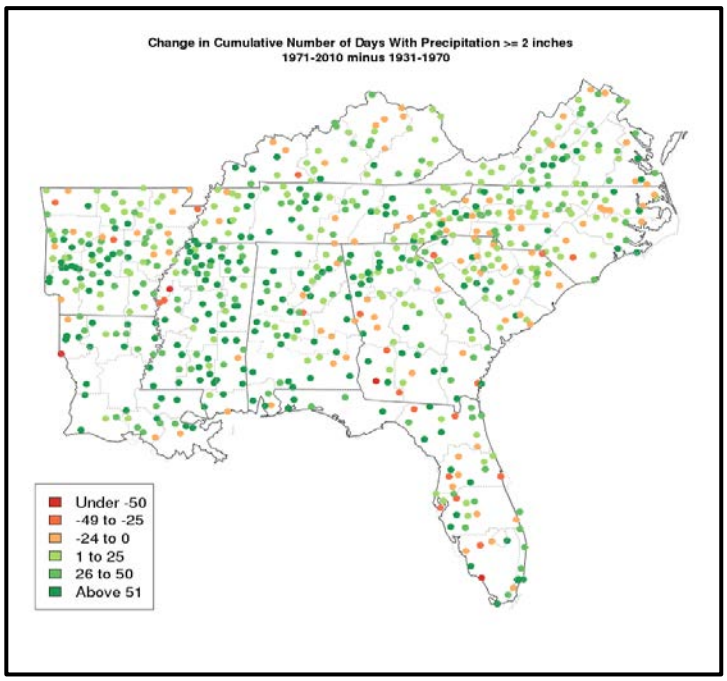

Figure 22. Difference in cumulative number of days with precipitation ≥2 inches between 1971-2010 and 1931-1970 for the Southeast region using data from the Global Historical Climatology Network (GHCN). Many stations across central portion of region show increases with southern areas showing a mix of increases and decreases. The overall field of differences is statistically significant at the 95% confidence level.

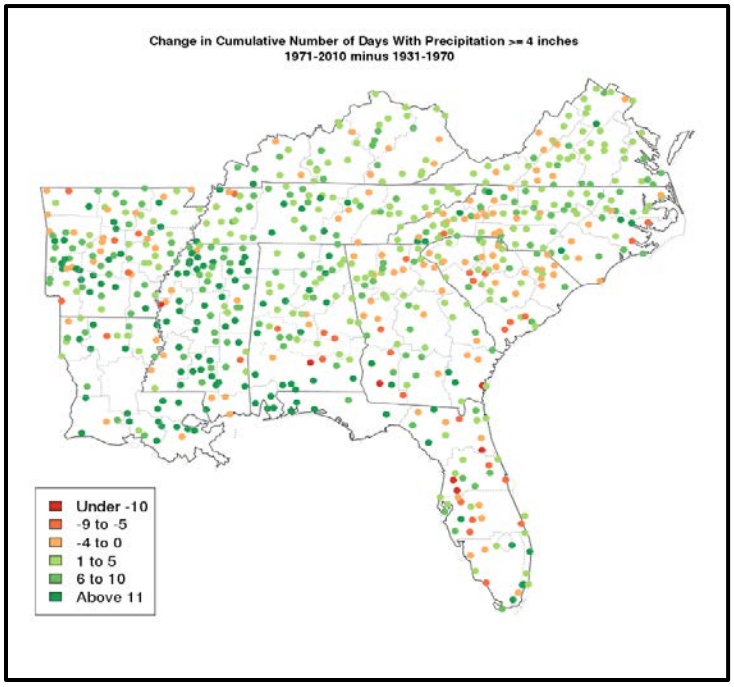

Figure 23. Same as Fig. 22 but for ≥4 inches. Many stations in the west show increases, while there is a mix of increases and decreases in the east. The overall field of differences is statistically significant at the 95% confidence level.

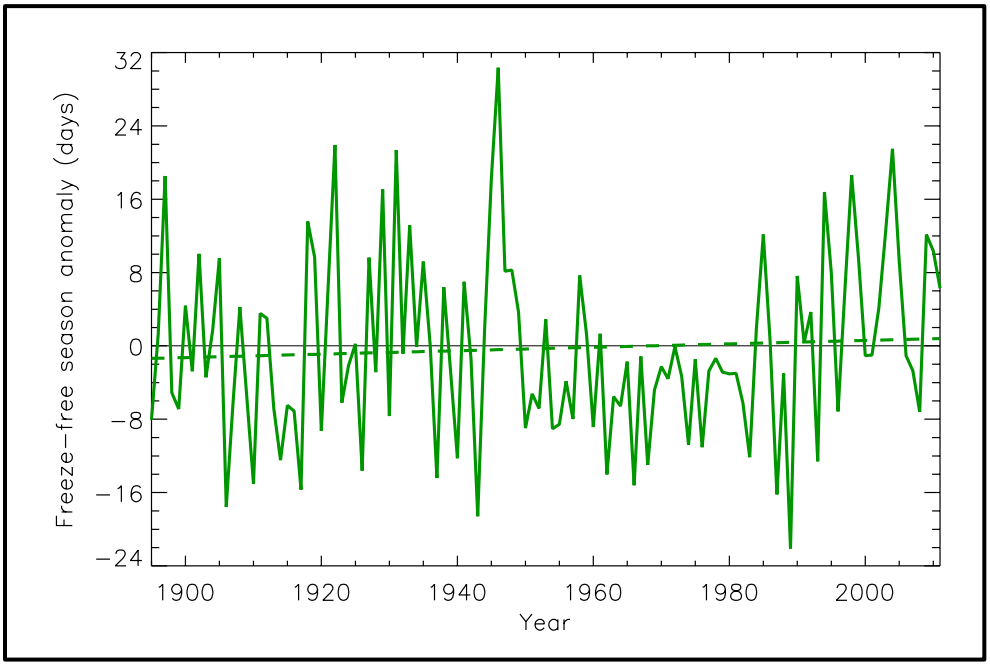

Figure 24. Freeze-free season anomalies shown as number of days per year. Length of the freeze-free season is defined as the period between the last occurrence of 32°F in the spring and first occurrence of 32°F in the fall. The dashed line is a linear fit. Based on daily COOP data from long-term stations in the National Climatic Data Center's Global Historical Climate Network data set. Only stations with less than 10% missing daily temperature data for the period 1895-2011 are used in this analysis. Freeze events are first identified for each individual station. Then, event dates for each year are averaged for 1x1° grid boxes. Finally, a regional average is determined by averaging the values for the individual grid boxes. There is no overall statistically significant trend.

2.4.8. Hurricanes

Many of the hurricanes that affect the United States make landfall in the SE. The decadal frequencies of both hurricane and major hurricane (category 3 and greater) landfalls have declined slightly over the last 100 years (Blake et al 2011); however, there is much inter-decadal variability in the record that relates to the AMO (Keim et al 2007; Klotzbach 2011) and ENSO (Klotzbach 2011). The AMO was most positive between 1930 and 1950, and 27 major hurricanes made landfall. In contrast, only 13 major hurricanes made landfall during the AMO negative phase between 1970 and 2000. During the last 10 years, there has been an increase in hurricanes as the AMO has shifted back to a positive phase. Tropical cyclone activity and landfall frequencies are typically lower during El Niño years, though this relationship is somewhat weaker during AMO positive phases (Klotzbach 2011).

Analyses of hurricanes and tropical cyclones over the entire Atlantic Basin provide differing perspectives regarding secular trends in activity. Holland and Webster (2007) and Mann and Emmanuel (2006) found increasing trends in tropical cyclone activity in the Atlantic basin extending back to 1900 and 1880, respectively. Landsea (2007), however, points out that the pre-satellite era (prior to the late 1960s) record of tropical activity is likely missing numerous storms and that the record may be worse before airplane reconnaissance began in the mid-1940s. Prior to the 1940s, storms were largely detected through landfalls and/or encounters with ships at sea. Even

when a ship route intersected a hurricane, the intensity of the storm was likely underestimated (Landsea et al. 2004). Landsea et al. (2010) also suggest that there has been a significant increase in the number of short-lived storms detected since the introduction of satellites that were likely missed in the earlier portions of the hurricane records.

When adjusted for these reporting and monitoring biases, the time series of Atlantic basin tropical cyclone frequency shows only a slight upward trend from 1878 to 2008 (Landsea et al. 2010). Examination of the accumulated cyclone energy (ACE) index, a metric that incorporates cyclone intensity (wind speed) and duration, reveals that, while global hurricane activity since 2006 has been at its lowest level since the 1970s, hurricane activity across the Atlantic basin has remained high over the past two decades (Maue 2011). Klotzbach (2011) examined the ACE index across the Atlantic basin and found an increasing trend from 1900 to 2009. Earlier work by Webster et al. (2005) and Klotzbach (2006) showed that the frequency of Category 4 and 5 hurricanes has increased across the Atlantic basin during the satellite era. These studies attribute increasing trends in ACE and major Atlantic basin hurricanes to anthropogenic global warming, multidecadal climate variability, and improved monitoring technology.

Trends in Atlantic basin tropical cyclone frequency and landfalls dating back 1500 years have been estimated using various proxy reconstructions that include the use of sediment records of storm surge over-wash (Mann et al. 2009). Results indicate a peak in tropical cyclone activity during the Medieval Period more than 1000 years ago with an overall declining trend into the mid-20th century. This result is also supported by Nyberg et al. (2007), who used coral and marine sediment cores in the Atlantic basin and found a declining trend in tropical cyclone frequencies from the mid-18th century to the early 1990s.

2.4.9. Sea Level Rise and Sea-Surface Temperature

Sea levels have slowly risen across the extensive coastline of the Southeast. Satellite altimetry records reveal spatial and temporal variations in the rates of sea level rise that relate to land motion (e.g., subsidence) as well as short-term climate variability (e.g., ENSO) (Mitchum et al. 2010). While similar variations are likely found along parts of the Southeast coast, there is currently no published data on local sea level rise for the region that varies from the global mean. Trends in global sea level dating back nearly 500,000 years have been assessed using coastal sediment cores. These records indicate variations in global sea level of as much as 100 meters that correspond with glacial and inter-glacial cycles (Church et al. 2010).

Variations in global sea level since the mid-19th century have been assessed using tidal gauge records, which indicate a rise of approximately 1.7 mm per year over most the 20th century (Church et al. 2010). However, satellite altimetry data indicate a global mean rise of between 3.0 and 3.5 mm per year since the early 1990s, or nearly double the average rate experienced over the 20th century (Prandi et al. 2009; Church et al. 2010) and near the upper bounds of sea level projections from the IPCC AR4 (Mitchum et al. 2010).

Variations in sea level rise are driven primarily by thermal expansion due to the warming of ocean waters and glacial melt (Domingues et al. 2008; Pritchard et al. 2009). Recent analysis of glacial melting on Greenland shows that the melt rate from 1996 to 2007 was above the long-term average (1973-2007), with 2007 exhibiting the highest melt rate on record by over 60 percent (Mote 2007).

Trends in SSTs over the 20th century reveal a cooling over the North Atlantic near Greenland. This cooling may be related to an infusion of melt water as well as an increase in wind speed and heat loss from the ocean surface connected with the upward trend in the NAO circulation over the latter half of the century (Deser et al. 2010). A marked warming trend in SST (1.6°C per century) is noted off of the East Coast of North America, and globally only the East coast of China exhibits a comparable trend (Deser et al. 2010).

3. FUTURE REGIONAL CLIMATE SCENARIOS

As noted above, the physical climate framework for the 2013 NCA report is based on climate model simulations of the future using the high (A2) and low (B1) SRES emissions scenarios. The resulting climate conditions are to be viewed as scenarios, not forecasts, and there are no explicit or implicit assumptions about the probability of occurrence of either scenario.

3.1. Description of Data Sources

This summary of future regional climate scenarios is based on the following model data sets:

- **Coupled Model Intercomparison Project phase 3 (CMIP3)** – Fifteen coupled Atmosphere-Ocean General Circulation Models (AOGCMs) from the World Climate Research Programme (WCRP) CMIP3 multi-model dataset (PCMDI 2012), as identified in the 2009 NCA report (Karl et al. 2009), were used (see Table 2). The spatial resolution of the great majority of these model simulations was 2-3° (a grid point spacing of approximately 100-200 miles), with a few slightly greater or smaller. All model data were re-gridded to a common resolution before processing (see below). The simulations from all of these models include:

  a) Simulations of the 20th century using best estimates of the temporal variations in external forcing factors (such as greenhouse gas concentrations, solar output, volcanic aerosol concentrations); and

  b) Simulations of the 21st century assuming changing greenhouse gas concentrations following both the A2 and B1 emissions scenarios. One of the fifteen models did not have a B1 simulation.

  These model simulations also serve as the basis for the following downscaled data set.

- **Downscaled CMIP3 (Daily_CMIP3)** – These temperature and precipitation data are at 1/8° (~8.6 miles latitude and ~6.0-7.5 miles longitude) resolution. The CMIP3 model data were initially downscaled on a monthly timescale using the bias-corrected spatial disaggregation (BCSD) method, for the period of 1961-2100. The starting point for this downscaling was an observationally-based gridded data set produced by Maurer et al. (2002). The climate model output was adjusted for biases through a comparison between this observational gridded data set and the model's simulation of the 20th century. Then, high-resolution gridded data for the future were obtained by applying change factors calculated as the difference between the model's present and future simulations (the so-called "delta" method).

  Daily statistically-downscaled data were then created by randomly sampling historical months and adjusting the values using the "delta" method (Hayhoe et al. 2004; 2008). Eight models with complete data for 1961-2100 were available and used in the Daily_CMIP3 analyses (Table 2).

- **North American Regional Climate Change Assessment Program (NARCCAP)** – This multi-institutional program is producing regional climate model (RCM) simulations in a coordinated experimental approach (NARCCAP 2012). At the time that this data analysis was initiated, simulations were available for 9 different combinations of an RCM driven by a general circulation model (GCM); during the development of these documents, two additional simulations became available and were incorporated into selected products. These 11 combinations involved four different GCMs and six different RCMs (see Table 3). The mean temperature and precipitation maps include all 11 combinations. For calculations and graphics

involving the distribution of NARCCAP models, analyses of only the original 9 model combinations were used. For graphics of the number of days exceeding thresholds and the number of degree days, the values were obtained from the Northeast Regional Climate Center, where only 8 of the model combinations were analyzed.

Each GCM-RCM combination performed simulations for the periods of 1971-2000, 1979-2004 and 2041-2070 for the high (A2) emissions scenario only. These simulations are at a resolution of approximately 50 km (~30 miles), covering much of North America and adjacent ocean areas. The simulations for 1971-2000 and 2041-2070 are "driven" (time-dependent conditions on the lateral boundaries of the domain of the RCM are provided) by global climate model simulations. The 1979-2004 simulations are driven by the NCEP/DOE Reanalysis II data set, which is an estimate of the actual time-dependent state of the atmosphere using a model that incorporates observations; thus the resulting simulations are the RCM's representation of historical observations. From this 1979-2004 simulation, the interval of 1980-2000 was selected for analysis.

Table 2. Listing of the 15 models used for the CMIP3 simulations (left column). The 8 models used in the daily statistically-downscaled (Daily_CMIP3) analyses are indicated (right column).

CMIP3 Models	**Daily_CMIP3**
CCSM3	X
CGCM3.1 (T47)	X
CNRM-CM3	
CSIRO-Mk3.0	
ECHAM5/MPI-OM	X
ECHO-G	X
GFDL-CM2.0	
GFDL-CM2.1	
INM-CM3.0	
IPSL-CM4	X
MIROC3.2 (medres)	X
MRI-CGCM2.3.2	X
PCM	X
UKMO-HadCM3	
UKMO-HadGEM1[2]	

[2] Simulations from this model are for the A2 scenario only.

Table 3. Combinations of the 4 GCMs and 6 RCMs that make up the 11 NARCCAP dynamically-downscaled model simulations.

		GCMs			
		CCSM3	CGCM3.1	GFDL-CM2.1	UKMO-HadCM3
RCMs	CRCM	X	X		
	ECPC			X[3]	
	HRM3			X[4]	X
	MM5I	X			X[3]
	RCM3		X	X	
	WRFG	X	X		

3.2. Analyses

Analyses are provided for the periods of 2021-2050, 2041-2070, and 2070-2099, with changes calculated with respect to an historical climate reference period (either 1971-1999, 1971-2000, or 1980-2000). These future periods will sometimes be denoted in the text by their midpoints of 2035, 2055, and 2085, respectively.

As noted above, three different intervals are used as the reference period for the historical climatology. Although a uniform reference period would be ideal, there were variations in data availability and in the needs of the author teams. For the NARCCAP maps of mean temperature and precipitation, the 1971-2000 period was used as the reference because that represents the full historical simulation period. The 1971-1999 period (rather than 1971-2000) was used as the reference for CMIP3 maps because some of the CMIP3 models' 20th century simulations ended in 1999, but we wanted to keep the same starting date of 1971 for both CMIP3 and NARCCAP mean temperature and precipitation maps. The 1980-2000 period was used as the historical reference for some of the NARCCAP maps (days over thresholds and degree days) because this is the analyzed period of the reanalysis-driven simulation, and we were requested to provide maps of the actual values of these variables for both the historical period and the future period, and not just a difference map. A U.S.-wide climatology based on actual observations was not readily available for all of these variables, and we chose to use the reanalysis-driven model simulation as an alternative. Since the reanalysis data set approximates observations, the reanalysis-driven RCM simulation will be free from biases arising from a driving GCM. To produce the future climatology map of actual values, we added the (future minus historical) differences to the 1980-2000 map values. For consistency then, the differences between future and present were calculated using the 1980-2000 subset of the 1971-2000 GCM-driven simulation.

Three different types of analyses are represented, described as follows:

[3] Data from this model combination were not used for simulations of the number of days exceeding thresholds or degree days.

[4] Data from these model combinations were not used for simulations of the number of days exceeding thresholds or degree days, or calculations and graphics involving the distribution of NARCCAP models.

- **Multi-model mean maps** – Model simulations of future climate conditions typically exhibit considerable model-to-model variability. In most cases, the future climate scenario information is presented as multi-model mean maps. To produce these, each model's data is first re-gridded to a common grid of approximately 2.8° latitude (~190 miles) by 2.8° longitude (~130-170 miles). Then, each grid point value is calculated as the mean of all available model values at that grid point. Finally, the mean grid point values are mapped. This type of analysis weights all models equally. Although an equal weighting does not incorporate known differences among models in their fidelity in reproducing various climatic conditions, a number of research studies have found that the multi-model mean with equal weighting is superior to any single model in reproducing the present-day climate (Overland et al. 2011). In most cases, the multi-model mean maps include information about the variability of the model simulations. In addition, there are several graphs that show the variability of individual model results. These should be examined to gain an awareness of the magnitude of the uncertainties in each scenario's future values.
- **Spatially-averaged products** – To produce these, all the grid point values within the Southeast region boundaries are averaged and represented as a single value. This is useful for general comparisons of different models, periods, and data sources. Because of the spatial aggregation, this product may not be suitable for many types of impacts analyses.
- **Probability density functions (pdfs)** – These are used here to illustrate the differences among models. To produce these, spatially-averaged values are calculated for each model simulation. Then, the distribution of these spatially-averaged values is displayed. This product provides an estimate of the uncertainty of future changes in a tabular form. As noted above, this information should be used as a complement to the multi-model mean maps.

3.3. Mean Temperature

Figure 26 shows the spatial distribution of multi-model mean simulated differences in average annual temperature for the three future time periods (2035, 2055, 2085) relative to the model reference period of 1971-1999, for both emissions scenarios, for the 14 (B1) or 15 (A2) CMIP3 models. The statistical significance regarding the change in temperature between each future time period and the model reference period was determined using a 2-sample *t*-test assuming unequal variances for those two samples. For each period (present and future climate), the mean and standard deviation were calculated using the 29 or 30 annual values. These were then used to calculate *t*. In order to assess the agreement between models, the following three categories were determined for each grid point, similar to that described in Tebaldi et al. (2011):

- *Category 1*: If less than 50% of the models indicate a statistically significant change then the multi-model mean is shown in color. Model results are in general agreement that simulated changes are within historical variations;
- *Category 2*: If more than 50% of the models indicate a statistically significant change, and less than 67% of the significant models agree on the sign of the change, then the grid points are masked out, indicating that the models are in disagreement about the direction of change;
- *Category 3*: If more than 50% of the models indicate a statistically significant change, and more than 67% of the significant models agree on the sign of the change, then the multi-model mean is shown in color with hatching. Model results are in agreement that simulated changes are statistically significant and in a particular direction.

It can be seen from Fig. 26 that all three periods indicate an increase in temperature with respect to the reference period; however, climatologically the Southeast has been one of the few regions not to exhibit an overall 20th century warming trend. Spatial variations are relatively small, with larger temperature changes in the northwest part of the region than the southeast, the smallest of which occur in southern Florida. This is consistent with global analyses that show relatively gradual spatial changes on a global scale (Meehl et al. 2007), a probable consequence of the generally high instantaneous spatial coherence of temperature and the smoothing effect of multi-model averaging. Increases are simulated for each future time period, and the differences between the high (A2) and low (B1) emissions scenarios are also simulated to increase over time. For 2035, values range from about 1.5 to 3.5°F for both emission scenarios. For 2055, warming in B1 ranges over 1.5-4.5°F and for A2, the range is from 3.5 to 5.5°F. Simulated temperature increases in 2085 are slightly larger than those in 2055 for the B1 emissions scenario (2.5-5.5°F), but are much larger for A2 at 4.5-8.5°F. The CMIP3 models indicate that temperature changes across the Southeast U.S., for all three future time periods and both emissions scenarios, are statistically significant. The models also agree on the sign of change, with all grid points satisfying category 3 above, i.e. the models are in agreement on temperature increases throughout the region for each future time period and scenario.

Figure 27 shows the multi-model mean simulated annual and seasonal 30-year average temperature changes between 2041-2070 and 1971-2000 for the high (A2) emissions scenario, for 11 NARCCAP regional climate model simulations. The simulated annual changes show a southeast-northwest gradient and are in the range of 3-5°F, similar to the CMIP3 simulations. The seasonal changes show more spatial variability. Winter differences range from 2.5 to 5°F, and the greatest warming occurs in the far north of the region. Springtime differences are similar with no systematic pattern to the warming. Summer shows the greatest warming, ranging from 3.5 to 6°F, with a maximum in the northwest part of the region. Increases in the fall range between 3 and 5°F, with the greatest warming occurring to the north and west. The agreement between models was again assessed using the three categories described in Fig. 26. The models agree on the sign of change, with all grid points satisfying category 3, annually, and for all seasons.

Figure 28 shows the simulated change in annual mean temperature for each future time period with respect to 1971-1999, for both emissions scenarios, averaged over the entire Southeast region for the 14 (B1) or 15 (A2) CMIP3 models. In addition, values 9 of the NARCCAP simulations and the 4 GCMs used in the NARCCAP experiment are shown for 2055 (A2 scenario only) with respect to 1971-2000. Both the multi-model mean and individual model values are shown. For the high (A2) emissions scenario, the CMIP3 models simulate average temperature increases of 2.7°F by 2035, 4.2°F by 2055, and over 7°F by 2085. The increases for the low (B1) emissions scenario are nearly as large in 2035 at 2.3°F, but by 2085 the increase of 4.0°F is over 3°F smaller than in the high A2 scenario. For 2055, the average temperature change simulated by the NARCCAP models (3.9°F) is comparable to the mean of the CMIP3 GCMs for the A2 scenario.

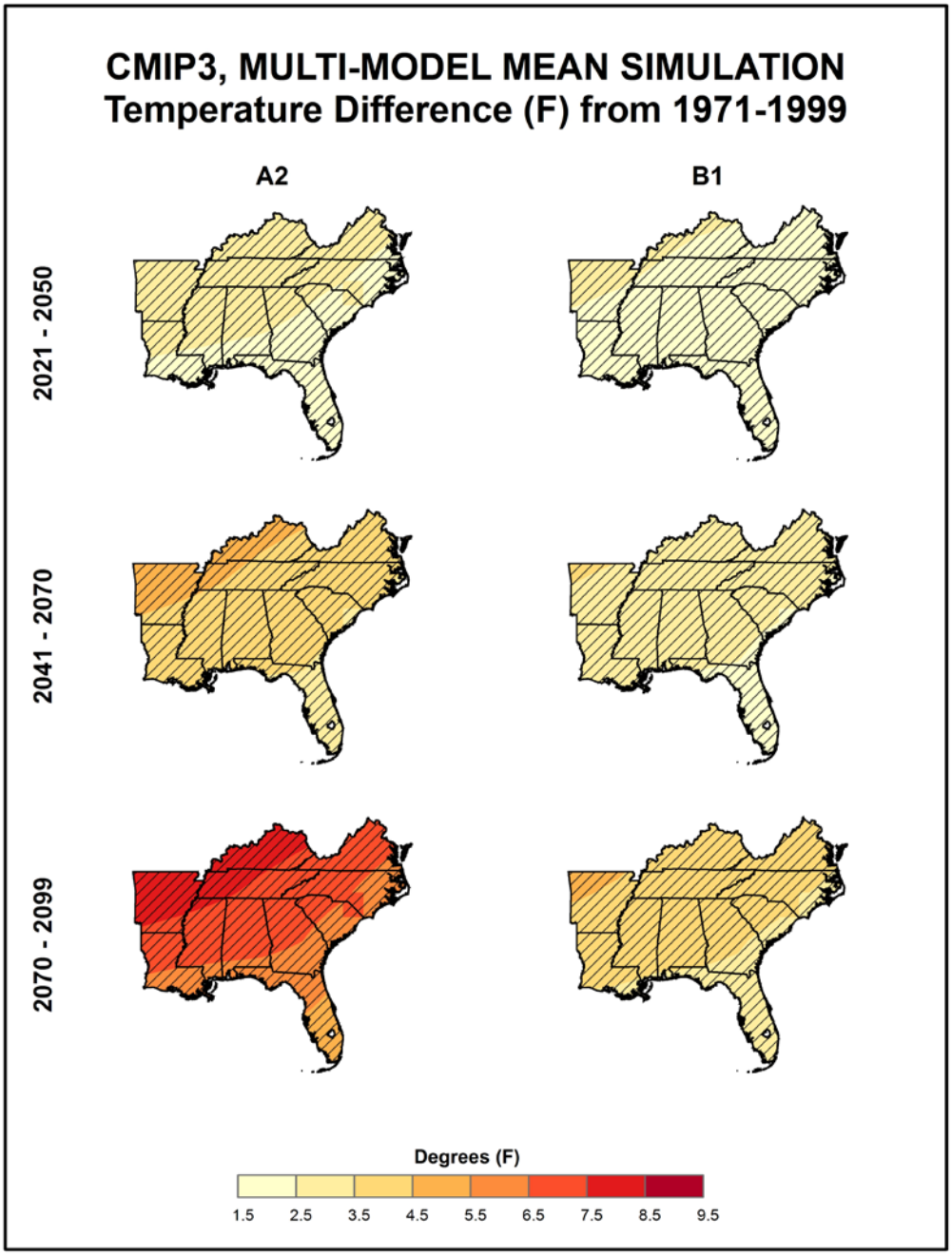

Figure 26. Simulated difference in annual mean temperature (°F) for the Southeast region, for each future time period (2021-2050, 2041-2070, and 2070-2099) with respect to the reference period of 1971-1999. These are multi-model means for the high (A2) and low (B1) emissions scenarios from the 14 (B1) or 15 (A2) CMIP3 global climate simulations. Color with hatching (category 3) indicates that more than 50% of the models show a statistically significant change in temperature, and more than 67% agree on the sign of the change (see text). Temperature changes increase throughout the 21st century, more rapidly for the high emissions scenario.

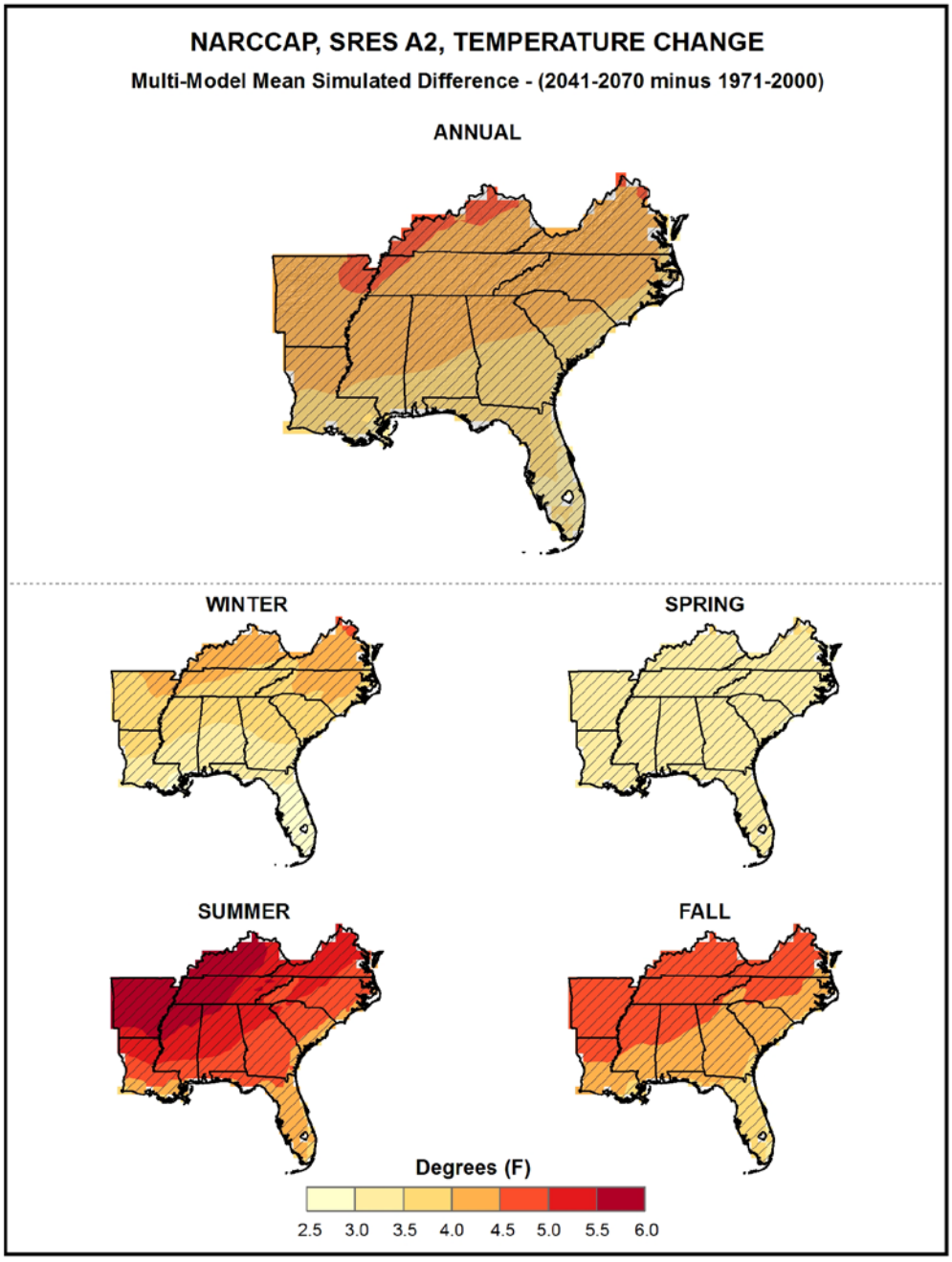

Figure 27. Simulated difference in annual and seasonal mean temperature (°F) for the Southeast region, for 2041-2070 with respect to the reference period of 1971-2000. . These are multi-model means from 11 NARCCAP regional climate simulations for the high (A2) emissions scenario. Color with hatching (category 3) indicates that more than 50% of the models show a statistically significant change in temperature, and more than 67% agree on the sign of the change (see text). Note that the color scale is different from that of Fig. 26. Temperature changes for the NARCCAP simulations are similar to those for the CMIP3 global models (Fig. 26, middle left panel). Seasonal changes are of greatest magnitude in summer, and least in spring.

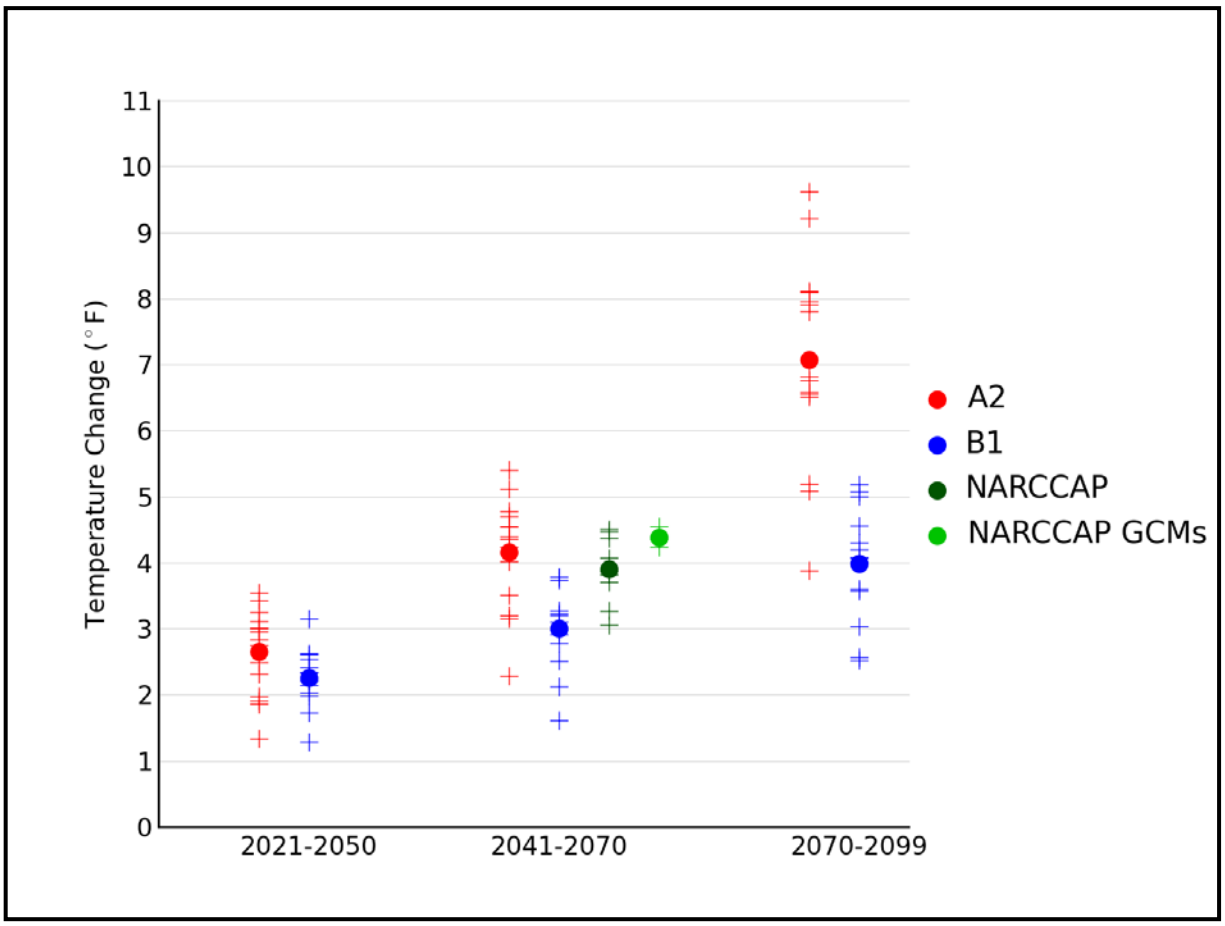

Figure 28. Simulated annual mean temperature change (°F) for the Southeast region, for each future time period (2021-2050, 2041-2070, and 2070-2099) with respect to the reference period of 1971-1999 for the CMIP3 models and 1971-2000 for the NARCCAP models. Values are given for the high (A2) and low (B1) emissions scenarios for the 14 (B1) or 15 (A2) CMIP3 models. Also shown for 2041-2070 (high emissions scenario only) are values for 9 NARCCAP models, as well as for the 4 GCMs used to drive the NARCCAP simulations. The small plus signs indicate each individual model and the circles depict the multi-model means. The range of model-simulated changes is large compared to the mean differences between A2 and B1 in the early and middle 21st century. By the end of the 21st century, the difference between A2 and B1 is comparable to the range of B1 simulations.

A key overall feature is that the simulated temperature changes are similar in value for the high and low emissions scenarios for 2035, but largely different for 2085. This indicates that early in the 21st century, the multi-model mean temperature changes are relatively insensitive to the emissions pathway, whereas late 21st century changes are quite sensitive to the emissions pathway. This arises because atmospheric CO_2 concentrations resulting from the two different emissions scenarios do not considerably diverge from one another until around 2050 (see Fig. 1). It can also be seen from Fig. 28 that the range of individual model changes is quite large, with considerable overlap between the A2 and B1 results, even for 2085. The range of temperature changes for the GCMs used to drive the NARCCAP simulations is small relative to the range for all CMIP3 models. This may be largely responsible for the relatively small range of the NARCCAP models.

Figure 29 shows the simulated change in seasonal mean temperature for each future time period with respect to 1971-1999 for the high (A2) emissions scenario, averaged over the entire Southeast region for the 15 CMIP3 models. Again, both the multi-model mean and individual model values are shown. Temperature increases are simulated to be largest in the summertime, with means of 3.1°F in 2035, 4.9°F in 2055, and 8.5°F in 2085. The least amount of warming is simulated for the winter season, with the mean temperature ranging from 2.2°F in 2035 to 5.4°F in 2085. The range of temperature changes for the individual models increases with each time period and is large relative to the differences between seasons.

The distribution of simulated changes in annual mean temperature for each future time period with respect to 1971-1999 for both emissions scenarios among the 14 (B1) or 15 (A2) CMIP3 models is shown in Table 4. Temperature changes simulated by the individual models vary from the lowest value of 1.3°F (in 2035 for the B1 scenario) to the highest value of 9.6°F (in 2085 for the A2 scenario). The interquartile range (the difference between the 75th and 25th percentiles) varies between 0.4 and 1.5°F across the three time periods. The NARCCAP simulated temperature changes have a smaller range than the comparable CMIP3 simulations, varying from 3.1°F to 4.5°F.

Table 4. Distribution of the simulated change in annual mean temperature (°F) from the 14 (B1) or 15 (A2) CMIP3 models for the Southeast region. The lowest, 25th percentile, median, 75th percentile and highest values are given for the high (A2) and low (B1) emissions scenarios, and for each future time period (2021-2050, 2041-2070, and 2070-2099) with respect to the reference period of 1971-1999. Also shown are values from the distribution of 9 NARCCAP models for 2041-2070, A2 only, with respect to 1971-2000.

Scenario	Period	Lowest	25th Percentile	Median	75th Percentile	Highest
A2	2021-2050	1.3	2.2	2.8	3.1	3.6
	2041-2070	2.3	3.8	4.4	4.6	5.4
	2070-2099	3.9	6.5	6.8	8.0	9.6
	NARCCAP (2041-2070)	*3.1*	*3.7*	*3.9*	*4.4*	*4.5*
B1	2021-2050	1.3	2.1	2.3	2.5	3.2
	2041-2070	1.6	2.8	3.1	3.3	3.8
	2070-2099	2.5	3.6	4.1	4.5	5.2

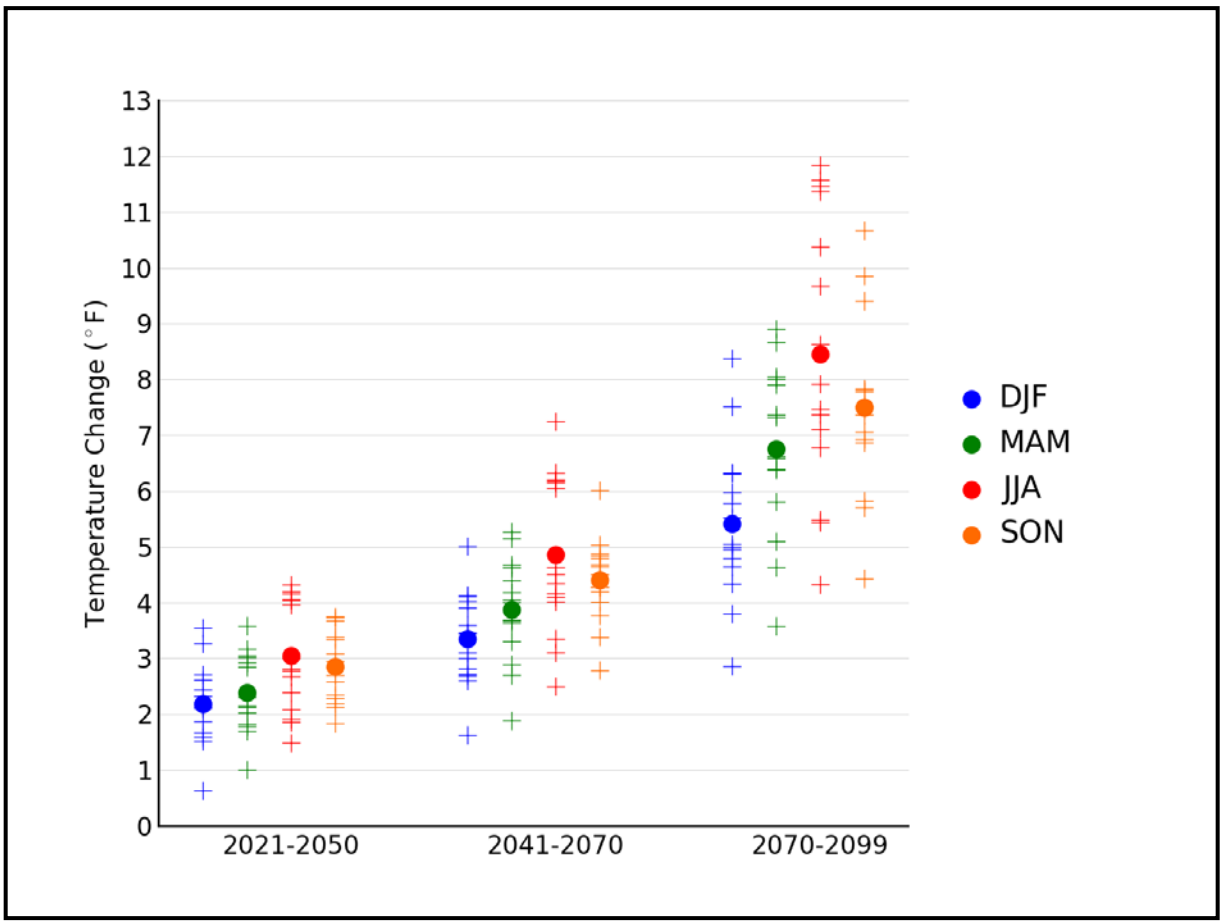

Figure 29. Simulated seasonal mean temperature change (°F) for the Southeast region, for each future time period (2021-2050, 2041-2070, and 2070-2099) with respect to the reference period of 1971-1999. Values are given for all 15 CMIP3 models for the high (A2) emissions scenario. The small plus signs indicate each individual model and the circles depict the multi-model means. Seasons are indicated as follows: winter (DJF, December-January-February), spring (MAM, March-April-May), summer (JJA, June-July-August), and fall (SON, September-October-November). The range of individual model-simulated changes is large compared to the differences among seasons and comparable to the differences between periods.

This table also illustrates the overall uncertainty arising from the combination of model differences and emission pathway. For 2035, the simulated changes range from 1.3°F to 3.6°F and are almost entirely due to differences in the individual models. By 2085, the range of simulated changes has increased to 2.5°F to 9.6°F, with roughly equal contributions to the range from model differences and emission pathway uncertainties.

3.4. Extreme Temperature

A number of metrics of extreme temperatures were calculated from the NARCCAP dynamically-downscaled and CMIP3 daily statistically-downscaled (Daily_CMIP3) data sets. Maps of a few select variables and a table summarizing all of the results follow. Each figure of NARCCAP data includes three map panels and the calculations used in each panel require some explanation. One panel (top) shows the difference between the 2055 period (2041-2070) simulation for the high (A2) emissions scenario and the 1980-2000 subset of the 1971-2000 simulation driven by the GCM. Since biases in the RCM simulations can arise from biases either in the driving global climate model or in the RCM, these two simulations include both sources of biases. It is usually assumed that such biases will be similar for historical and future periods. When taking the difference of these, the biases should at least partially cancel. As noted above, we were requested to include actual values of the variables, not just the future minus historical differences. We decided that the best model representation of the present-day values is the 1980-2000 simulation because it is driven by reanalysis data (NOAA 2012b) and thus will not include biases from a driving global climate model (although the reanalysis data used to drive the RCM is not a perfect representation of the actual state of the atmosphere). Any biases should be largely from the RCM. Thus, the lower left panel in the following figures shows the actual values from the 1980-2000 simulation. The lower right panel shows the actual values for the future period, calculated by adding the differences (the 2041-2070 simulation minus the 1980-2000 subset of the 1971-2000 simulation) to the 1980-2000 simulation. If our assumption that the differencing of present and future at least partially cancels out model biases is true, then the predominant source of biases in the future values in the lower right hand panel is from the RCM simulation of the present-day, 1980-2000. The agreement among models was once again assessed using the three categories described in Fig. 26.

The selection of threshold temperatures to calculate extremes metrics is somewhat arbitrary because impacts-relevant thresholds are highly variable due to the very diverse climate of the U.S., with the exception of the freezing temperature, which is a universal physical threshold. In terms of high temperature thresholds, the values of 90°F, 95°F, and 100°F have been utilized in various studies of heat stress, although it is obvious that these thresholds have very different implications for the impacts on northern, cooler regions compared to southern, warmer regions. The threshold of 95°F has physiological relevance for maize production because the efficiency of pollination drops above that threshold. The low temperature thresholds of 10°F and 0°F also have varying relevance on impacts related to the background climate of a region. Fortunately, our analysis results are not qualitatively sensitive to the chosen thresholds. Thus, the results for these somewhat arbitrary choices nevertheless provide general guidance into scenarios of future changes.

Figure 30 shows the spatial distribution of the multi-model mean change in the average annual number of days with a maximum temperature exceeding 95°F between 2055 and the model reference period of 1980-2000, for the high (A2) emissions scenario, for 8 NARCCAP regional climate model simulations. Over the 20th century the number of 95°F days has declined overall;

however, an upward trend has been seen since the 1970s. Model simulations indicate further increases throughout the region, with the largest increases of more than 35 days occurring in south central Florida, where the climate of 2055 is simulated to feature 40-50 days over 95°F during the year. The smallest increases of 4-10 days per year occur in the highest elevation areas along the spine of the Appalachians, where the historical period averages less than 10 days exceeding 95°F in a given year. The NARCCAP model changes in the number of 95°F days across the Southeast are statistically significant. The models are in agreement on the sign of change, with all grid points satisfying category 3, i.e. the number of days above 95°F will increase throughout the region under this scenario.

Figure 31 shows the NARCCAP multi-model mean change in the average annual number of days with a minimum temperature of less than 10°F between 2055 and the model reference period of 1980-2000, for the high (A2) emissions scenario. The largest changes occur across the northern tier of the region, with some areas decreasing by up to 14 days. There is little to no change in the number of days with minimum temperatures below 10°F in coastal and southern areas where the number of occurrences in the climatology is already extremely small or zero. The changes in days with a minimum temperature of less than 10°F are not statistically significant for most models (category 1) over the southern half of the region. For the northern half of the region, however, most models indicate statistically significant changes (category 3) under this scenario.

Figure 32 shows the NARCCAP multi-model mean change in the average annual number of days with a minimum temperature of less than 32°F between 2055 and the model reference period of 1980-2000, for the high (A2) emissions scenario. Model simulated decreases are largest (decreases of more than 20 days) in the northern part of the region. The least amount of change is simulated in Florida, where the number of freezes in the historical period is low. All grid points satisfy category 3, with the models indicating that the change in the number days below 32°F across the Southeast is statistically significant. The models also agree on the sign of change, i.e. they are in agreement that the number of days with a minimum temperature of less than 32°F will decrease throughout the region under this scenario.

Consecutive warm days can have large impacts on a geographic area and its population, and are analyzed here as one metric of heat waves. Figure 33 shows the NARCCAP multi-model mean change in the average annual maximum number of consecutive days with maximum temperatures exceeding 95°F between 2055 and the model reference period of 1980-2000, for the high (A2) emissions scenario. Historically, the western portion of the region experiences the largest number of consecutive days with maximum temperatures over 95°F, with average annual maximum runs of up to 20 days. This same area is simulated to experience the largest increase by 2055, with an increase of 16-20 days. The smallest increases once again occur along the Appalachian Mountains, with increases of up to 4 days. The NARCCAP models indicate that the changes in the number of consecutive days over 95°F across the Southeast are statistically significant. The models also agree on the sign of change, with all grid points satisfying category 3, i.e. the models are in agreement that the number of consecutive days above 95°F will increase throughout the region under this scenario.

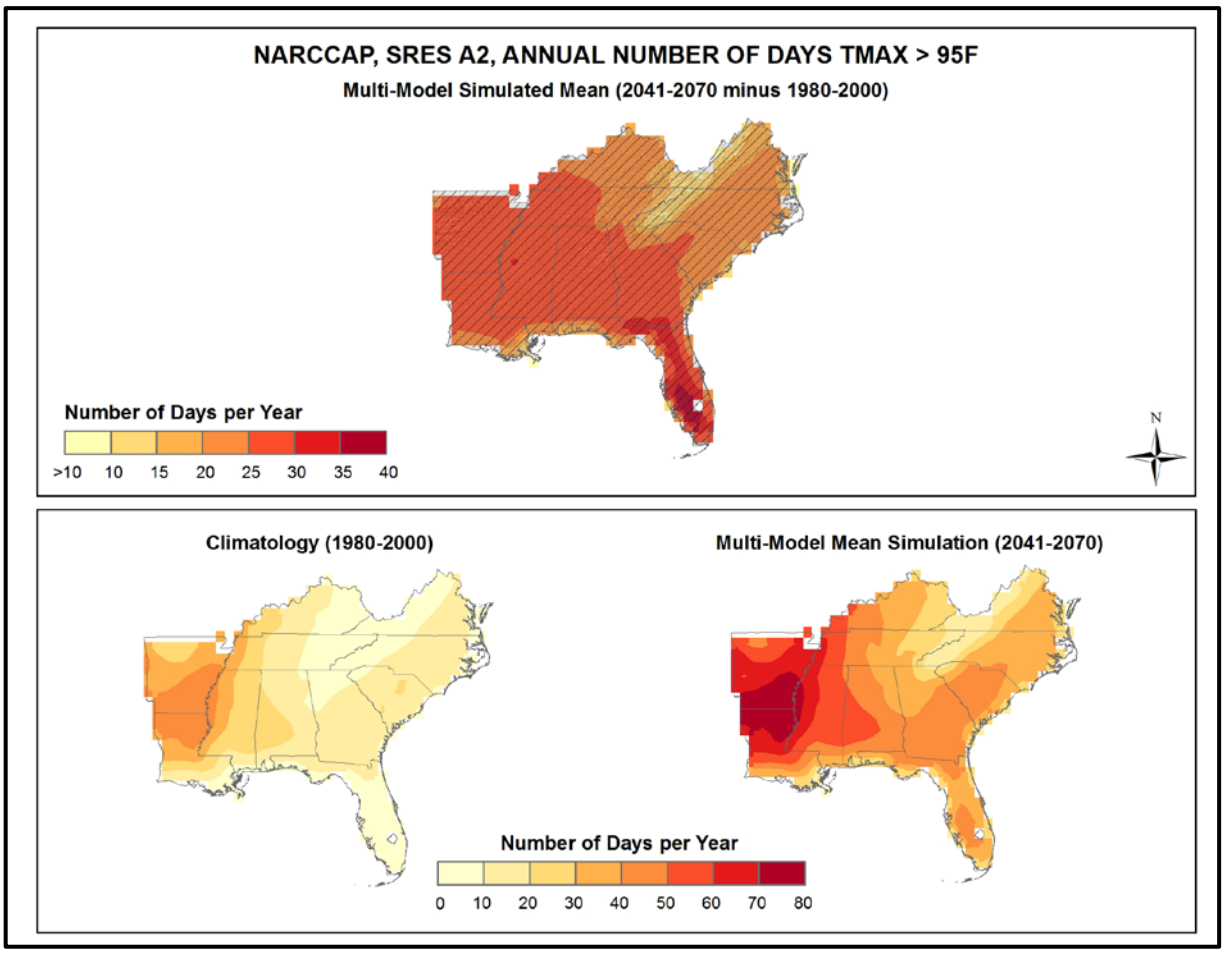

Figure 30. Simulated difference in the mean annual number of days with a maximum temperature greater than 95°F (T_{max} > 95°F) for the Southeast region, for the 2041-2070 time period with respect to the reference period of 1980-2000 (top). Color with hatching (category 3) indicates that more than 50% of the models show a statistically significant change in the number of days, and more than 67% agree on the sign of the change (see text). Mean annual number of days with T_{max} > 95°F for the 1980-2000 reference period (bottom left). Simulated mean annual number of days with T_{max} > 95°F for the 2041-2070 future time period (bottom right). These are multi-model means from 8 NARCCAP regional climate simulations for the high (A2) emissions scenario. Note that top and bottom color scales are different. The changes are upward everywhere. Increases are smallest at high elevations and largest in the south of the region.

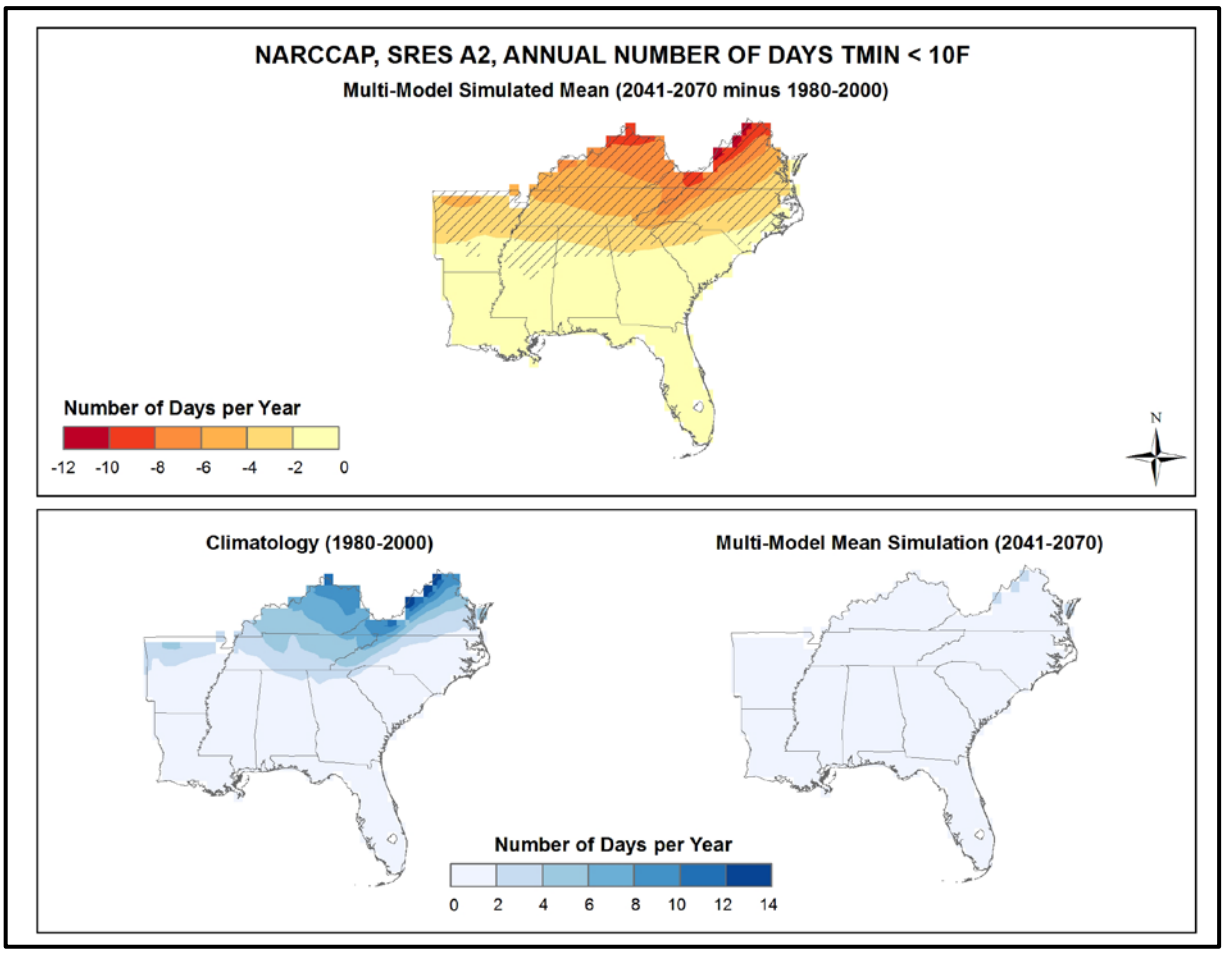

Figure 31. Simulated difference in the mean annual number of days with a minimum temperature less than 10°F (T_{min} < 10°F) for the Southeast region, for the 2041-2070 time period with respect to the reference period of 1980-2000 (top). Color only (category 1) indicates that less than 50% of the models show a statistically significant change in the number of days. Color with hatching (category 3) indicates that more than 50% of the models show a statistically significant change in the number of days, and more than 67% agree on the sign of the change (see text). Mean annual number of days with T_{min} < 10°F for the 1980-2000 reference period (bottom left). Simulated mean annual number of days with T_{min} < 10°F for the 2041-2070 future time period (bottom right). These are multi-model means from 8 NARCCAP regional climate simulations for the high (A2) emissions scenario. Decreases are largest in the north and become smaller southward, in a pattern similar to the present-day climatology.

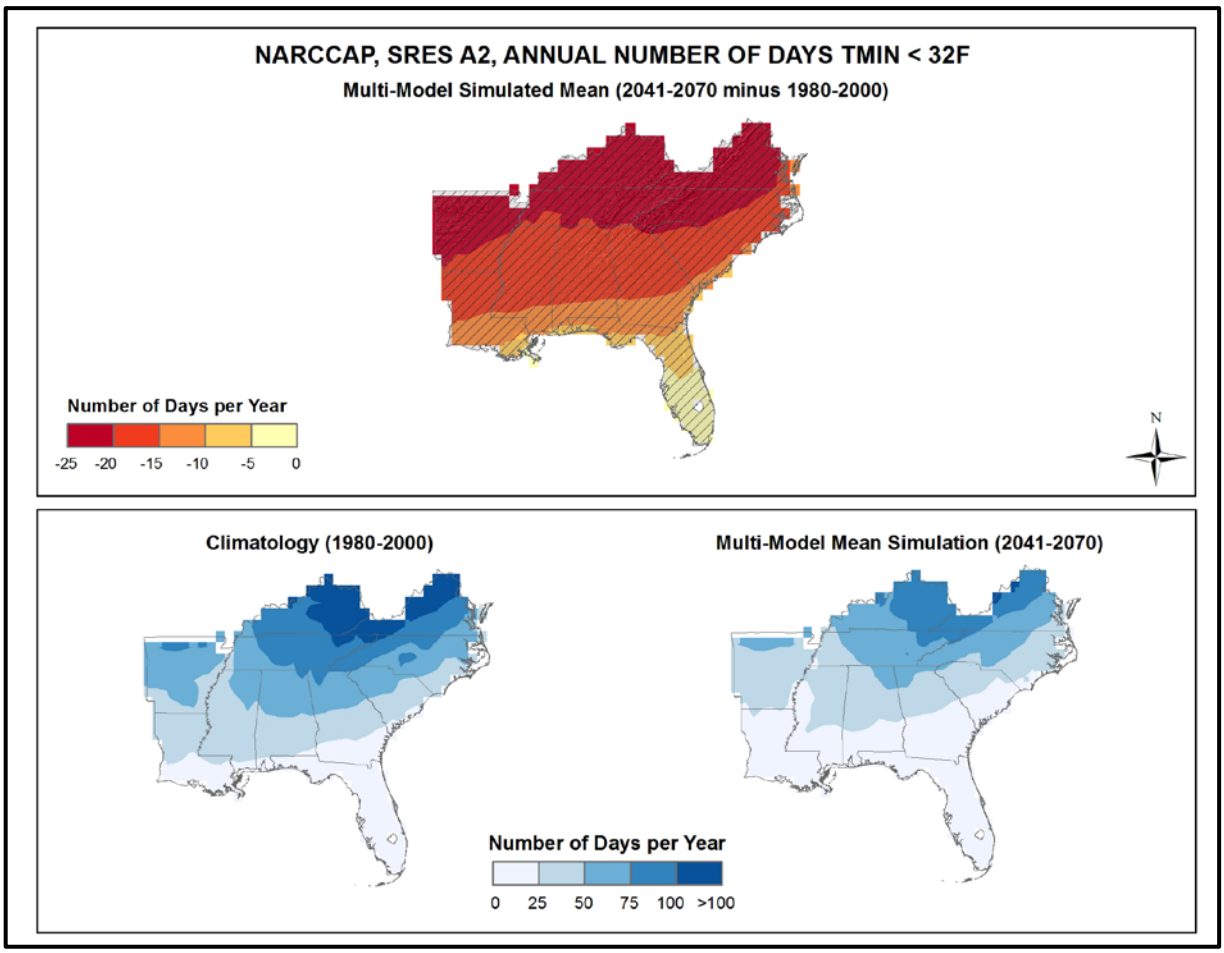

Figure 32. Simulated difference in the mean annual number of days with a minimum temperature less than 32°F (T_{min} < 32°F) for the Southeast region, for the 2041-2070 time period with respect to the reference period of 1980-2000 (top). Color with hatching (category 3) indicates that more than 50% of the models show a statistically significant change in the number of days, and more than 67% agree on the sign of the change (see text). Mean annual number of days with T_{min} < 32°F for the 1980-2000 reference period (bottom left). Simulated mean annual number of days with T_{min} < 32°F for the 2041-2070 future time period (bottom right). These are multi-model means from 8 NARCCAP regional climate simulations for the high (A2) emissions scenario. Changes are downward everywhere. Decreases are largest in the north of the region and smallest in the southeast.

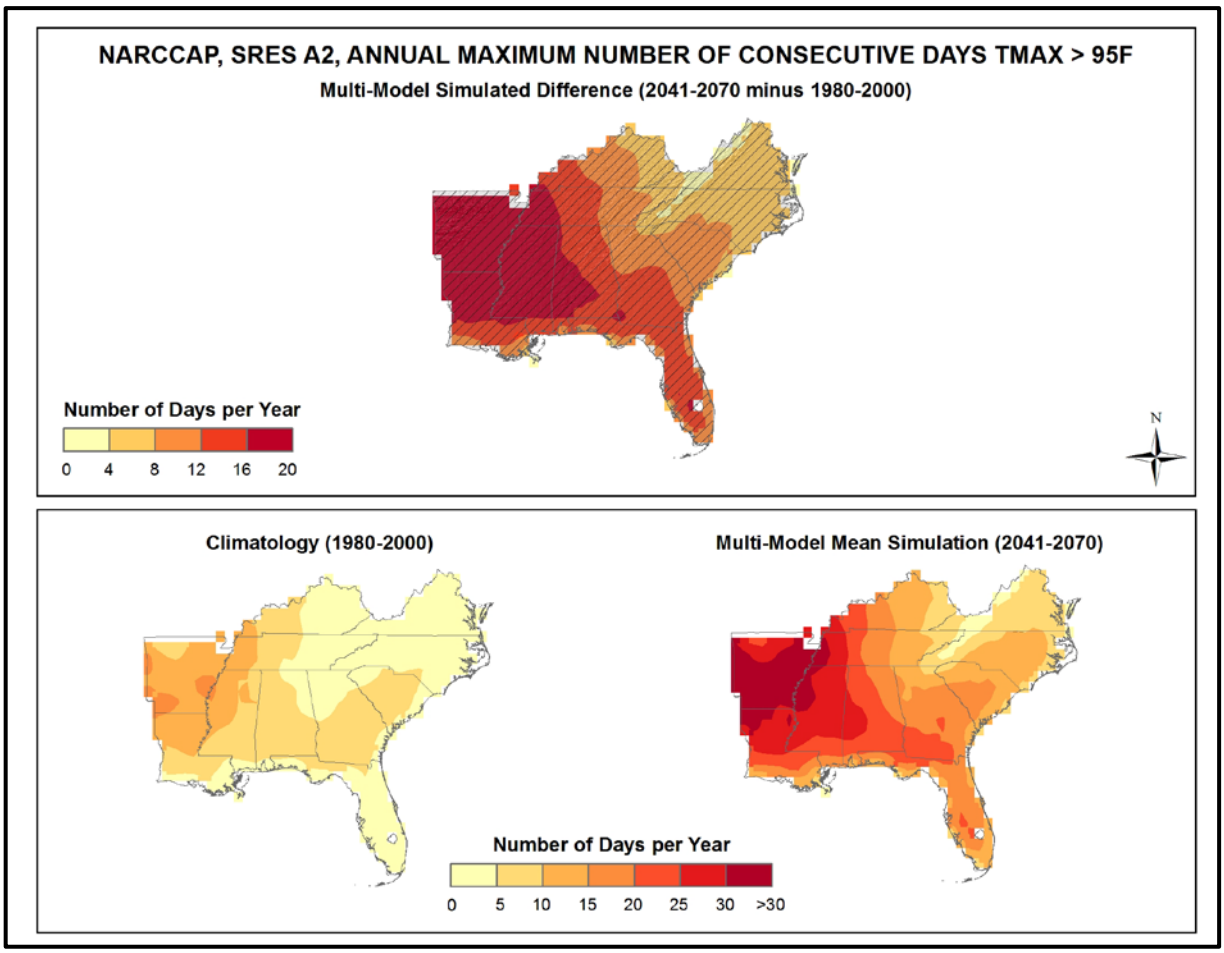

Figure 33. Simulated difference in the mean annual maximum number of consecutive days with a maximum temperature greater than 95°F (T_{max} > 95°F) for the Southeast region, for the 2041-2070 time period with respect to the reference period of 1980-2000 (top). Color with hatching (category 3) indicates that more than 50% of the models show a statistically significant change in the number of consecutive days, and more than 67% agree on the sign of the change (see text). Mean annual maximum number of consecutive days with T_{max} > 95°F for the 1980-2000 reference period (bottom left). Simulated mean annual maximum number of consecutive days with T_{max} > 95°F for the 2041-2070 future time period (bottom right). These are multi-model means from 8 NARCCAP regional climate simulations for the high (A2) emissions scenario. Note that top and bottom color scales are different. Increases are largest in the west and smallest in areas of high elevation, with a pattern similar to the present-day climatology

3.5. Other Temperature Variables

The spatial distribution of the NARCCAP multi-model mean change in the average length of the freeze-free season between 2055 and the model reference period of 1980-2000, for the high (A2) emissions scenario, is shown in Fig. 34. The freeze-free season is defined as the period of time between the last spring frost (a daily minimum temperature of less than 32°F) and the first fall frost. Increases are simulated throughout the Southeast region. The largest increases are mainly found across the northern tier of the region and Louisiana, where the length of the freeze-free season is simulated to increase by 25-30 days. The smallest simulated changes are seen in southern Florida, where increases are 0-15 days. But, freezes are not an annual occurrence in the present climate of south Florida, and these results indicate that freezes are simulated to become even less common under this scenario. All grid points satisfy category 3, with the models indicating that the changes in the length of the freeze-free season across the Southeast are statistically significant. The models also agree on the sign of change, i.e. the models are in agreement that the freeze-free season length will increase throughout the region under this scenario.

Cooling and heating degree days are accumulative metrics related to energy use, more specifically regarding the cooling and heating of buildings, with a base temperature of 65°F, assumed to be the threshold below which heating is required and above which cooling is required. Heating degree days provide a measure of the extent (in degrees), and duration (in days), that the daily mean temperature is below the base temperature. Cooling degree days measure the extent and duration that the daily mean temperature is above the base temperature.

Figure 35 shows the NARCCAP multi-model mean change in the average annual number of cooling degree days between 2055 and the model reference period of 1980-2000, for the high (A2) emissions scenario. Simulated changes are largest (greater than 950 cooling degree days) in the hottest areas of the region, mainly south Florida. Elsewhere increases of at least 450 cooling degree days (CDDs) are simulated, with the smallest increases of 450-550 CDDs across the higher terrain. For the Appalachian Mountains, a change of this magnitude is nearly a doubling of the current climate conditions. The models indicate that the changes in cooling degree days across the Southeast are statistically significant. The models also agree on the sign of change, with all grid points satisfying category 3, i.e. the models are in agreement that the number of CDDs will increase throughout the region under this scenario.

The NARCCAP multi-model mean change in the average annual number of heating degree days between 2055 and the model reference period of 1980-2000, for the high (A2) emissions scenario, is shown in Fig. 36. In general, the entire region is simulated to experience a decrease in heating degree days (HDDs). The areas that are simulated to have a larger increase in cooling degree days will have a smaller increase of heating degree days, and vice versa. The largest changes are simulated to occur in higher elevation areas, with decreases of up to 1,100 HDDs. Parts of southern Florida are simulated to see the smallest decreases, with between 0 and 300 fewer HDDs. The models once again indicate that the changes across the Southeast are statistically significant. All grid points satisfy category 3, i.e. the models are in agreement that the number of HDDs will decrease throughout the region under this scenario.

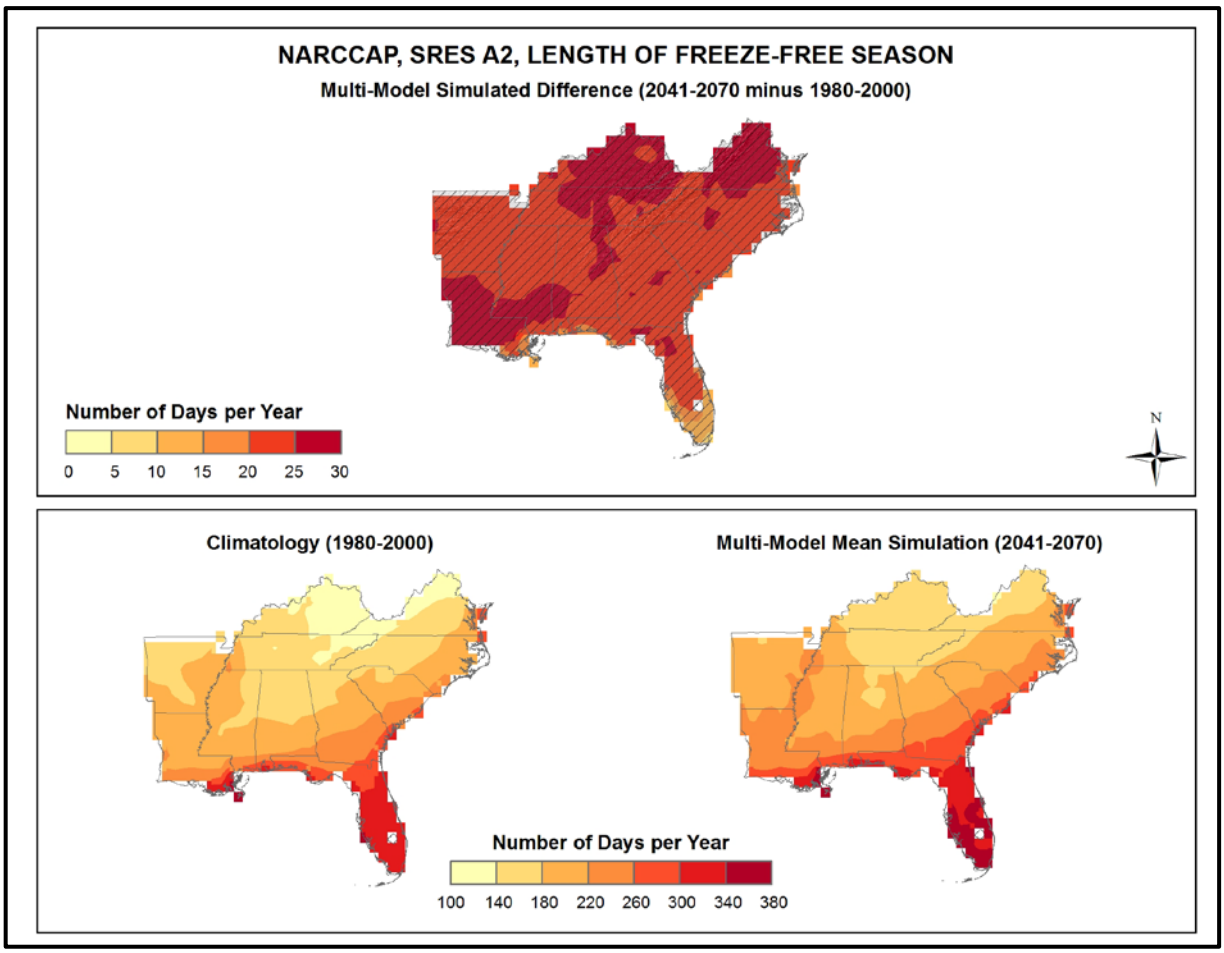

Figure 34. Simulated difference in the mean annual length of the freeze-free season for the Southeast region, for the 2041-2070 time period with respect to the reference period of 1980-2000 (top). Color with hatching (category 3) indicates that more than 50% of the models show a statistically significant change in the length of the freeze-free season, and more than 67% agree on the sign of the change (see text). Annual mean length of the freeze-free season for the 1980-2000 reference period (bottom left). Simulated mean annual length of the freeze-free season for the 2041-2070 future time period (bottom right). These are multi-model means from 8 NARCCAP regional climate simulations for the high (A2) emissions scenario. Note that top and bottom color scales are different. The length of the freeze-freeze season is simulated to increase throughout the region, with changes mostly in the 20-30 day range.

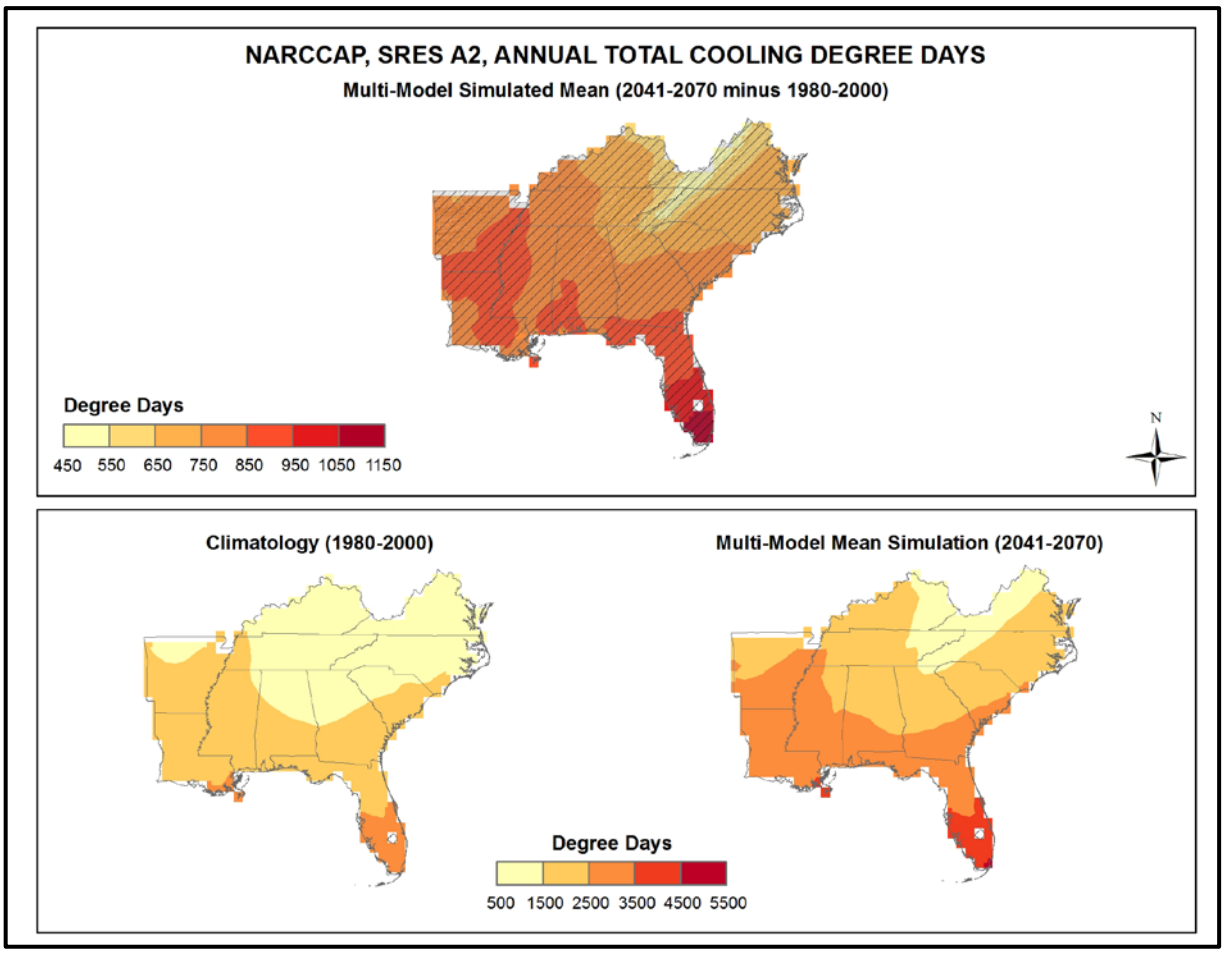

Figure 35. Simulated difference in the mean annual number of cooling degree days for the Southeast region, for the 2041-2070 time period with respect to the reference period of 1980-2000 (top). Color with hatching (category 3) indicates that more than 50% of the models show a statistically significant change in the number of cooling degree days, and more than 67% agree on the sign of the change (see text). Mean annual number of cooling degree days for the 1980-2000 reference period (bottom left). Simulated mean annual number of cooling degree days for the 2041-2070 future time period (bottom right). These are multi-model means from 8 NARCCAP regional climate simulations for the high (A2) emissions scenario. Note that top and bottom color scales are different. There are increases everywhere with the changes becoming larger from north to south.

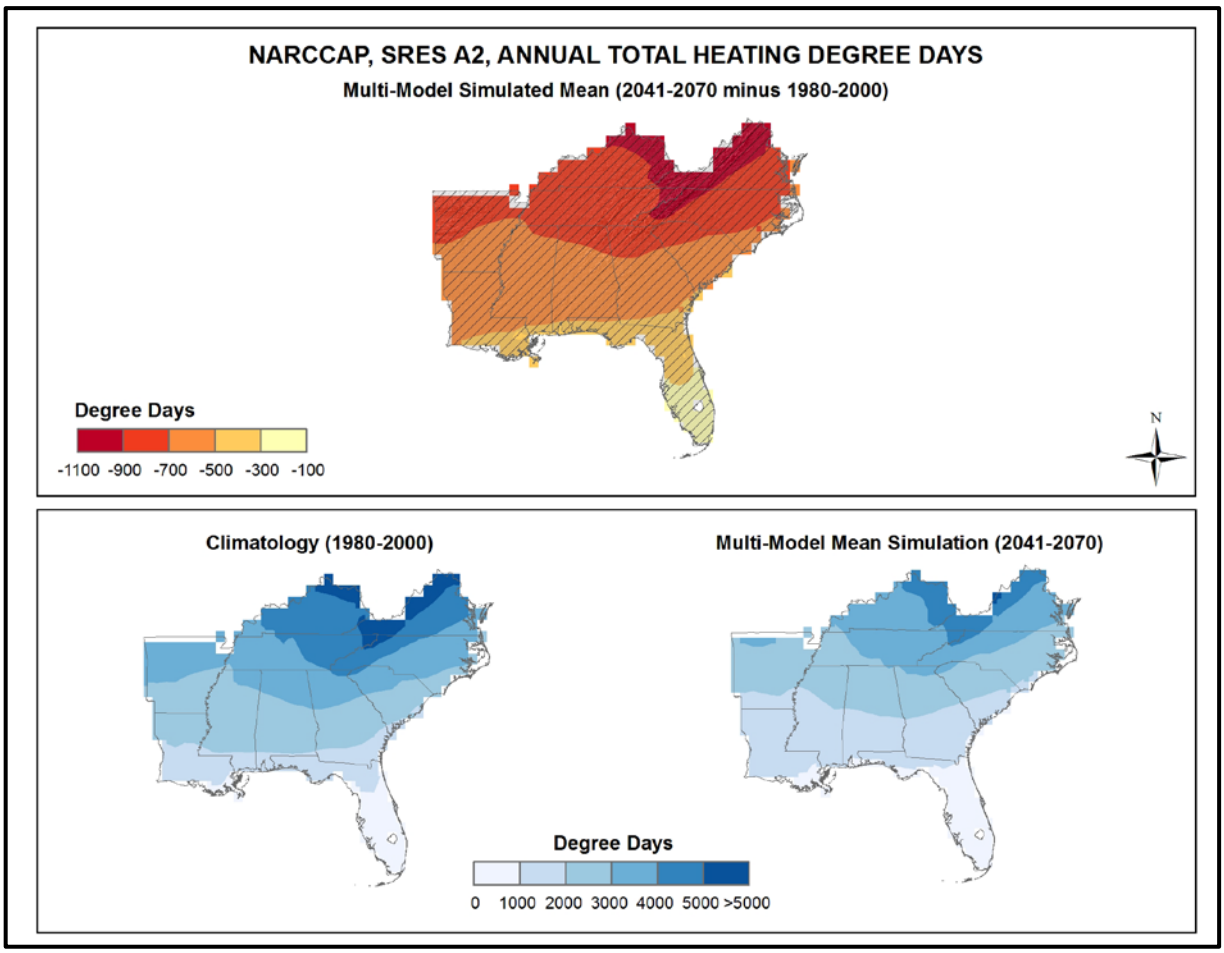

Figure 36. Simulated difference in the mean annual number of heating degree days for the Southeast region, for the 2041-2070 time period with respect to the reference period of 1980-2000 (top). Color with hatching (category 3) indicates that more than 50% of the models show a statistically significant change in the number of heating degree days, and more than 67% agree on the sign of the change (see text). Mean annual number of heating degree days for the 1980-2000 reference period (bottom left). Simulated mean annual number of heating degree days for the 2041-2070 future time period (bottom right). These are multi-model means from 8 NARCCAP regional climate simulations for the high (A2) emissions scenario. There are decreases everywhere with the largest changes in the north.

3.6. Tabular Summary of Selected Temperature Variables

The mean changes for select temperature-based variables derived from 8 NARCCAP simulations for 2055 with respect to the model reference period of 1971-2000, for the high (A2) emissions scenario, are summarized in Table 5. These were determined by first calculating the derived variable at each grid point. The spatially-averaged value of the variable was then calculated for the reference and future periods. Finally, the difference or ratio between the two periods was calculated from the spatially-averaged values. In addition, these same variables were calculated from the 8 CMIP3 daily statistically-downscaled data set (Daily_CMIP3) simulations for comparison.

Table 5. Multi-model means and standard deviations of the simulated annual mean change in select temperature variables from 8 NARCCAP simulations for the Southeast region. Multi-model means from the 11 Daily_CMIP3 simulations are also shown for comparison. Analyses are for the 2041-2070 time period with respect to the reference period of 1971-2000, for the high (A2) emissions scenario.

Temperature Variable	**NARCCAP Mean**	**NARCCAP Standard Deviation**	**Daily_CMIP3 Mean**
Freeze-free period	+24 days	5 days	+22 days
#days T_{max} > 90°F	+31 days	6 days	+42 days
#days T_{max} > 95°F	+27 days	9 days	+33 days
#days T_{max} > 100°F	+20 days	9 days	+10 days
#days T_{min} < 32°F	-17 days	2 days	-18 days
#days T_{min} < 10°F	-2 days	2 days	-1 day
#days T_{min} < 0°F	-1 day	1 day	0 days
Consecutive #days > 95°F	+97%	53%	+207%
Consecutive #days > 100°F	+132%	88%	+513%
Heating degree days	-19%	2%	-23%
Cooling degree days	+49%	9%	+42%
Growing degree days (base 50°F)	+24%	3%	+22%

For the NARCCAP simulations, the multi-model mean freeze-free period over the Southeast region is simulated to increase by 24 days, comparable to the 22 days calculated for the CMIP3 daily statistically-downscaled data. The number of days with daily maximum temperatures greater than 90°F, 95°F, and 100°F are simulated to increase by 31, 27, and 20 days, respectively, for the NARCCAP models. For the Daily_CMIP3 data, corresponding increases are 42, 33, and 10 days.

The number of days with minimum temperatures of less than 32°F, 10°F, and 0°F are simulated to decrease by 18, 2, and 1 days, respectively, for the NARCCAP models. Corresponding values for the Daily_CMIP3 simulations are comparable decreases of 18, 1, and 0 days.

The multi-model mean annual maximum number of consecutive days exceeding 95°F and 100°F (our heat wave metric) are simulated to increase by 97% and 132% respectively for the NARCCAP data, a substantial increase in the length of such hot periods. These increases are greater for the Daily_CMIP3 simulations, with values of 207% for the 95°F threshold, and 513% for the 100°F threshold.

Table 5 indicates that, for the high (A2) emissions scenario, the number of heating degree days are simulated by the NARCCAP simulations to decrease by 19% (23% for Daily_CMIP3), while the number of cooling degree days are simulated to increase by 49% (42% for Daily_CMIP3). The number of growing degree days (base 50°F) are also comparable for both data sets, increasing by 24% and 22% for NARCCAP and Daily_CMIP3, respectively.

3.7. Mean Precipitation

Figure 37 shows the spatial distribution of multi-model mean simulated differences in average annual precipitation for the three future time periods (2035, 2055, 2085) with respect to 1971-1999, for both emissions scenarios, for the 14 (B1) or 15 (A2) CMIP3 models. There is a consistent difference between the increasingly wet areas of North Carolina and Virginia (+3 to +6%) by 2085 and the substantial drying that is simulated across Louisiana (up to -12%). This gradient in precipitation changes gradually increases in magnitude as time progresses and is largest in 2085. The agreement among models was once again assessed using the three categories described in Fig. 26. It can be seen that for the 2035 time period the changes in precipitation are not significant for most models (category 1) over the majority of grid points. This means that most models are in agreement that any changes will be smaller than the normal year-to-year variations that occur. For the low emissions scenario in 2085, most models indicate changes that are larger than these normal variations (category 3) in the eastern half of the region. For the high emissions scenario, the models are mostly in agreement that precipitation will increase in the far northeast and decrease in the southwest. Across the majority of the region, however, the models are in disagreement about the sign of the changes (category 2).

Table 6 shows the distribution of changes in annual mean precipitation for each future time period with respect to 1971-1999, for both emissions scenarios, among the 14 (B1) or 15 (A2) CMIP3 models. The distribution of 9 NARCCAP simulations (for 2055, A2 scenario only) is also shown for comparison, with respect to 1971-2000. For all three time periods and both scenarios, the CMIP3 model simulate both increases and decreases in precipitation. The median values are all positive and less than 4%. The inter-model range of changes in precipitation (i.e. the difference between the highest and lowest model values) varies from 14% to 34%. For example, in the high (A2) emissions scenario the precipitation change for 2055 varies from a low of -14% to a high of +8%. The range of the NARCCAP values is 17% (for A2, 2055). The interquartile range (the difference between the 75^{th} and 25^{th} percentiles) of precipitation changes across all of the GCMs is 10% or less for all time periods, except A2, 2085.

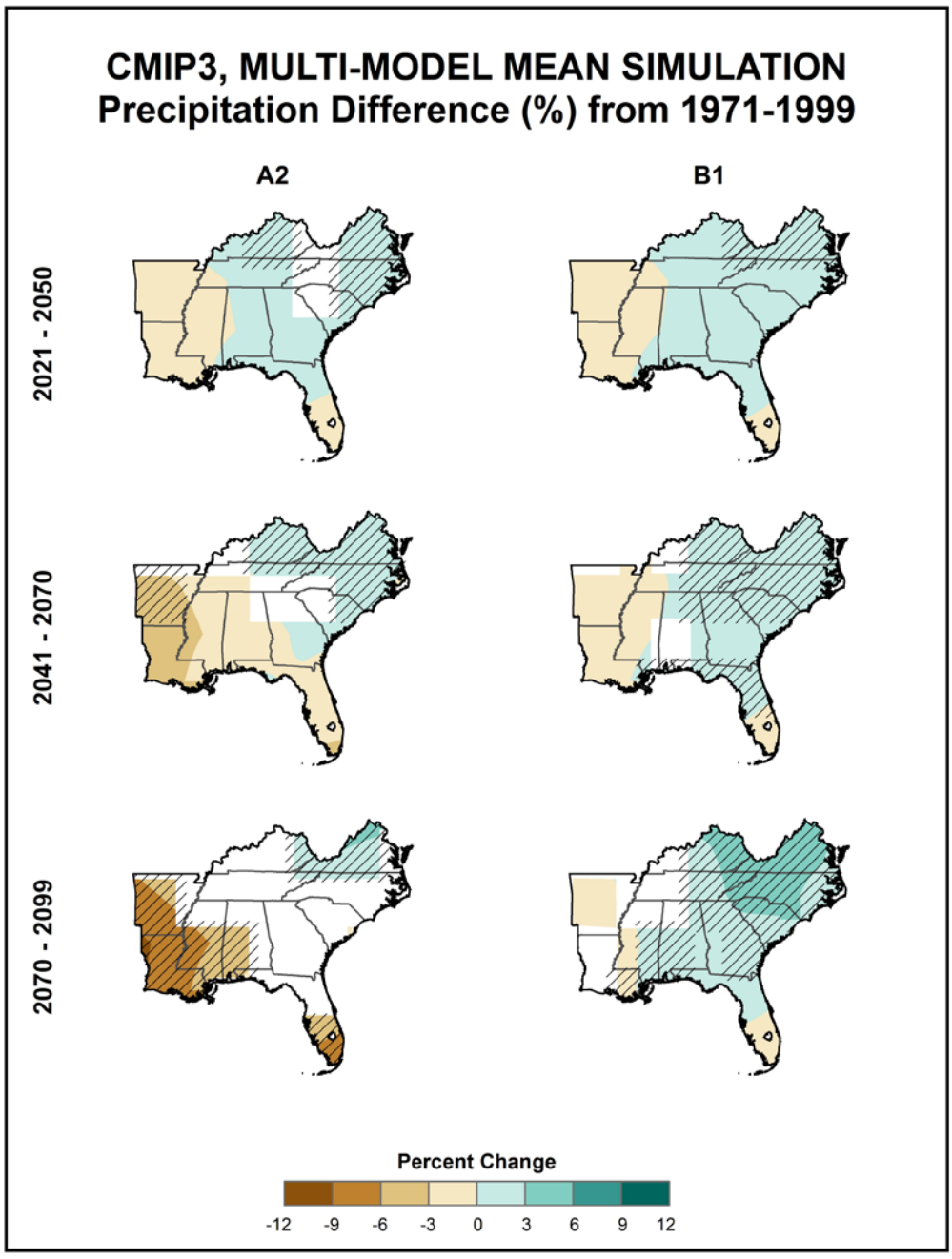

Figure 37. Simulated difference in annual mean precipitation (%) for the Southeast region, for each future time period (2021-2050, 2041-2070, and 2070-2099) with respect to the reference period of 1971-1999. These are multi-model means for the high (A2) and low (B1) emissions scenarios from the 14 (B1) or 15 (A2) CMIP3 global climate simulations. Color only (category 1) indicates that less than 50% of the models show a statistically significant change in precipitation. Color with hatching (category 3) indicates that more than 50% of the models show a statistically significant change in precipitation, and more than 67% agree on the sign of the change. Whited out areas (category 2) indicate that more than 50% of the models show a statistically significant change in precipitation, but less than 67% agree of the sign of the change (see text). Generally, the models simulate increases in the north and east and decreases in the south and west parts of the region.

Table 6. Distribution of the simulated change in annual mean precipitation (%) from the 14 (B1) or 15 (A2) CMIP3 models for the Southeast region. The lowest, 25th percentile, median, 75th percentile and highest values are given for the high (A2) and low (B1) emissions scenarios, and for each future time period (2021-2050, 2041-2070, and 2070-2099) with respect to the reference period of 1971-1999. Also shown are values from the distribution of 9 NARCCAP models for 2041-2070, A2 only, with respect to 1971-2000.

Scenario	Period	Lowest	25th Percentile	Median	75th Percentile	Highest
A2	2021-2050	-9	-2	2	3	8
	2041-2070	-14	-6	2	4	8
	2070-2099	-23	-12	4	6	11
	NARCCAP (2041-2070)	*-5*	*-3*	*3*	*5*	*12*
B1	2021-2050	-9	-1	1	3	5
	2041-2070	-11	-1	3	4	7
	2070-2099	-12	-1	4	5	9

Figure 38 shows the multi-model mean annual and seasonal 30-year average precipitation change between 2041-2070 and 1971-2000 for the high (A2) emissions scenario, for 11 NARCCAP regional climate model simulations. Over the last 100 years no discernible annual trend has been seen in the region. The simulated changes in precipitation are mostly upward with the largest increases of 9-12% along the Gulf Coast, while decreases of up to 6% are simulated for southern Florida. There are also small (less than 3%) decreases in the far western part of the region. There are notable seasonal variations in changes. For the winter, spring, and fall, precipitation is mostly simulated to increase. For the winter, the largest increases of more than 15% occur in the northern part of the region and central Florida. For the spring season, increases of 15-20% occur in the interior and north of the region. For the fall, the largest simulated increases of more than 15% occur along the Gulf Coast. By contrast, the models simulate mostly precipitation decreases in the summer with the largest decreases of more than 10% occurring in southern Florida and the far west of the region. Little change or slight increases are simulated along much of the Atlantic and Gulf Coasts. The agreement between models was again assessed using the three categories described in Fig. 26. It can be seen that for the winter, spring, and fall seasons the simulated changes in precipitation are not statistically significant for most models over all grid points (category 1). Annually, and for summer, however, there are some areas in the south and east of the region where the models are in agreement (category 3). For summer, there are also some parts of southern Louisiana, southern Georgia, and northern Florida, where the models are in disagreement about the sign of the change (category 2).

Table 7 shows the distribution of simulated changes in seasonal mean precipitation among the 14 (B1) or 15 (A2) CMIP3 models between 2070-2099 and 1971-1999, for both emissions scenarios. On a seasonal basis, the range of model-predicted changes is quite large. For example, in the high (A2) emissions scenario, the change in summer precipitation varies from a decrease of 51% to an increase of 24%. In the winter, summer, and fall, a few models simulate sizeable increases in precipitation of more than 10%. In the low (B1) emissions scenario, the range of changes in precipitation is generally smaller. The central feature of the results in Table 7 is the large uncertainty in seasonal precipitation changes.

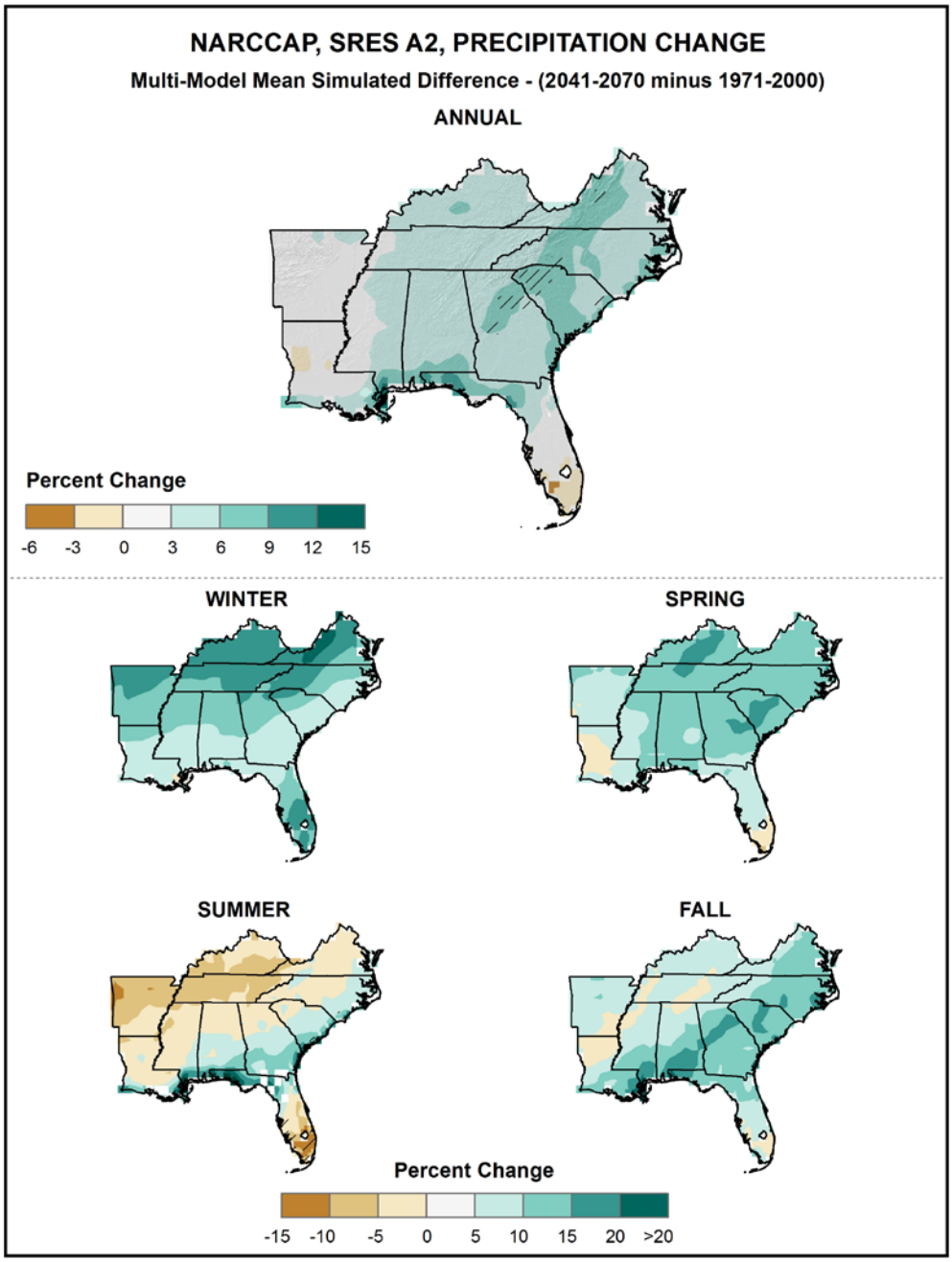

Figure 38. Simulated difference in annual and seasonal mean precipitation (%) for the Southeast region, for 2041-2070 with respect to the reference period of 1971-2000. These are multi-model means from 11 NARCCAP regional climate simulations for the high (A2) emissions scenario. Color only (category 1) indicates that less than 50% of the models show a statistically significant change in precipitation. Color with hatching (category 3) indicates that more than 50% of the models show a statistically significant change in precipitation, and more than 67% agree on the sign of the change. Whited out areas (category 2) indicate that more than 50% of the models show a statistically significant change in precipitation, but less than 67% agree of the sign of the change (see text). Note that top and bottom color scales are unique, and different from that of Fig. 37. The annual change is near zero in the west and downward in southern Florida, with increases of 2-6% throughout the remainder of the region. Changes are mostly upward in winter, spring, and fall, and downward in summer.

Table 7. Distribution of the simulated change in seasonal mean precipitation (%) from the 14 (B1) or 15 (A2) CMIP3 models for the Southeast region. The lowest, 25th percentile, median, 75th percentile and highest values are given for the high (A2) and low (B1) emissions scenarios, and for the 2070-2099 time period with respect to the reference period of 1971-1999.

Scenario	Period	Season	Lowest	25th Percentile	Median	75th Percentile	Highest
A2	2070-2099	DJF	-34	-4	3	7	14
		MAM	-26	-16	2	4	11
		JJA	-50	-22	0	9	24
		SON	-16	-5	3	13	17
B1	2070-2099	DJF	-25	-7	2	5	9
		MAM	-14	0	2	6	8
		JJA	-24	-3	5	10	18
		SON	-11	-3	3	7	13

Figure 39 shows the simulated change in annual mean precipitation for each future time period with respect to 1971-1999, for both emissions scenarios, averaged over the entire Southeast region for the 14 (B1) or 15 (A2) CMIP3 models. In addition, averages for 9 of the NARCCAP simulations (relative to 1971-2000) and the 4 GCMs used in the NARCCAP experiment are shown for 2055 (A2 scenario only). Both the multi-model mean and individual model values are shown. There is considerable spread in the magnitude of the simulated changes, although the multi-model mean values are rather small overall. For the high (A2) emissions scenario, the multi-model mean CMIP3 changes are simulated to be +1 by 2035, -1% by 2055, and -3% by 2085. The mean changes for the low (B1) emissions scenario are less than 2% for all three time periods. The multi-model mean of the NARCCAP simulations is positive (+3%), compared to a negative change for CMIP3, but is comparable to that of the 4 GCMs used in the NARCCAP experiment (which do not include the 3 driest CMIP3 models). The inter-model range of changes in Fig. 39 is large compared to the differences in the multi-model means, as also illustrated in Table 6. In fact, for both emissions scenarios, the individual model range is much larger than the differences in the CMIP3 multi-model means between time periods.

Figure 40 shows the simulated change in seasonal mean precipitation for each future time period with respect to 1971-1999, for the high (A2) emissions scenario, averaged over the entire Southeast region for the 15 CMIP3 models, as well as the NARCCAP models for 2055, relative to 1971-2000. Again, both the multi-model mean and individual model values are shown. The CMIP3 models simulate mean decreases in precipitation for the spring and summer seasons but increases for fall. Both increases and decreases are simulated for winter. For 2055, the NARCCAP models are wetter than the CMIP3 models for the winter, spring, and fall. This may in part be due to the choice of the 4 GCMs in the NARCCAP experiment (which do not include the driest CMIP3 models. As was the case for the annual totals in Fig. 39, the model ranges in Fig. 40 are large compared to the multi-model mean differences. This illustrates the large uncertainty in the precipitation estimates using these simulations.

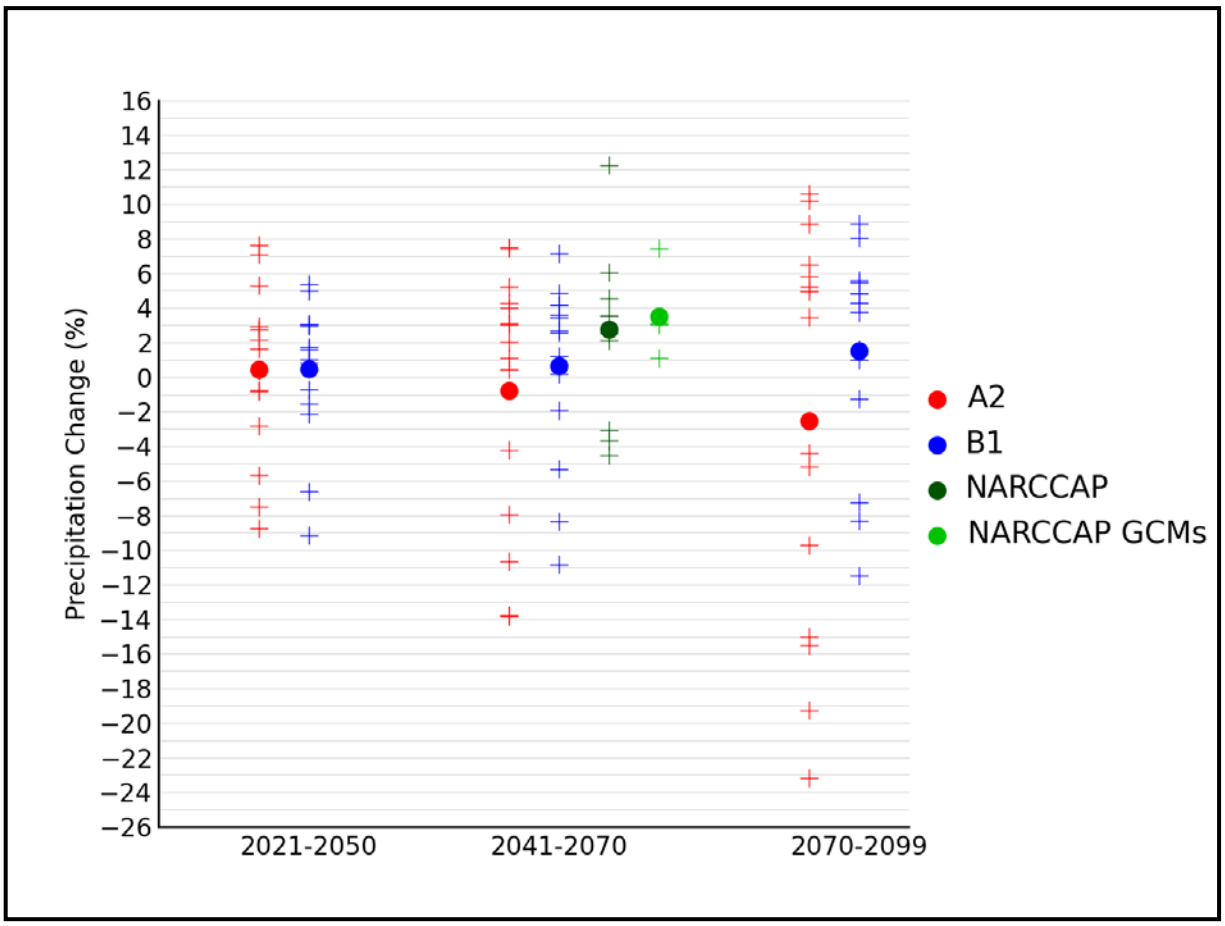

Figure 39. Simulated annual mean precipitation change (%) for the Southeast region, for each future time period (2021-2050, 2041-2070, and 2070-2099) with respect to the reference period of 1971-1999. Values are given for the high (A2) and low (B1) emissions scenarios for the 14 (B1) or 15 (A2) CMIP3 models. Also shown for 2041-2070 (high emissions scenario only) are values (relative to 1971-2000) for 9 NARCCAP models, as well as for the 4 GCMs used to drive the NARCCAP simulations. The small plus signs indicate each individual model and the circles depict the multi-model means. The ranges of model-simulated changes are very large compared to the mean changes and to differences between the A2 and B1 scenarios.

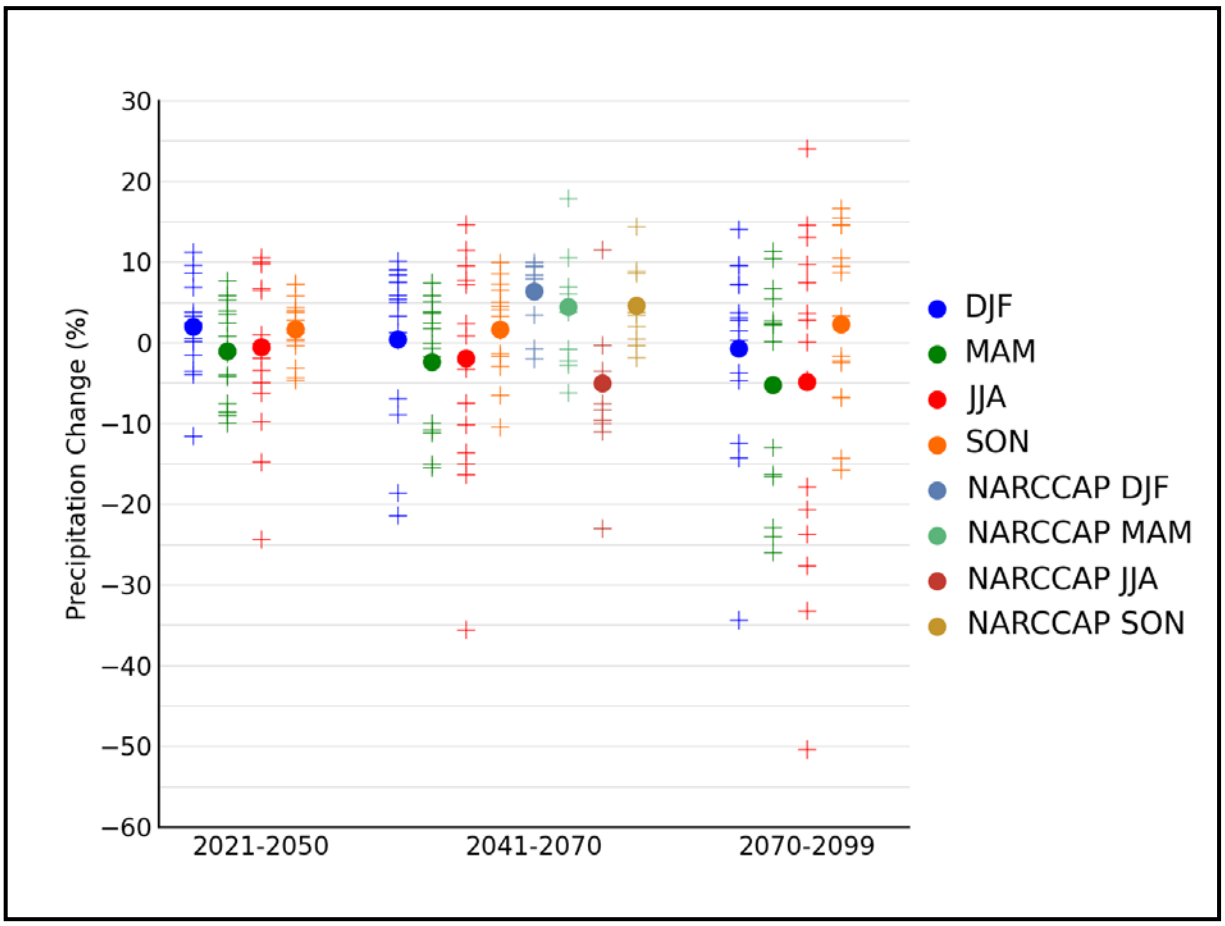

Figure 40. Simulated seasonal mean precipitation change (%) for the Southeast region, for each future time period (2021-2050, 2041-2070, and 2070-2099) with respect to the reference period of 1971-1999. Values are given for all 15 CMIP3 models for the high (A2) emissions scenario. Also shown are values (relative to 1971-2000) for 9 NARCCAP models for 2041-2070. The small plus signs indicate each individual model and the circles depict the multi-model means. Seasons are indicated as follows: winter (DJF, December-January-February), spring (MAM, March-April-May), summer (JJA, June-July-August), and fall (SON, September-October-November). The ranges of model-simulated changes are large compared to the mean changes and to differences between the seasons.

3.8. Extreme Precipitation

Figure 41 shows the spatial distribution of the multi-model mean change in the average annual number of days with precipitation exceeding 1 inch, for 8 NARCCAP regional climate model simulations. Again this is the difference between the period of 2041-2070 and the 1980-2000 model reference period, for the high (A2) emissions scenario. In addition to this difference map, maps of the model simulations of the actual values for historical conditions (NARCCAP models driven by the NCEP Reanalysis II) and for the future are also displayed for comparison. All areas exhibit simulated increases. The largest changes are seen across the Appalachian Mountains with increases of 20-25%. The smallest increases of less than 10% are seen mainly in Arkansas, Louisiana, and Mississipi. Changes in days exceeding 1 inch are not statistically significant for most models (category 1) over the majority of grid points. This means that most models are in agreement that any changes will be smaller than the normal year-to-year variations that occur under this scenario. For high elevation areas, however, most models indicate increases in days with precipitation of more than 1 inch that are larger than these normal variations (category 3).

Consecutive days with little or no precipitation reduce soil moisture levels and put stress on plants. Figure 42 shows the NARCCAP multi-model mean change in the average annual maximum number of consecutive days with precipitation less than 0.1 inches (3 mm) between 2055 and the model reference period of 1980-2000, for the high (A2) emissions scenario. In general, a large part of the interior Southeast is simulated to see little or no change in the number of consecutive days with precipitation less than 0.1 inches. The biggest exceptions are areas along the Gulf Coast, where these consecutive dry days are simulated to increase by up to 12 days. Changes in the number of consecutive days with precipitation of less than 0.1 inches are not statistically significant for most models (category 1) over the majority of grid points. This means that most models are in agreement that any changes will be smaller than the normal year-to-year variations that occur under this scenario. For grid points where the largest decreases are simulated, however, most models indicate statistically significant changes (category 3). In some areas, such as central and northern Florida, the models are in disagreement about the sign of the changes (category 2).

3.9. Tabular Summary of Selected Precipitation Variables

The mean changes for select precipitation-based variables derived from 8 NARCCAP simulations for 2055 with respect to the model reference period of 1971-2000, for the high (A2) emissions scenario, are summarized in Table 8. The same variables from the 8 CMIP3 statistically-downscaled (Daily_CMIP3) simulations are also shown for comparison. These spatially-averaged values were calculated as described for Table 5.

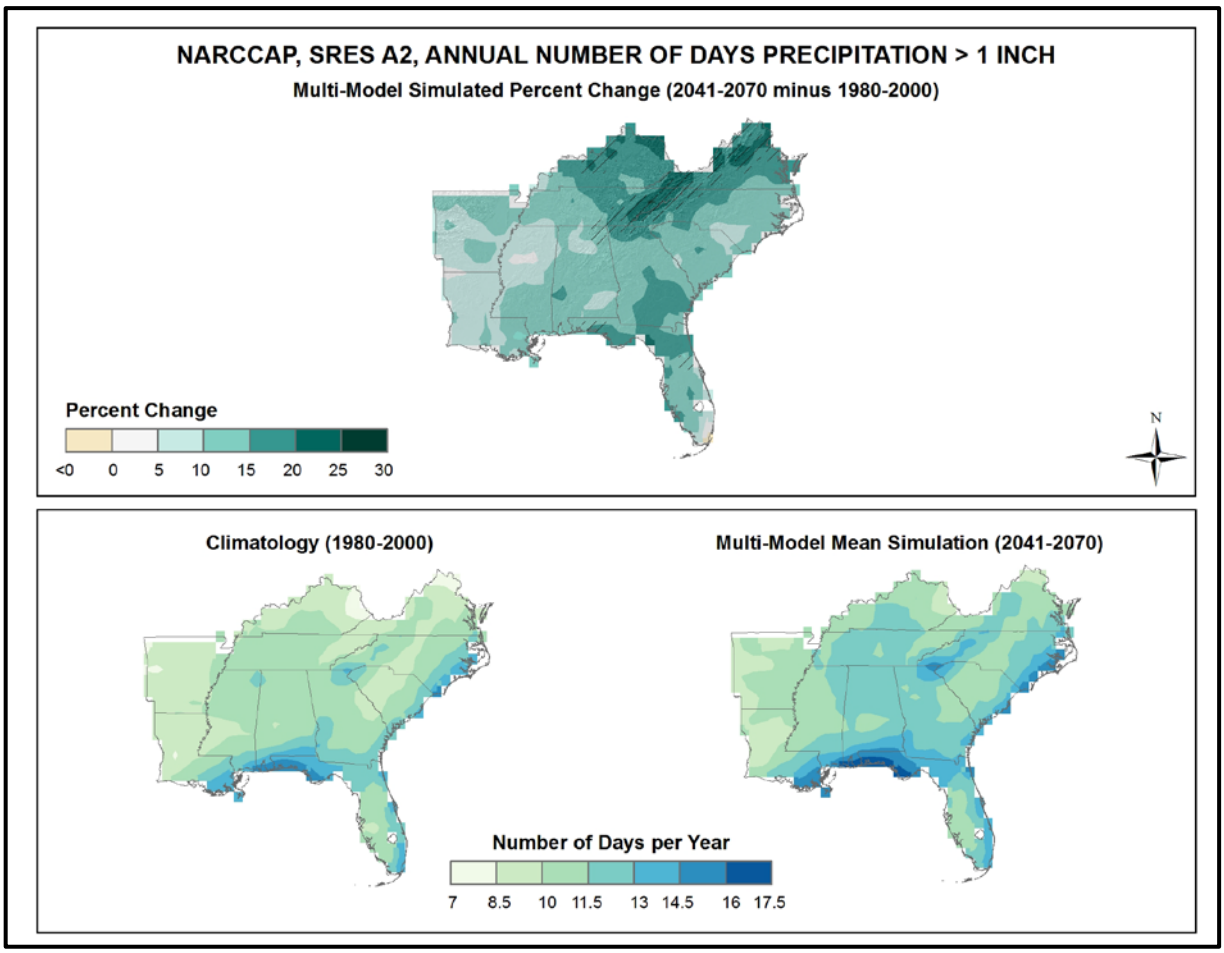

Figure 41. Simulated percentage difference in the mean annual number of days with precipitation of greater than one inch for the Southeast region, for the 2041-2070 time period with respect to the reference period of 1980-2000 (top). Color only (category 1) indicates that less than 50% of the models show a statistically significant change in the number of days. Color with hatching (category 3) indicates that more than 50% of the models show a statistically significant change in the number of days, and more than 67% agree on the sign of the change (see text). Mean annual number of days with precipitation of greater than one inch for the 1980-2000 reference period (bottom left). Simulated mean annual number of days with precipitation of greater than one inch for the 2041-2070 future time period (bottom right). These are multi-model means from 8 NARCCAP regional climate simulations for the high (A2) emissions scenario. The models simulate general increases with the largest changes in the north.

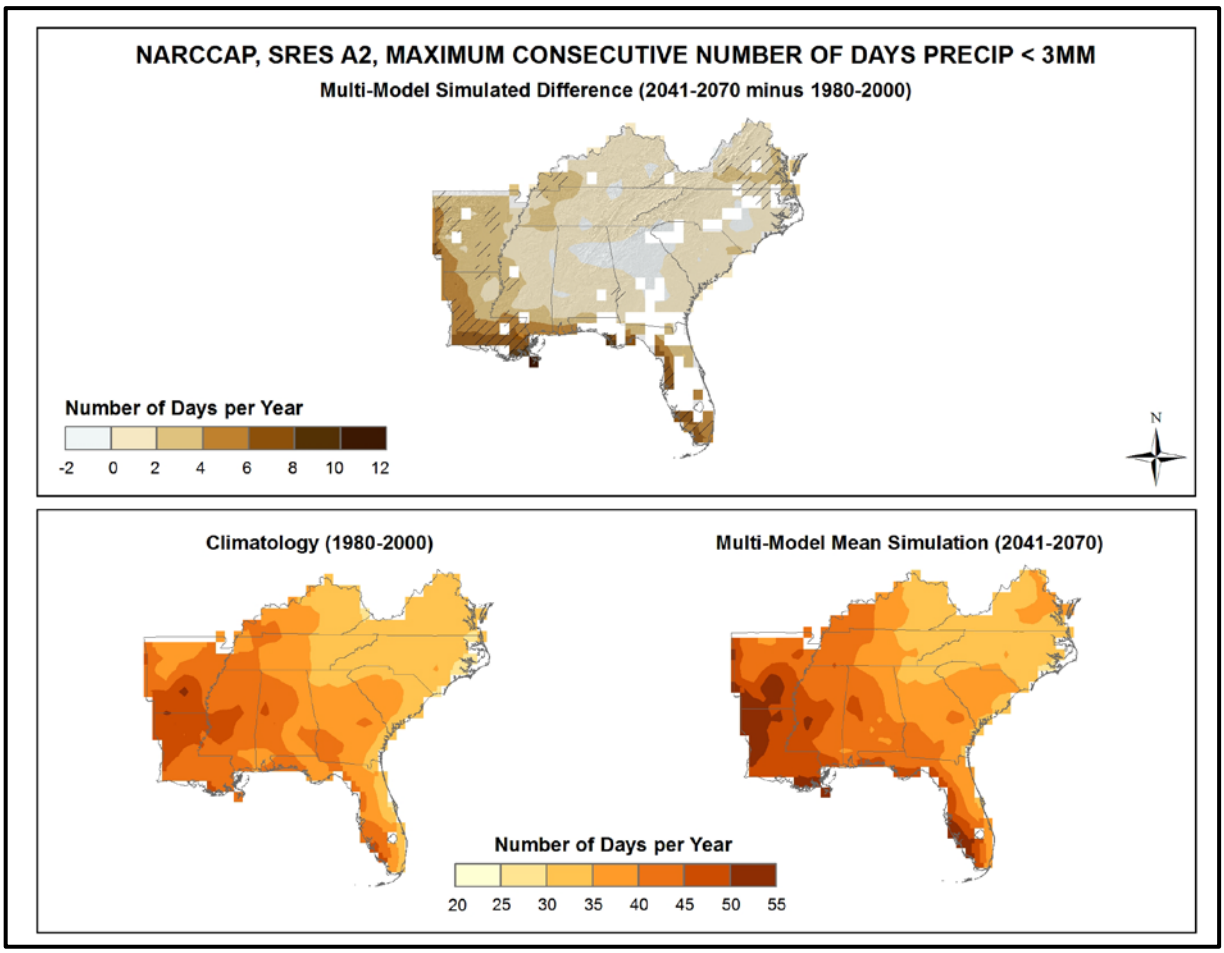

Figure 42. Simulated difference in the mean annual maximum number of consecutive days with precipitation of less than 0.1 inches/3 mm for the Southeast region, for the 2041-2070 time period with respect to the reference period of 1980-2000 (top). Color only (category 1) indicates that less than 50% of the models show a statistically significant change in the number of consecutive days. Color with hatching (category 3) indicates that more than 50% of the models show a statistically significant change in the number of consecutive days, and more than 67% agree on the sign of the change. Whited out areas (category 2) indicate that more than 50% of the models show a statistically significant change in the number of consecutive days, but less than 67% agree of the sign of the change (see text). Mean annual maximum number of consecutive days with precipitation of less than 0.1 inches/3 mm for the 1980-2000 reference period (bottom left). Simulated mean annual maximum number of consecutive days with precipitation of less than 0.1 inches/3 mm for the 2041-2070 future time period (bottom right). These are multi-model means from 8 NARCCAP regional climate simulations for the high (A2) emissions scenario. The models simulate little change over the majority of the region, with slight increases in the south.

Table 8. Multi-model means and standard deviations of the simulated annual mean change in select precipitation variables from 8 NARCCAP simulations for the Southeast region. Multi-model means from the 8 Daily_CMIP3 simulations are also shown for comparison. Analyses are for the 2041-2070 time period with respect to the reference period of 1971-2000, for the high (A2) emissions scenario.

Precipitation Variable	NARCCAP Mean	NARCCAP Standard Deviation	Daily_CMIP3 Mean
#days > 1 inch	+13%	10%	+6%
#days > 2 inches	+32%	24%	+20%
#days > 3 inches	+48%	39%	+39%
#days > 4 inches	+60%	49%	+65%
Consecutive #days < 0.1 inches	+2 days	4 days	+1 day

Recent climatology shows an increase in extreme precipitation events in recent years, a trend which is simulated to continue by both the NARCCAP and Daily_CMIP3 simulations. For the NARCCAP data, the multi-model mean number of days with precipitation exceeding 1, 2, 3, and 4 inches are simulated to increase for the high (A2) emissions scenario, with changes of between +13% for a threshold of 1 inch and +60% for 4 inches. Similar to the temperature variables in Table 5, greater increases are seen in Table 8 for the more extreme thresholds. As for the temperature variables, changes for the Daily_CMIP3 data between each threshold and the next become greater as the thresholds become more extreme. The average annual maximum number of consecutive days with precipitation less than 0.1 inches is simulated to increase by 2 days. The corresponding Daily_CMIP3 simulations indicate a comparable increase of 1 day.

3.10. Comparison Between Model Simulations and Observations

In this section, some selected comparisons between CMIP3 model simulations and observations are presented. These are limited to annual and seasonal temperature and precipitation. The model simulations of the 20th century that are shown herein are based on estimated historical forcings of the climate system, including such factors as greenhouse gases, volcanic eruptions, solar variations, and aerosols. Also shown are the simulations of the 21st century for the high (A2) emissions scenario.

In these comparisons, both model and observational data are expressed as deviations from the 1901-1960 average. As explained in Section 2.4 (Climatic Trends), acceleration of the anthropogenic forcing occurs shortly after 1960. Thus, for the purposes of comparing net warming between periods of different anthropogenic forcing, 1960 is a rational choice for the ending date of a reference period. It is not practical to choose a beginning date earlier than about 1900 because many model simulations begin in 1900 or 1901 and the uncertainties in the observational time series increase substantially prior to 1900. Therefore, the choice of 1901-1960 as the reference period is well suited for this purpose (comparing the net warming between periods of different anthropogenic forcing). However, there are some uncertainties in the suitability of the 1901-1960 reference period for this purpose. Firstly, there is greater uncertainty in the natural climate forcings (e.g., solar variations) during this time period than in the latter half of the 20th century. If there are sizeable errors in the estimated natural forcings used in climate models, then the simulations will be affected; this type of error does not represent a model deficiency. Secondly, the 1930s “Dust Bowl” era is included in this period. The excessive temperatures experienced then, particularly during the

summers, are believed to be caused partially by poor land management through its effects on the surface energy budget. Climate models do not incorporate land management changes and there is no expectation that models should simulate the effects of such. Thirdly, there are certain climate oscillations that occur over several decades. These oscillations have important effects on regional temperatures. A 60-year period is too short to sample entire cycles of some of these, and thus only represents a partial sampling of the true baseline climate.

Figure 43 shows observed (using the same data set as shown in Fig. 10) and simulated decadal mean annual temperature changes for the Southeast U.S. from 1900 to 2100, expressed as deviations from the 1901-1960 average. The observed rate of warming from 1900 into the 1930s was not simulated by any of the models. Similarly the observed rate of cooling from the 1930s into the 1960s was also not simulated by any model. However, since the 1960s, the observed rate of warming is similar to that of the models. For the winter and summer seasons (Fig. 44, left column), observed temperatures for the 1930s are higher than any model simulation and the observed temperatures for the 1960s/70s are lower than any model simulation. For spring and fall (right column), the observations are generally within the envelope of the model simulations, but do not show a substantial increase in temperature over the time period. This lack of 20th century warming in the Southeast U.S. and some adjacent areas is well-known and has been dubbed the "warming hole". Research on the causes of this feature is active and ongoing.

The 21st century portions of the time series indicate that the simulated future warming is much larger than the observed and simulated temperature changes for the 20th century.

Observed and model-simulated decadal mean precipitation changes (using the same data set as shown in Fig. 18) can be seen in Fig. 45 for annual and Fig. 46 for seasonal values. The observed variability tends to be somewhat higher than the model simulations, although the decadal values are within the envelope of the model simulations for annual, spring, and summer and the overall trend is within the envelope of model simulations for all seasons except fall. However, for the fall, the observed upward trend is not simulated by any model and many decadal values are outside the envelope of the model simulations. The 21st century portions of the time series show increased variability among the model simulations. It can be seen that the majority of the models simulate an overall increase in precipitation for winter, spring, and fall.

The CMIP3 archive contains a total of 74 simulations of the 20th century, 40 simulations of the 21st century for the high (A2) emissions scenario, and 32 simulations of the 21st century for the low (B1) emissions scenario from a total of 23 different models (many models performed multiple simulations for these periods). An exploratory analysis of the entire archive was performed, limited to temperature and to the year as a whole. As before, the data were processed using 1901-1960 as the reference period to calculate anomalies.

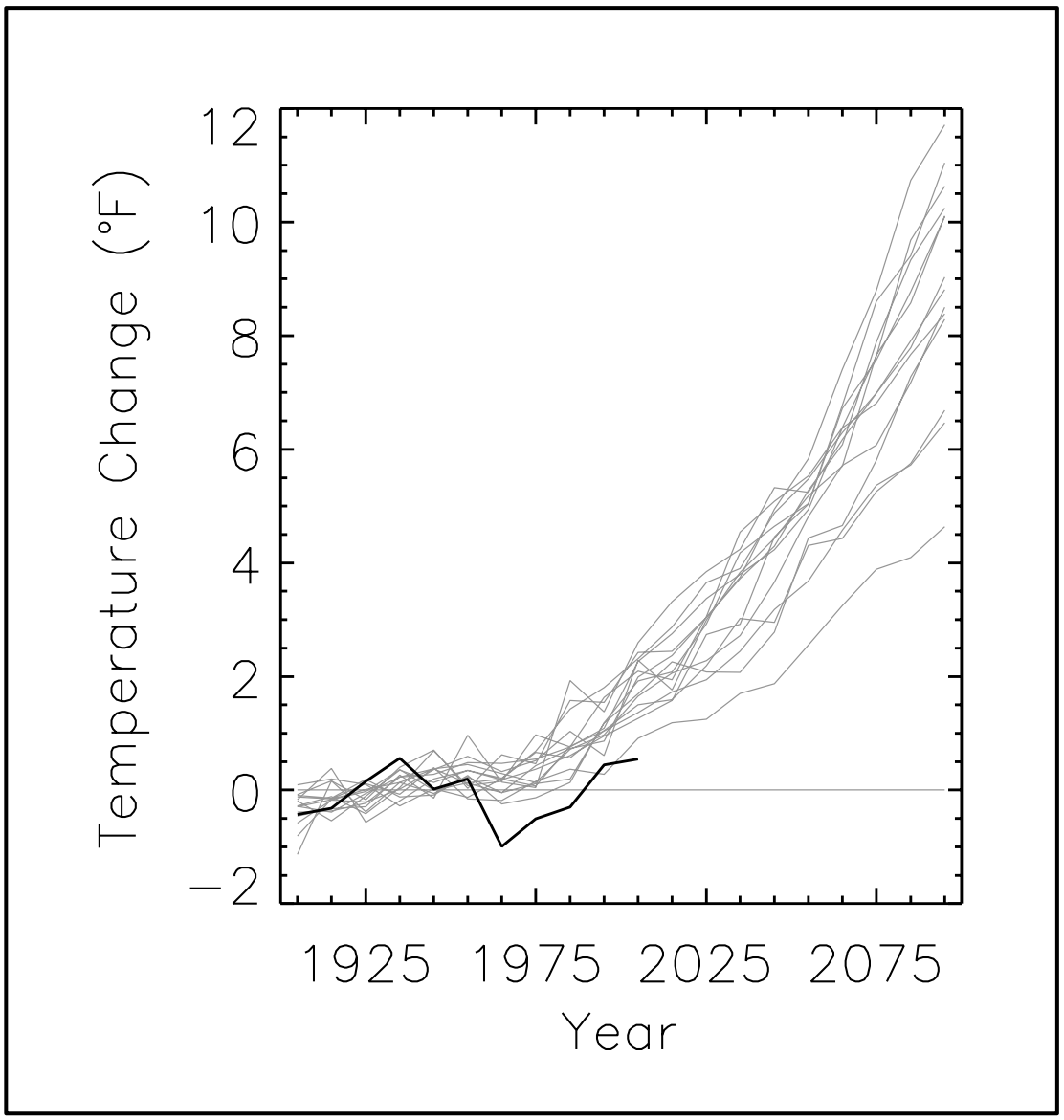

Figure 43. Observed decadal mean annual temperature change (deviations from the 1901-1960 average, °F) for the Southeast U.S. (black line). Based on a new gridded version of COOP data from the National Climatic Data Center, the CDDv2 data set (R. Vose, personal communication, July 27, 2012). Gray lines indicate the 20th and 21st century simulations from 15 CMIP3 models, for the high (A2) emissions scenario. The early 20th century rate of warming and the mid-century rate of cooling are not simulated by the models, but the late-century rate of warming is similar to the rate of warming in the models.

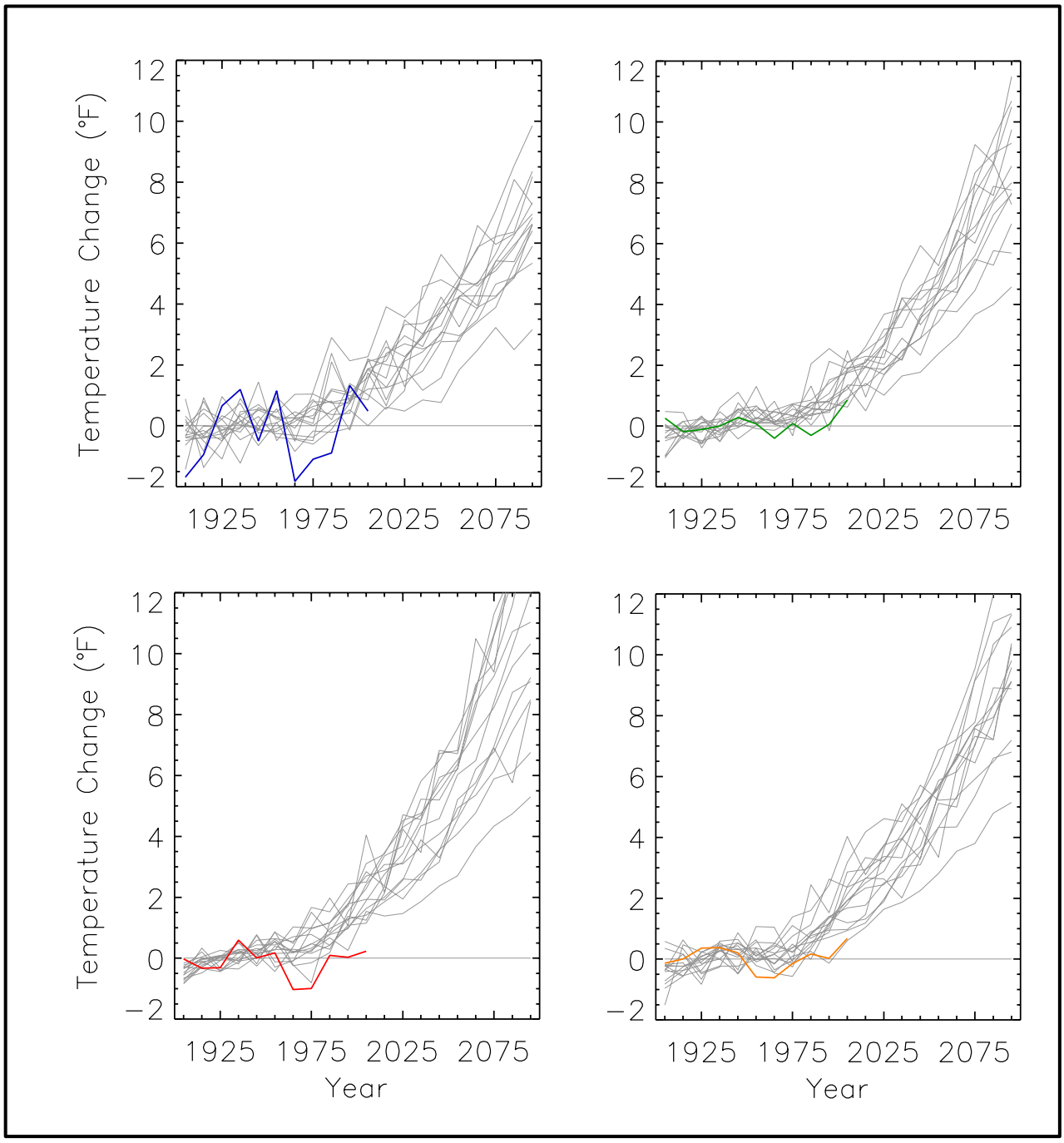

Figure 44. Observed decadal mean temperature change (deviations from the 1901-1960 average, °F) for the Southeast U.S. for winter (top left, blue line), spring (top right, green line), summer (bottom left red line), and fall (bottom right, orange line Based on a new gridded version of COOP data from the National Climatic Data Center, the CDDv2 data set (R. Vose, personal communication, July 27, 2012). Gray lines indicate 20th and 21st century simulations from 15 CMIP3 models, for the high (A2) emissions scenario. The observed amount of 20th century warming is within the envelope of model simulates in winter and spring, but it is less than model simulations in summer and fall.

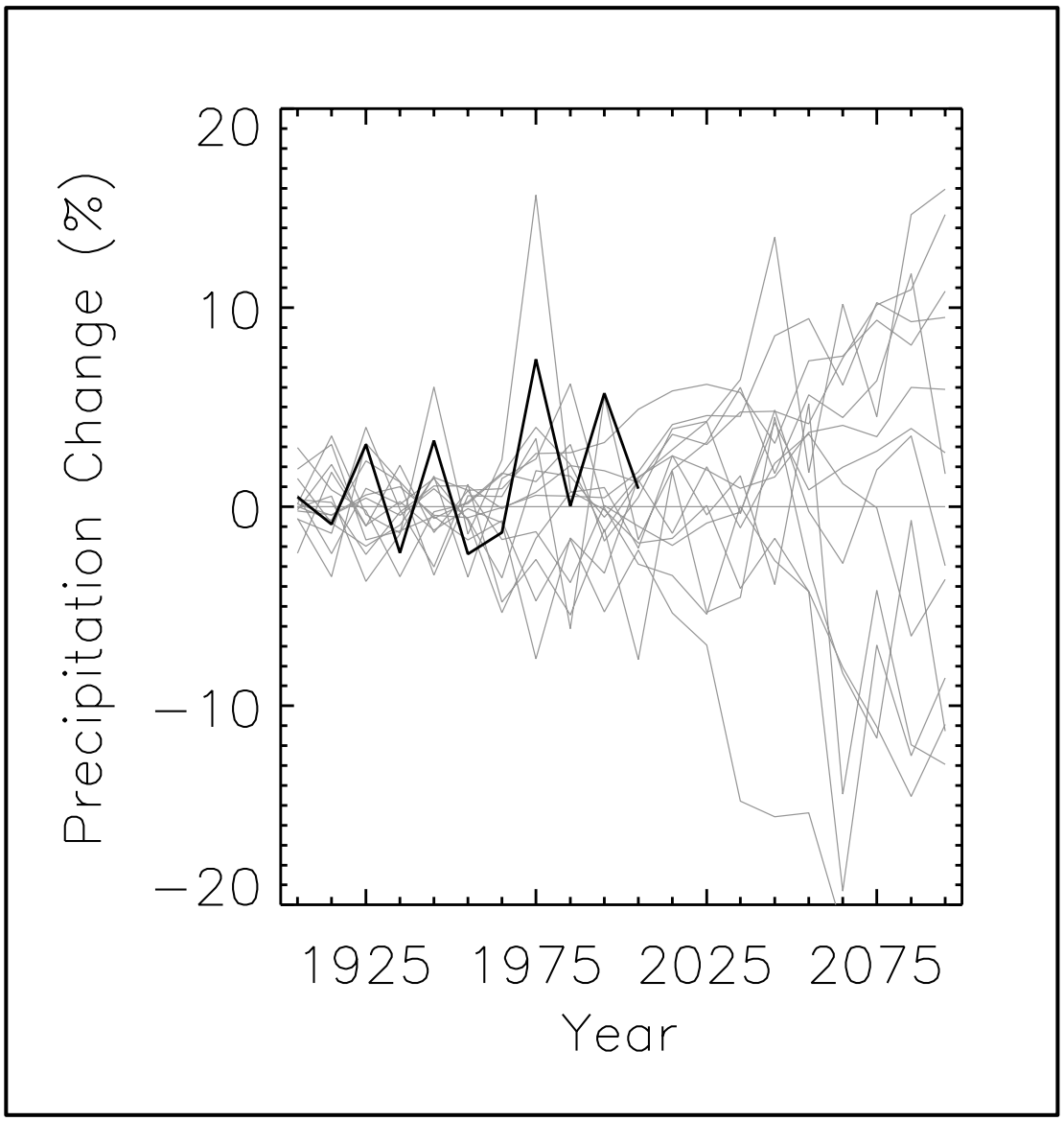

Figure 45. Observed decadal mean annual precipitation change (deviations from the 1901-1960 average, %) for the Southeast U.S. (black line). Based on a new gridded version of COOP data from the National Climatic Data Center, the CDDv2 data set (R. Vose, personal communication, July 27, 2012). Gray lines indicate the 20th and 21st century simulations from 15 CMIP3 models, for the high (A2) emissions scenario. Observed precipitation variations are within the model simulations.

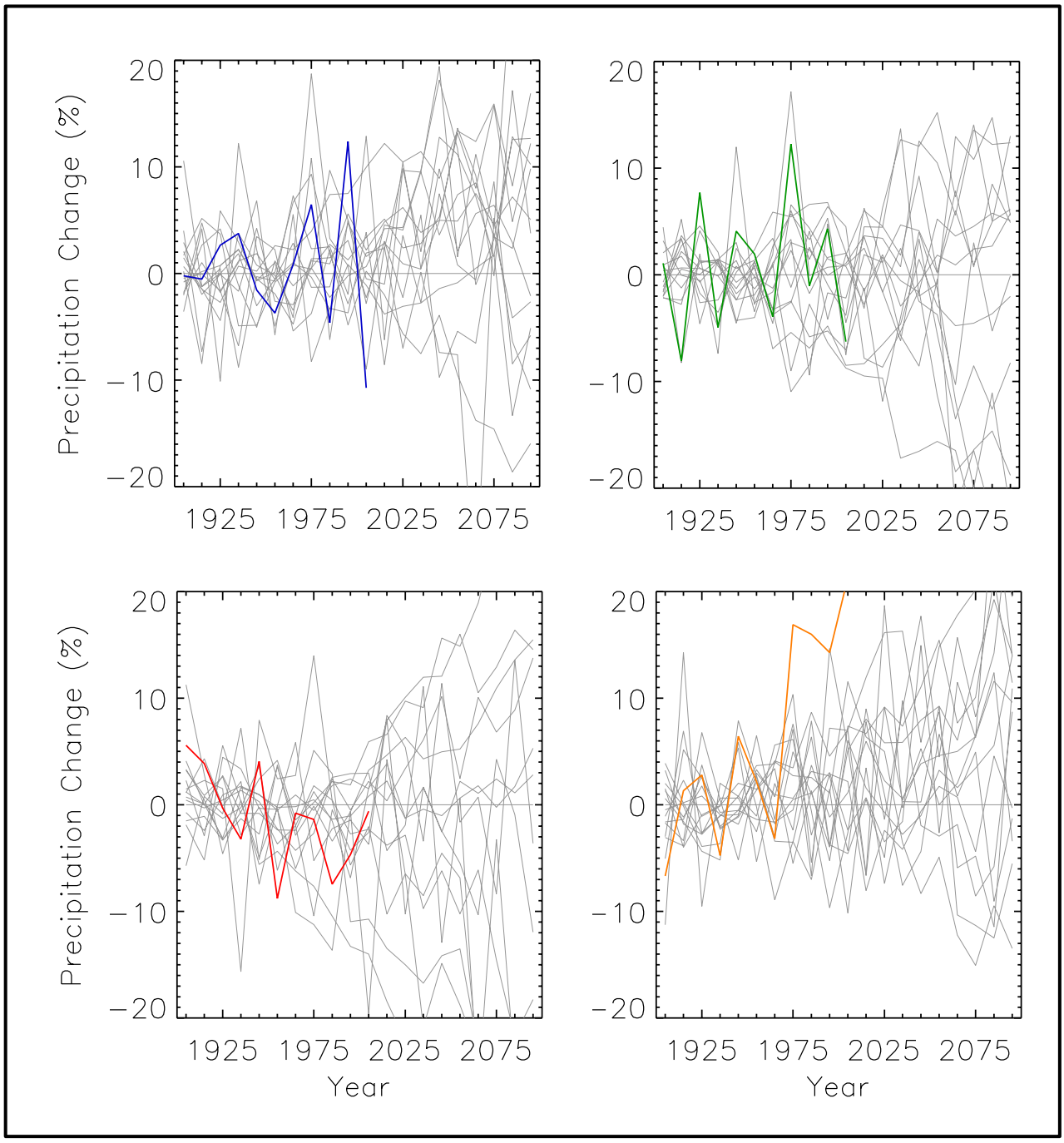

Figure 46. Observed decadal mean precipitation change (deviations from the 1901-1960 average, %) for the Southeast U.S. for winter (top left, blue line), spring (top right, green line), summer (bottom left red line), and fall (bottom right, orange line). Based on a new gridded version of COOP data from the National Climatic Data Center, the CDDv2 data set (R. Vose, personal communication, July 27, 2012). Gray lines indicate 20th and 21st century simulations from 15 CMIP3 models, for the high (A2) emissions scenario. Observed seasonal precipitation variations are within model simulations except for the fall where the observed increase in precipitation is not simulated by any of these models.

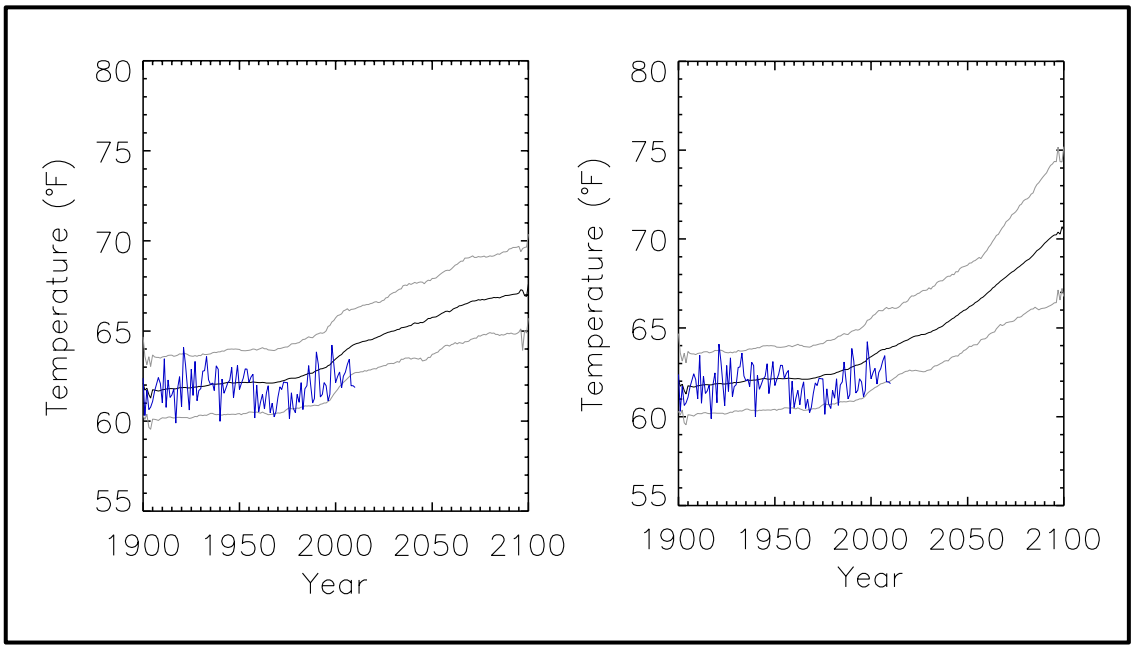

Figure 47. Time series of mean annual temperature for the Southeast region from observations (blue) and from all available CMIP3 global climate model simulations (black and grey). Black represents the mean and grey indicates the 5 and 95% limits of the model simulations. Model mean and percentile limits were calculated for each year separately and then smoothed. Results are shown for the low (B1) emissions scenario (left) and the high (A2) emissions scenario (right). A total of 74 simulations of the 20th century were used. For the 21st century, there were 40 simulations for the high emissions scenario and 32 for the low emissions scenario. For each model simulation, the annual temperature values were first transformed into anomalies by subtracting the simulation's 1901-1960 average from each annual value. Then, the mean bias between model and observations was removed by adding the observed 1901-1960 average to each annual anomaly value from the simulation. For each year, all available model simulations were used to calculate the multi-model mean and the 5th and 95th percentile bounds for that year. Then, the mean and 5th and 95th percentile values were smoothed with a 10-year moving boxcar average.

Figure 47 compares observations of annual temperature with the entire suite of model simulations. For each model, the annual anomalies were first calculated using the 1901-1960 period as the reference. Then the mean 1901-1960 value from the observations was added to each annual anomaly, essentially removing the model mean bias. In this presentation, the multi-model mean and the 5th and 95th percentile bounds of the model simulations are shown. The mean and percentile values were calculated separately for each year. Then, the curves were smoothed with a 10-year moving boxcar average. The observational time series is not smoothed. During the first half of the 20th century, the observed annual values vary around the model mean because that is the common reference period. These values occasionally fall outside the 5th/95th percentile bounds for the model simulations. During the 1950s, the observed values decline substantially but this does not occur in the model simulations. After about 1960, the observed values are generally within the 5th/95th percentile bounds but on the lower end of the distribution. The rate of observed warming after 1960 is similar to that of the multi-model mean, a similar result to that found in Fig. 43 for a subset of the CMIP3 models. A few values are below the 5th percentile bound while none are above the 95th percentile bound after 1960.

On decadal time scales, climate variations arising from natural factors can be comparable to or larger than changes arising from anthropogenic forcing. An analysis of change on such time scales was performed by examining the decadal changes simulated by the CMIP3 models with respect to the most recent historical decade of 2001-2010. Figure 48 shows the simulated change in decadal mean values of annual temperature for each future decadal time period with respect to the most recent historical decade of 2001-2010, averaged over the entire Southeast region for the 14 (B1) or 15 (A2) CMIP3 models. For the 2011-2020 decade, the temperature increases are not statistically significant relative to the 2001-2010 decade for most of the models. As the time period increases, more of the individual models simulate statistically significant temperature changes, with all being significant at the 95% confidence level by 2045 for the high emissions scenario (2075 for the low emissions scenario). By this point, all of the model decadal mean values lie outside the 10-90th percentile range of the historical annual temperature anomalies. As also shown in Fig. 43, the model simulations show increased variability over time, with the inter-model range of temperature changes for 2091-2100 being more than double that for 2051-2060 (for the high emissions scenario).

The corresponding simulated change in decadal mean values of annual precipitation can be seen in Fig. 49. Unlike for temperature, many of the model values of precipitation change are not statistically significant in all decades out to 2091-2099. For the high (A2) emissions scenario (Fig. 49, top) positive changes in multi-model mean precipitation are simulated up to the 2051-2060 period, with negative changes indicated after this time. Also, the variability in the model simulations becomes greater over time, with a larger number of models lying outside the 10-90th percentile range for each increasing time period. However, for the low (B1) emissions scenario (Fig. 49, bottom) increases in multi-model mean precipitation are simulated for all time periods, with little change in variability over time.

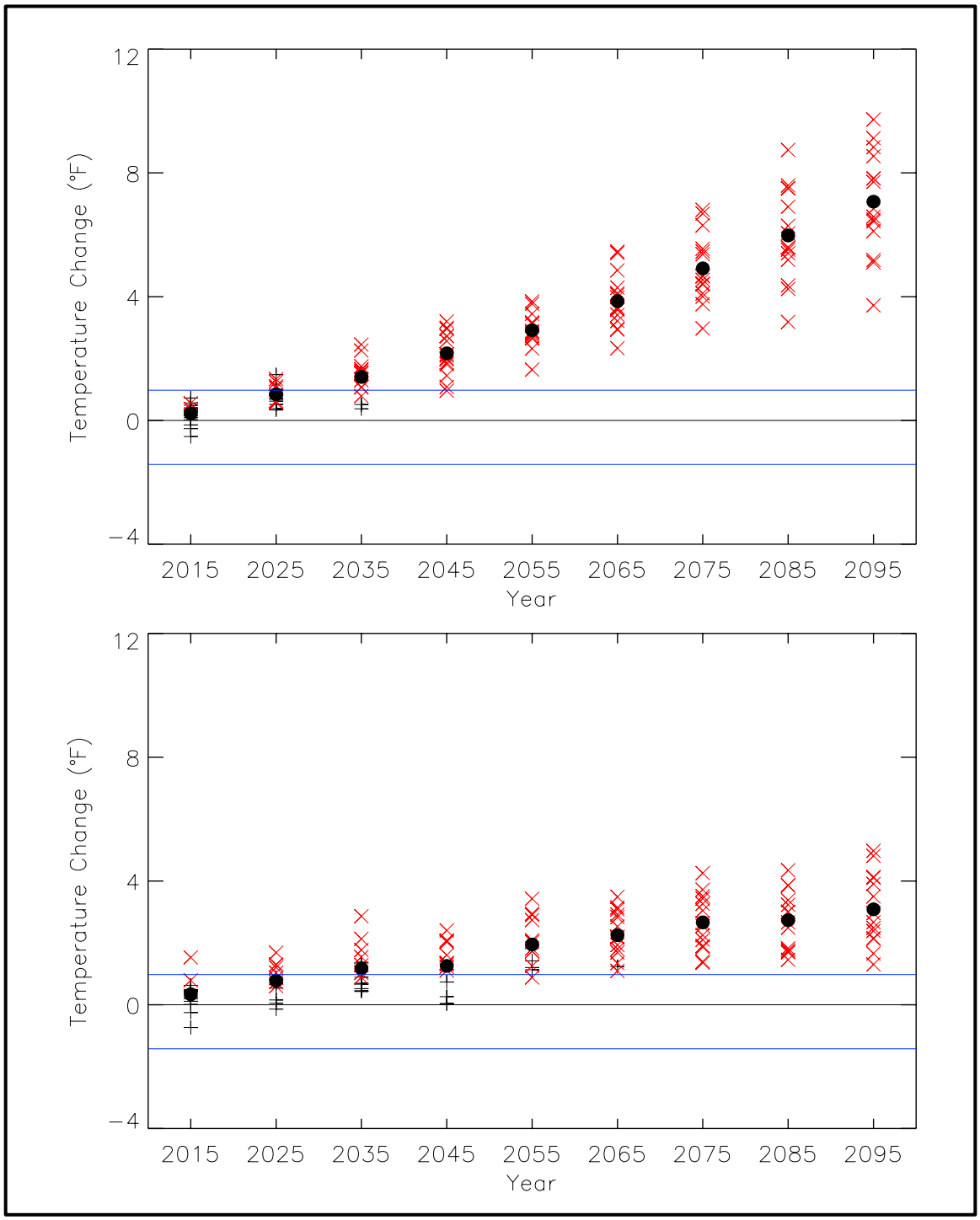

Figure 48. Simulated decadal mean change in annual temperature (°F) for the Southeast U.S. for each future decadal time period (represented by their approximate midpoints, e.g., 2015 = 2011-2020), with respect to the reference period of 2001-2010 Values are given for the high (A2, top) and low (B1, bottom) emissions scenarios for the 14 (B1) or 15 (A2) CMIP3 models. Large circles depict the multi-model means. Each individual model is represented by a black plus sign (+), or a red x if the value is statistically significant at the 95% confidence level. Blue lines indicate the 10th and 90th percentiles of 30 annual anomaly values from 1981-2010. The model simulated warming by 2015 is not statistically significant but by mid-21st century, all models simulate statistically significant warming.

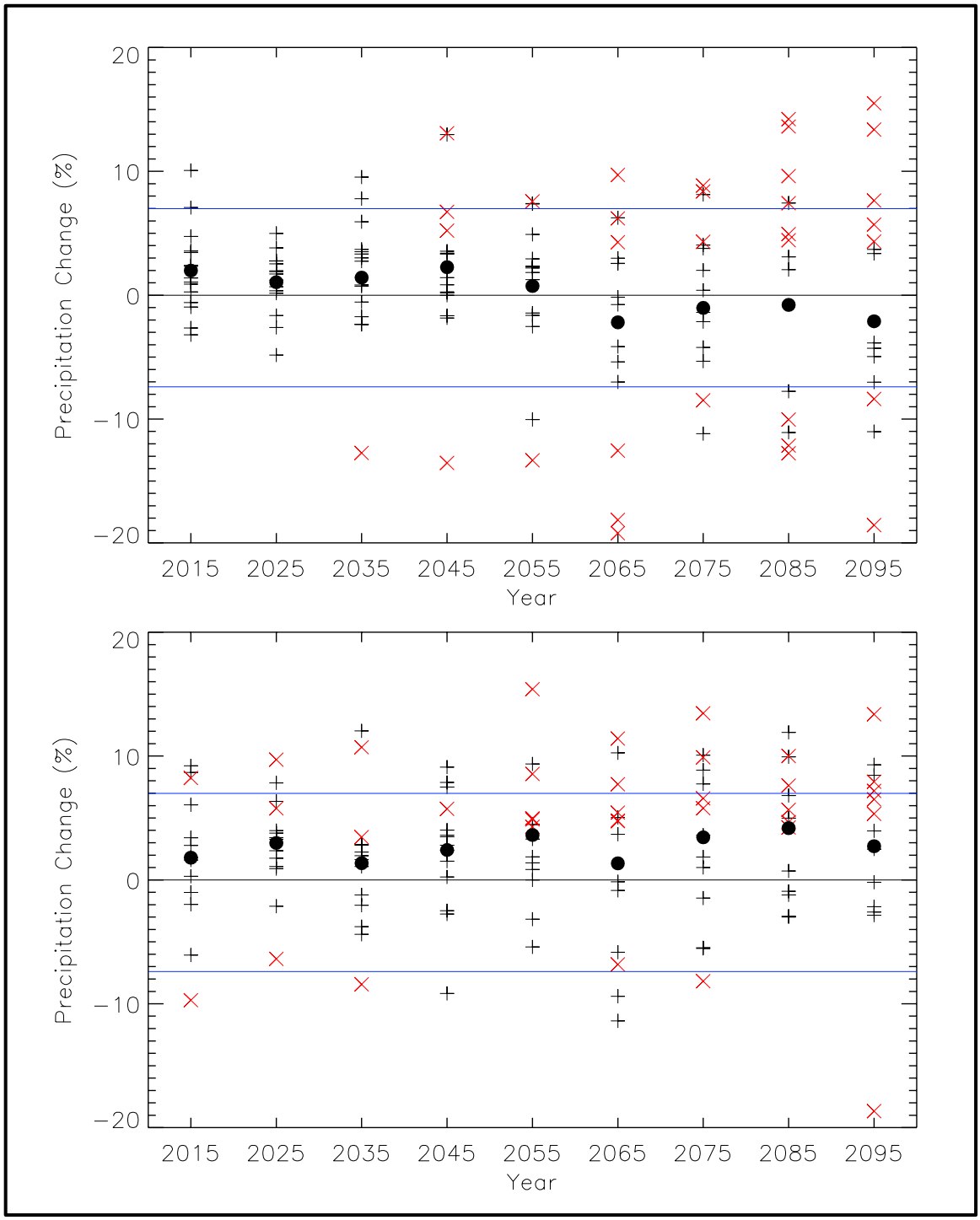

Figure 49. Simulated decadal mean change in annual precipitation (%) for the Southeast U.S. for each future decadal time period (represented by their approximate midpoints, e.g., 2015 = 2011-2020), with respect to the reference period of 2001-2010. Values are given for the high (A2, top) and low (B1, bottom) emissions scenarios for the 14 (B1) or 15 (A2) CMIP3 models. Large circles depict the multi-model means. Each individual model is represented by a black plus sign (+), or a red x if the value is statistically significant at the 95% confidence level. Blue lines indicate the 10th and 90th percentiles of the 30 annual anomaly values from 1981-2010. Many models simulate precipitation changes that are not statistically significant out to the end of the 21st century.

4. SUMMARY

The primary purpose of this document is to provide physical climate information for potential use by the authors of the 2013 National Climate Assessment report. The document contains two major sections. One section summarizes historical conditions in the Southeast U.S and primarily focuses on trends in temperature and precipitation metrics that are important in the region. The core observational data set used is that of the National Weather Service's Cooperative Observer Network (COOP).

The second section summarizes climate model simulations for two scenarios of the future path of greenhouse gas emissions, the IPCC SRES high (A2) and low (B1) emissions scenarios. These simulations incorporate analyses from multiple sources, the core source being Climate Model Intercomparison Project 3 (CMIP3) simulations. Additional sources consist of statistically- and dynamically-downscaled data sets, including simulations from the North American Regional Climate Change Assessment Program (NARCCAP). Analyses of the simulated future climate are provided for the periods of 2021-2050, 2041-2070, and 2070-2099, with changes calculated with respect to an historical climate reference period (1971-1999, 1971-2000, or 1980-2000). The resulting climate conditions are to be viewed as scenarios, not forecasts, and there are no explicit or implicit assumptions about the probability of occurrence of either scenario. The basis for these climate scenarios (emissions scenarios and sources of climate information) were considered and approved by the National Climate Assessment Development and Advisory Committee.

Some key characteristics of the historical climate include:

- Climatic phenomena that have major impacts on the Southeast include: heavy rainfall and floods, drought, extreme heat and cold, winter storms (in northern regions), severe thunderstorms and tornadoes, and tropical cyclones.
- The Southeast is one of the few regions globally not to exhibit an overall warming trend in surface temperature over the 20th century (IPCC 2007a). This "warming hole" also includes parts of the Great Plains and Midwest regions in the summer.
- Temperatures increased rapidly in the early part of the 20th century, then decreased rapidly during the middle of the 20th century. Since the 1960s, temperatures have been increasing. Recent increases in temperature are most pronounced during the summer season, particularly along the Gulf and Atlantic coasts. Temperature trends over the period of 1895-2011 are found to not be statistically significant for any season.
- The number of extreme hot days has tended to decrease or remain the same while the number of very warm summer nights has tended to increase. The number of extreme cold days has tended to decrease.
- Day-to-day and week-to-week variations in the positioning of the Bermuda High can have a strong influence on precipitation patterns across the region. The highest amounts of precipitation are found along the Atlantic coast and across the Florida Peninsula, with tropical cyclones contributing significantly to annual precipitation totals.
- In most cases, there are no long-term trends in precipitation across the Southeast over the last 100 years. Along the northern Gulf Coast precipitation has increased annually and in summer.

For the region as a whole, long-term trends are statistically significant for fall, which shows an upward trend, and summer, which shows a slight downward trend.

- Inter-annual variability in precipitation has increased over the last several decades across much of the region, with more exceptionally wet and dry summers, which is at least partly related to the mean positioning of the Bermuda High. The frequency of extreme precipitation events has been increasing across the Southeast region, particularly over the past two decades
- Average annual snowfall totals across the Southeast have declined since the late 1930s.
- The decadal frequencies of both hurricane and major hurricane (category 3 and greater) landfalls have declined slightly over the last 100 years; however, there is large inter-decadal variability.
- Sea levels have slowly risen across the extensive coastline of the Southeast.

The climate characteristics simulated by climate models for the two emissions scenarios have the following key features:

- Both the CMIP3 and NARCCAP simulations indicate that spatial variations in temperature increase are relatively small, with the greatest temperature increases simulated in the northwest, and the least in the southeast part of the region. The CMIP3 models indicate that temperature increases across the Southeast are statistically significant (for all three future time periods and both emissions scenarios).
- Temperature increases are simulated to be similar in magnitude for the high and low emissions scenarios for the near future, whereas late in the 21st century the high emissions scenario indicates approximately double the amount of warming.
- The range of model-simulated temperature changes is substantial, indicating substantial uncertainty in the magnitude of warming associated with each scenario. However, in each model simulation, the warming is unequivocal and large compared to historical variations. This is also true for all of the derived temperature variables described below.
- NARCCAP model simulations indicate increases in the number of days with a maximum temperature of more than 95°F, from less than 15 days in the extreme north to more than 35 days in south central Florida (for the A2 scenario at mid-century). The number of consecutive warm days is simulated to increase the most in the western portion of the region.
- The number of days with minimum temperatures below 10°F, varying from zero in Florida to about 10 in the far north in the present-day climate, becomes near zero everywhere by mid-century in the A2 scenario. The number of days below 32°F are simulated to decrease by more than 20 days across the northern tier of the region (for the A2 scenario at mid-century).
- Increases in the length of the freeze-free season are in the range of 20 to 30 days across most of the region (for the A2 scenario at mid-century).
- Cooling degree days increase by less than 650 in the north to more than 1,050 in south Florida; these are increases of 25-100% or more (for the A2 scenario at mid-century). Correspondingly, heating degree days are simulated to decrease by more than 900 in the north to less than 300 in south Florida.

- Precipitation in the Southeast is simulated by both the CMIP3 and NARCCAP models to generally increase, with the greatest changes seen in the north and east of the region. Decreases are simulated in the far south and west, however, which are greatest in the summer season. However, for the most part, these changes are either not statistically significant or the models are not in agreement on the sign of the changes. The one exception is the modeled decreases in the south and west for 2070-2099 for the high emissions scenario. The range of model-simulated precipitation changes is considerably larger than the multi-model mean change in most cases. Thus, there is great uncertainty associated with future precipitation changes in these scenarios.
- The Southeast is simulated by the NARCCAP models to see an increase in the number of days with precipitation exceeding 1 inch across the region, with the greatest changes indicated across the Appalachian Mountains (for the A2 scenario at mid-century).
- Little or no change in the number of consecutive days with precipitation less than 0.1 inches is simulated across large parts of the Southeast; however, increases in these dry spells of up to 12 days are indicated in areas along the Gulf coast (for the A2 scenario at mid-century).
- Most models do not indicate a statistically significant change in decadal-average temperature (with respect to 2001-2010) for the near future; however, as the time period increases, a greater number of models simulate statistically significant decadal-average temperature changes, with all being significant at the 95% confidence level by 2045 (for the high emissions scenario).
- Many of the modeled values of decadal precipitation change are not statistically significant, with respect to 2001-2010, out to 2091-2099.

A comparison of model simulations of the 20th century with observations indicates the following:

- The observed early 20th century increase and mid-20th century decrease in temperature are not simulated by any model, while the rate of warming since the 1960s is similar to most of the models. 21st century simulations of temperature indicate that future warming is much larger than the observed and simulated values for the 20th century.
- The variability in observed precipitation change tends to be somewhat higher than that of the models, although decadal values are generally within the envelope of the model simulations.

5. REFERENCES

AchutaRao, K., and K.R. Sperber, 2002: Simulation of the El Niño Southern Oscillation: Results from the Coupled Model Intercomparison Project. *Clim. Dyn.*, **19,** 191–209.

Arakawa, A., 2004: The cumulus parameterization problem: Past, present, and future. *J. Climate*, **17**, 2493-2525.

Ashley, S. T., and W. S. Ashley, 2008: Flood fatalities in the United States. *J. Appl. Meteorol. Climatol.*, **47,** 805-818.

Ashley, W. S., 2007: Spatial and temporal analysis of tornado fatalities in the United States: 1880-2005. *Weather Forecast.*, **22,** 1214-1228.

Ashley, W. S., and C. W. Gilson, 2009: A Reassessment of U. S. Lightning Mortality. *Bull. Am. Meteorol. Soc.*, **90,** 1501-1518.

Bader D. C., C. Covey, W. J. Gutowski Jr., I. M. Held, K. E. Kunkel, R. L. Miller, R. T. Tokmakian, and M. H. Zhang, 2008: *Climate models: An Assessment of Strengths and Limitations*. U.S. Climate Change Science Program Synthesis and Assessment Product 3.1. Department of Energy, Office of Biological and Environmental Research, 124 pp.

Blake, E. S., C. W. Landsea, and E. J. Gibney, 2011: The Deadliest, Costliest and Most Intense United States Tropical Cyclones from 1851 to 2010 (and other Frequently Requested Hurricane Facts). NOAA Technical Memorandum NWS NHC-6, 47 pp. [Available online at http://www.nhc.noaa.gov/pdf/nws-nhc-6.pdf.]

Brooks, H., and C. A. Doswell, 2001: Some aspects of the international climatology of tornadoes by damage classification. *Atmos. Res.*, **56,** 191-201.

Brooks, H., C. Doswell, and M. Kay, 2003: Climatological estimates of local daily tornado probability for the United States. *Weather Forecast.*, **18,** 626-640.

Campbell, J. D., M. A. Taylor, T. S. Stephenson, R. A. Watson, and F. S. Whyte, 2011: Future climate of the Caribbean from a regional climate model. *Int. J. Climatol.*, **31,** 1866-1878.

Carbone, G. J., J. Rhee, H. P. Mizzell, and R. Boyles, 2008: DECISION SUPPORT: A regional-scale drought monitoring tool for the Carolinas. *Bull. Am. Meteorol. Soc.*, **89,** 20-28.

Changnon, S., D. Changnon, and T. Karl, 2006: Temporal and spatial characteristics of snowstorms in the contiguous United States. *J. Appl. Meteorol. Climatol.*, **45,** 1141-1155.

Changnon, S. A., 1999: Impacts of 1997-98 El Niño-generated weather in the United States. *Bull. Am. Meteorol. Soc.*, **80,** 1819-1828.

Changnon, S. A., and T. R. Karl, 2003: Temporal and spatial variations of freezing rain in the contiguous United States: 1948-2000. *J. Appl. Meteorol.*, **42,** 1302-1315.

Chen, Q., L. Wang, and R. Tawes, 2008: Hydrodynamic response of northeastern Gulf of Mexico to hurricanes. *Estuaries Coasts*, **31,** 1098-1116.

Church, J. A., and Coauthors, 2010: Sea-level rise and variability: synthesis and outlook for the future. *Understanding Sea-Level Rise and Variability*, J.A. Church, P.L. Woodworth, T. Aarup, and W. S. Wilson, Eds., Wiley-Blackwell, 402-419.

Curtis, S., 2008: The Atlantic multidecadal oscillation and extreme daily precipitation over the US and Mexico during the hurricane season. *Clim. Dyn.*, **30,** 343-351.

DeGaetano, A. T., and R. J. Allen, 2002: Trends in twentieth-century temperature extremes across the United States. *J. Climate*, **15,** 3188-3205.

Deser, C., A. S. Phillips, and M. A. Alexander, 2010: Twentieth century tropical sea surface temperature trends revisited. *Geophys. Res. Lett.*, **37,** L10701.

Dixon, P. G., A. E. Mercer, J. Choi, and J. S. Allen, 2011: Tornado risk analysis – Is Dixie Alley an extension of Tornado Alley? *Bull. Am. Meteorol. Soc.*, **92,** 433-441.

Domingues, C. M., J. A. Church, N. J. White, P. J. Gleckler, S. E. Wijffels, P. M. Barker, and J. R. Dunn, 2008: Improved estimates of upper-ocean warming and multi-decadal sea-level rise. *Nature*, **453,** 1090-1093.

Downton, M. W., and K. A. Miller, 1993: The freeze risk to Florida citrus. Part II: Temperature variability and circulation patterns. *J. Climate*, **6,** 364-372.

Dufresne, J.-L., and S. Bony. 2008. An assessment of the primary sources of spread of global warming estimates from coupled ocean–atmosphere models. *J. Climate*, **21**, 5135-5144.

Durkee, J., J. Frye, C. Fuhrmann, M. Lacke, H. Jeong, and T. Mote, 2008: Effects of the North Atlantic Oscillation on precipitation-type frequency and distribution in the eastern United States. *Theor. Appl. Climatol.*, **94,** 51-65.

Fall, S., A. Watts, J. Nielsen-Gammon, E. Jones, D. Niyogi, J. R. Christy, and R. A. Pielke Sr, 2011: Analysis of the impacts of station exposure on the US Historical Climatology Network temperatures and temperature trends. *J. Geophys. Res.*, **116,** D14120.

Fuhrmann, C. M., C. E. Konrad, and L. E. Band, 2008: Climatological perspectives on the rainfall characteristics associated with landslides in western North Carolina. *Phys. Geogr.*, **29,** 289-305.

Gamble, D. W., D. B. Parnell, and S. Curtis, 2008: Spatial variability of the Caribbean mid-summer drought and relation to north Atlantic high circulation. *Int. J. Climatol.* **28,** 343-350.

Goto-Maeda, Y., D. Shin, and J. J. O'Brien, 2008: Freeze probability of Florida in a regional climate model and climate indices. *Geophys. Res. Lett.*, **35,** L11703.

Groisman, P., and R. Knight, 2008: Prolonged dry episodes over the conterminous United States: New tendencies emerging during the last 40 years. *J. Climate*, **21,** 1850-1862.

Hayhoe, K., and Coauthors, 2004: Emission pathways, climate change, and impacts on California. *P. Natl. Acad. Sci. USA*, **101,** 12422-12427.

Hayhoe, K., and Coauthors, 2008: Regional climate change projections for the Northeast USA. *Mitig. Adapt. Strateg. Glob. Change*, **13,** 425-436.

Hayhoe, K. A., 2010: A standardized framework for evaluating the skill of regional climate downscaling techniques. Ph.D. thesis, University of Illinois, 153 pp. [Available online at https://www.ideals.illinois.edu/handle/2142/16044.]

Hirsch, R., and K. Ryberg, 2012: Has the magnitude of floods across the USA changed with global CO2 levels? *Hydrolog. Sci. J.*, **57,** 1-9.

Holland, G. J., and P. J. Webster, 2007: Heightened tropical cyclone activity in the North Atlantic: natural variability or climate trend? *Philos. Trans. R. Soc. A*, **365,** 2695-2716.

Hubbard, K., and X. Lin, 2006: Reexamination of instrument change effects in the US Historical Climatology Network. *Geophys. Res. Lett.*, **33,** L15710.

IPCC, 2000: *Special Report on Emissions Scenarios: A Special Report of Working Group III of the Intergovernmental Panel on Climate Change*, N. Nakicenovic, and R. Swart, Eds., Cambridge University Press, 570 pp.

——, 2007a: *Climate Change 2007: The Physical Science Basis. Contribution of Working Group I to the Fourth Assessment Report of the Intergovernmental Panel on Climate Change*, Solomon, S., D. Qin, M. Manning, Z. Chen, M. Marquis, K.B. Averyt, M. Tignor, and H.L. Miller, Eds., Cambridge University Press, 996 pp.

——, 2007b: *Climate Change 2007: Synthesis Report. Contribution of Working Groups I, II and III to the Fourth Assessment Report of the Intergovernmental Panel on Climate Change*, Pachauri, R. K, and Reisinger, A., Eds., IPCC, 104 pp.

——, cited 2012: IPCC Data Distribution Centre. [Available online at http://www.ipcc-data.org/ddc_co2.html.]

Irish, J. L., D. T. Resio, and J. J. Ratcliff, 2008: The influence of storm size on hurricane surge. *J. Phys. Oceanogr.*, **38,** 2003-2013.

Jones, K. F., A. C. Ramsay, and J. N. Lott, 2004: Icing Severity in the December 2002 freezing-rain storm from ASOS data. *Mon. Wea. Rev.*, **132,** 1630-1644.

Jones, P. D., P. Y. Groisman, M. Coughlan, N. Plummer, W. C. Wang, and T. R. Karl, 1990: Assessment of urbanization effects in time series of surface air temperature over land. *Nature*, **347,** 169-172.

Jury, M., B. A. Malmgren, and A. Winter, 2007: Subregional precipitation climate of the Caribbean and relationships with ENSO and NAO. *J. Geophys. Res.*, **112,** D16107.

Karl, T. R., C. N. Williams Jr, P. J. Young, and W. M. Wendland, 1986: A model to estimate the time of observation bias associated with monthly mean maximum, minimum and mean temperatures for the United States. *J. Appl. Meteorol.*, **25,** 145-160.

Karl, T. R., H. F. Diaz, and G. Kukla, 1988: Urbanization: Its detection and effect in the United States climate record. *J. Climate*, **1,** 1099-1123.

Karl, T. R., J. M. Melillo, and T. C. Peterson, Eds, 2009: *Global Climate Change Impacts in the United States.* Cambridge University Press, 188 pp.

Keim, B. D., 1996: Spatial, synoptic, and seasonal patterns of heavy rainfall in the southeastern United States. *Phys. Geogr.*, **17,** 313-328.

Keim, B. D., R. A. Muller, and G. W. Stone, 2007: Spatiotemporal patterns and return periods of tropical storm and hurricane strikes from Texas to Maine. *J. Climate*, **20,** 3498-3509.

Keim, B. D., R. Fontenot, C. Tebaldi, and D. Shankman, 2011: Hydroclimatology of the US Gulf Coast under global climate change scenarios. *Phys. Geogr.*, **32,** 561-582.

Kilbourne, K., T. Quinn, R. Webb, T. Guilderson, J. Nyberg, and A. Winter, 2008: Paleoclimate proxy perspective on Caribbean climate since the year 1751: Evidence of cooler temperatures and multidecadal variability. *Paleoceanography*, **23,** PA3220.

Klotzbach, P. J., 2006: Trends in global tropical cyclone activity over the past twenty years (1986-2005). *Geophys. Res. Lett.*, **33,** L10805.

——, 2011: El Nino-Southern Oscillation's impact on Atlantic basin hurricanes and U.S. landfalls. *J. Climate*, **24**, 1252-1263

Knight, D. B., and R. E. Davis, 2007: Climatology of tropical cyclone rainfall in the southeastern United States. *Phys Geogr*, **28,** 126-147.

——, 2009: Contribution of tropical cyclones to extreme rainfall events in the southeastern United States. *J. Geophys. Res.*, **114,** D23102.

Knutti, R., 2010: The end of model democracy? *Climatic Change*, **102,** 395-404.

Konrad, C. E., and L. B. Perry, 2010: Relationships between tropical cyclones and heavy rainfall in the Carolina region of the USA. *Int. J. Climatol.*, **30,** 522-534.

Kruk, M. C., E. J. Gibney, D. H. Levinson, and M. Squires, 2010: A Climatology of Inland Winds from Tropical Cyclones for the Eastern United States. *J. Appl. Meteorol. Climatol.*, **49,** 1538-1547.

Kunkel, K. E., X.-Z. Liang, J. Zhu, and Y. Lin, 2006: Can CGCMs Simulate the Twentieth-Century "Warming Hole" in the Central United States? *J. Climate*, **19,** 4137-4153.

Kunkel, K. E., M. Palecki, L. Ensor, K. G. Hubbard, D. Robinson, K. Redmond, and D. Easterling, 2009: Trends in twentieth-century US snowfall using a quality-controlled dataset. *J. Atmos. Oceanic Technol.*, **26,** 33-44.

Landsea, C., and Coauthors, 2004: The Atlantic Hurricane Database Reanalysis Project: Documentation for the 1851-1910 Alterations and Additions to the HURDAT Database. *Hurricanes and Typhoons: Past, Present, and Future*, R. Murnane, and K.-b. Liu, Eds., Columbia University Press, 177-221.

Landsea, C., 2007: Counting Atlantic Tropical Cyclones Back in Time. *Eos, Trans. Am. Geophys. Union*, **88,** 197-203.

Landsea, C. W., G. A. Vecchi, L. Bengtsson, and T. R. Knutson, 2010: Impact of Duration Thresholds on Atlantic Tropical Cyclone Counts. *J. Climate*, **23,** 2508-2519.

Li, L., W. Li, and Y. Kushnir, 2011: Variation of the North Atlantic subtropical high western ridge and its implication to Southeastern US summer precipitation. *Clim. Dyn.***,** 1-12.

Lirman, D., and Coauthors, 2011: Severe 2010 cold-water event caused unprecedented mortality to corals of the Florida Reef Tract and reversed previous survivorship patterns. *PLoS ONE*, **6,** e23047.

LSU, cited 2012a: Climate Trends. [Available online at http://charts.srcc.lsu.edu/trends/.]

——, cited 2012b: Threshold Exceedance Trends. [Available online at http://charts.srcc.lsu.edu/ghcn/.]

Malmgren, B. A., A. Winter, and D. Chen, 1998: El Niño-southern oscillation and North Atlantic oscillation control of climate in Puerto Rico. *J. Climate*, **11,** 2713-2717.

Mann, M. E., and K. A. Emanuel, 2006: Atlantic hurricane trends linked to climate change. *Eos, Trans. Am. Geophys*, **87,** 233, 244.

Mann, M. E., J. D. Woodruff, J. P. Donnelly, and Z. Zhang, 2009: Atlantic hurricanes and climate over the past 1,500 years. *Nature*, **460,** 880-883.

Manuel, J., 2008: Drought in the Southeast: Lessons for water management. *Environ. Health Persp.*, **116,** A168.

Marshall, C. H., R. A. Pielke Sr., and L. T. Steyaert, 2004a: Has the conversion of natural wetlands to agricultural land increased the incidence and severity of damaging freezes in south Florida? *Mon. Wea. Rev.*, **132,** 2243-2258.

Marshall, C. H., R. A. Pielke, L. T. Steyaert, and D. A. Willard, 2004b: The impact of anthropogenic land-cover change on the Florida Peninsula sea breezes and warm season sensible weather. *Mon. Wea. Rev.*, **132,** 28-52.

Maue, R. N., 2011: Recent historically low global tropical cyclone activity. *Geophys. Res. Lett.*, **38**, L14803.

Maurer, E. P., A. W. Wood, J. C. Adam, D. P. Lettenmaier, and B. Nijssen, 2002: A long-term hydrologically based dataset of land surface fluxes and states for the conterminous United States. *J. Climate*, **15,** 3237–3251.

Maxwell, J. T., P. T. Soulé, J. T. Ortegren, and P. A. Knapp, 2011: Drought-Busting Tropical Cyclones in the Southeastern Atlantic United States: 1950–2008.

Meehl, G. A., W. M. Washington, T. M. L. Wigley, J. M. Arblaster, and A. Dai, 2003: Solar and Greenhouse Gas Forcing and Climate Response in the Twentieth Century. *J. Climate*, **16,** 426-444.

Meehl, G. A., and Coauthors, 2007: Global climate projections. *Climate Change 2007: The Physical Basis. Contribution of Working Group I to the Fourth Assessment Report of the Intergovernmental Panel on Climate Change*, Solomon, S., D. Qin, M. Manning, Z. Chen, M. Marquis, K.B. Averyt, M. Tignor, and H.L. Miller, Eds., Cambridge University Press, 747-845.

Menne, M. J., C. N. Williams, and R. S. Vose, 2009: The US Historical Climatology Network monthly temperature data, version 2. *Bull. Am. Meteorol. Soc.*, **90,** 993-1007.

Menne, M. J., C. N. Williams, and M. A. Palecki, 2010: On the reliability of the U.S. surface temperature record. *J. Geophys. Res.*, **115,** D11108.

Misra, V., L. Moeller, L. Stefanova, S. Chan, J. J. O'Brien, T. J. Smith III, and N. Plant, 2011: The influence of the Atlantic Warm Pool on the Florida panhandle sea breeze. *J. Geophys. Res*, **116,** D00Q06.

Mitchum, G. T., R. S. Nerem, M. A. Merrifield, and R. Gehrels, 2010: Modern Sea-Level-Change Estimates. *Understanding Sea-level Rise and Variability*, J.A. Church, P.L. Woodworth, T. Aarup, and W. S. Wilson, Eds., Wiley-Blackwell, 122-142.

Mo, K. C., J. K. E. Schemm, and S. H. Yoo, 2009: Influence of ENSO and the Atlantic multidecadal oscillation on drought over the United States. *J. Climate*, **22,** 5962-5982.

Monahan, A.H., and A. Dai, 2004: The spatial and temporal structure of ENSO nonlinearity. *J. Climate*, **17,** 3026–3036.

Mote, T. L., 2007: Greenland surface melt trends 1973–2007: Evidence of a large increase in 2007. *Geophys. Res. Lett.*, **34,** L22507.

NARCCAP, cited 2012: North American Regional Climate Change Assessment Program. [Available online at http://www.narccap.ucar.edu/.]

Needham, H., and B. D. Keim, 2011: Storm surge: physical processes and an impact scale. *Recent Hurricane Research-Climate, Dynamics, and Societal Impacts*, Lupo E., *Ed.*, InTech, 385-406. [Available online at http://www.intechopen.com/books/recent-hurricane-research-climate-dynamics-and-societal-impacts/.]

New, M., M. Todd, M. Hulme, and P. Jones, 2001: Precipitation measurements and trends in the twentieth century. *Int. J. Climatol.*, **21,** 1889-1922.

NOAA, cited 2011: Billion Dollar Weather/Climate Disasters. [Available online at http://www.ncdc.noaa.gov/billions/.]

——, cited 2012a: Cooperative Observer Program. [Available online at http://www.nws.noaa.gov/om/coop/.]

——, cited 2012b: NCEP/DOE AMIP-II Reanalysis. [Available online at http://www.cpc.ncep.noaa.gov/products/wesley/reanalysis2/.]

Norton, C. W., P.-S. Chu, and T. A. Schroeder, 2011: Projecting changes in future heavy rainfall events for Oahu, Hawaii: A statistical downscaling approach. *J. Geophys. Res.*, **116,** D17110.

NWS, 1993: Cooperative Program Operations. National Weather Service Observing Handbook No. 6, 56 pp. [Available online at http://www.srh.noaa.gov/srh/dad/coop/coophb6.pdf.]

Nyberg, J., B. A. Malmgren, A. Winter, M. R. Jury, K. H. Kilbourne, and T. M. Quinn, 2007: Low Atlantic hurricane activity in the 1970s and 1980s compared to the past 270 years. *Nature*, **447,** 698-701.

Overland, J. E., M. Wang, N. A. Bond, J. E. Walsh, V. M. Kattsov, and W. L. Chapman, 2011: Considerations in the selection of global climate models for regional climate projections: The Arctic as a case study. *J. Climate*, **24,** 1583-1597.

PCMDI, cited 2012: CMIP3 Climate Model Documentation, References, and Links. [Available online at http://www-pcmdi.llnl.gov/ipcc/model_documentation/ipcc_model_documentation.php.]

Pan, Z., R. W. Arritt, E. S. Takle, W. J. Gutowski Jr., C. J. Anderson, and M. Segal, 2004: Altered hydrologic feedback in a warming climate introduces a "warming hole." *Geophys. Res. Lett.*, **31,** L17109,

Perry, L. B., C. E. Konrad, D. G. Hotz, and L. G. Lee, 2010: Synoptic classification of snowfall events in the Great Smoky Mountains, USA. *Phys. Geogr.*, **31,** 156-171.

Portmann, R. W., S. Solomon, and G. C. Hegerl, 2009: Spatial and seasonal patterns in climate change, temperatures, and precipitation across the United States. *P. Natl. Acad. Sci. USA*, **106,** 7324.

Prandi, P., A. Cazenave, and M. Becker, 2009: Is coastal mean sea level rising faster than the global mean? A comparison between tide gauges and satellite altimetry over 1993–2007. *Geophys. Res. Lett.*, **36,** L05602.

Pritchard, H. D., R. J. Arthern, D. G. Vaughan, and L. A. Edwards, 2009: Extensive dynamic thinning on the margins of the Greenland and Antarctic ice sheets. *Nature*, **461,** 971-975.

Puma, M. J., and B. I. Cook, 2010: Effects of irrigation on global climate during the 20th century. *J. Geophys. Res.*, **115,** D16120.

Quayle, R. G., D. R. Easterling, T. R. Karl, and P. Y. Hughes, 1991: Effects of recent thermometer changes in the cooperative station network. *Bull. Am. Meteorol. Soc.,* **72,** 1718-1723.

Randall, D.A., and Coauthors, 2007: Climate models and their evaluation. *Climate Change 2007: The Physical Basis. Contribution of Working Group I to the Fourth Assessment Report of the Intergovernmental Panel on Climate Change*, Solomon, S., D. Qin, M. Manning, Z. Chen, M. Marquis, K.B. Averyt, M. Tignor, and H.L. Miller, Eds., Cambridge University Press, 590-662.

Rappaport, E. N., 2000: Loss of life in the United States associated with recent Atlantic tropical cyclones. *Bull. Am. Meteorol. Soc.*, **81,** 2065-2073.

Robinson, W. A., R. Reudy, and J. E. Hansen, 2002: General circulation model simulations of recent cooling in the east-central United States. *J. Geophys. Res.*, **107,** 4748.

Rogers, J. C., and R. V. Rohli, 1991: Florida citrus freezes and polar anticyclones in the Great Plains. *J. Climate*, **4,** 1103-1113.

Seager, R., A. Tzanova, and J. Nakamura, 2009: Drought in the Southeastern United States: Causes, Variability over the Last Millennium, and the Potential for Future Hydroclimate Change. *J. Climate*, **22,** 5021-5045.

Seager, R., Y. Kushnir, J. Nakamura, M. Ting, and N. Naik, 2010: Northern Hemisphere winter snow anomalies: ENSO, NAO and the winter of 2009/10. *Geophys. Res. Lett.*, **37,** L14703.

Shepherd, M., T. Mote, J. Dowd, M. Roden, P. Knox, S. C. McCutcheon, and S. E. Nelson, 2011: An overview of synoptic and mesoscale factors contributing to the disastrous Atlanta flood of 2009. *Bull. Am. Meteorol. Soc.*, **92,** 861-870.

Taylor, M., and E. Alfaro, 2005: Climate of Central America and the Caribbean. *The Encyclopedia of World Climatology*, J. E. Oliver, Ed., Springer, 193-189.

Tebaldi, C., J. M. Arblaster, and R. Knutti, 2011: Mapping model agreement on future climate projections. *Geophys. Res. Lett.*, **38,** L23701.

Trewartha, G. T., 1981: *The Earth's Problem Climates.* University of Wisconsin Press, 371 pp.

U.S. Census Bureau, cited 2011: Metropolitan and Micropolitan Statistical Areas. [Available online at http://www.census.gov/popest/data/metro/totals/2011/.]

Verbout, S. M., H. E. Brooks, L. M. Leslie, and D. M. Schultz, 2006: Evolution of the U.S. tornado database: 1954–2003. *Weather Forecast.*, **21,** 86-93.

Vose, R. S., C. N. Williams, Jr., T. C. Peterson, T. R. Karl, and D. R. Easterling, 2003: An evaluation of the time of observation bias adjustment in the U.S. Historical Climatology Network. *Geophys. Res. Lett.*, **30,** 2046.

Wang, H., R. Fu, A. Kumar, and W. Li, 2010: Intensification of summer rainfall variability in the southeastern United States during recent decades. *J. Hydrometeorol.*, **11,** 1007-1018.

Webster, P. J., G. J. Holland, J. A. Curry, and H. R. Chang, 2005: Changes in tropical cyclone number, duration, and intensity in a warming environment. *Science*, **309,** 1844-1846.

Wilby, R. L., and T. Wigley, 1997: Downscaling general circulation model output: a review of methods and limitations. *Prog. Phys. Geog.*, **21,** 530.

Williams, C. N., M. J. Menne, and P. W. Thorne, 2011: Benchmarking the performance of pairwise homogenization of surface temperatures in the United States. *J. Geophys. Res.*, **52,** 154-163.

Winter, A., and Coauthors, 2011: Evidence for 800 years of North Atlantic multi-decadal variability from a Puerto Rican speleothem. *Earth Planet. Sc. Lett*., **308,** 23-28.

6. ACKNOWLEDGEMENTS

6.1. Regional Climate Trends and Important Climate Factors

We thank Kevin Robbins, David Sathiaraj, and Luigi Romolo of the Southern Regional Climate Center, and Ryan Boyles and Ashley Frazier of the North Carolina State Climate Office, for producing many of the figures in this document. Document and analysis support was provided by Brooke Stewart of the Cooperative Institute for Climate and Satellites (CICS), and by Fred Burnett and Clark Lind of TBG Inc. Analysis support was provided by Russell Vose of NOAA's National Climatic Data Center (NCDC).

6.2. Future Regional Climate Scenarios

We acknowledge the modeling groups, the Program for Climate Model Diagnosis and Intercomparison (PCMDI) and the WCRP's Working Group on Coupled Modelling (WGCM) for their roles in making available the WCRP CMIP3 multi-model dataset. Support of this dataset is provided by the Office of Science, U.S. Department of Energy. Analysis of the CMIP3 GCM simulations was provided by Michael Wehner of the Lawrence Berkeley National Laboratory, and by Jay Hnilo of CICS. Analysis of the NARCCAP simulations was provided by Linda Mearns and Seth McGinnis of the National Center for Atmospheric Research, and by Art DeGaetano and William Noon of the Northeast Regional Climate Center. Additional programming and graphical support was provided by Byron Gleason of NCDC, and by Andrew Buddenberg of CICS.

A partial listing of reports appears below:

NESDIS 102 **NOAA Operational Sounding Products From Advanced-TOVS Polar Orbiting Environmental Satellites. Anthony L. Reale, August 2001.**

NESDIS 103 **GOES-11 Imager and Sounder Radiance and Product Validations for the GOES-11 Science Test. Jaime M. Daniels and Timothy J. Schmit, August 2001.**

NESDIS 104 **Summary of the NOAA/NESDIS Workshop on Development of a Coordinated Coral Reef Research and Monitoring Program. Jill E. Meyer and H. Lee Dantzler, August 2001.**

NESDIS 105 **Validation of SSM/I and AMSU Derived Tropical Rainfall Potential (TRaP) During the 2001 Atlantic Hurricane Season. Ralph Ferraro, Paul Pellegrino, Sheldon Kusselson, Michael Turk, and Stan Kidder, August 2002.**

NESDIS 106 **Calibration of the Advanced Microwave Sounding Unit-A Radiometers for NOAA-N and NOAA-N=. Tsan Mo, September 2002.**

NESDIS 107 **NOAA Operational Sounding Products for Advanced-TOVS: 2002. Anthony L. Reale, Michael W. Chalfant, Americo S. Allegrino, Franklin H. Tilley, Michael P. Ferguson, and Michael E. Pettey, December 2002.**

NESDIS 108 **Analytic Formulas for the Aliasing of Sea Level Sampled by a Single Exact-Repeat Altimetric Satellite or a Coordinated Constellation of Satellites. Chang-Kou Tai, November 2002.**

NESDIS 109 **Description of the System to Nowcast Salinity, Temperature and Sea nettle (*Chrysaora quinquecirrha*) Presence in Chesapeake Bay Using the Curvilinear Hydrodynamics in3-Dimensions (CH3D) Model. Zhen Li, Thomas F. Gross, and Christopher W. Brown, December 2002.**

NESDIS 110 **An Algorithm for Correction of Navigation Errors in AMSU-A Data. Seiichiro Kigawa and Michael P. Weinreb, December 2002.**

NESDIS 111 **An Algorithm for Correction of Lunar Contamination in AMSU-A Data. Seiichiro Kigawa and Tsan Mo, December 2002.**

NESDIS 112 **Sampling Errors of the Global Mean Sea Level Derived from Topex/Poseidon Altimetry. Chang-Kou Tai and Carl Wagner, December 2002.**

NESDIS 113 **Proceedings of the International GODAR Review Meeting: Abstracts. Sponsors: Intergovernmental Oceanographic Commission, U.S. National Oceanic and Atmospheric Administration, and the European Community, May 2003.**

NESDIS 114 **Satellite Rainfall Estimation Over South America: Evaluation of Two Major Events. Daniel A. Vila, Roderick A. Scofield, Robert J. Kuligowski, and J. Clay Davenport, May 2003.**

NESDIS 115 **Imager and Sounder Radiance and Product Validations for the GOES-12 Science Test. Donald W. Hillger, Timothy J. Schmit, and Jamie M. Daniels, September 2003.**

NESDIS 116 **Microwave Humidity Sounder Calibration Algorithm. Tsan Mo and Kenneth Jarva, October 2004.**

NESDIS 117 **Building Profile Plankton Databases for Climate and EcoSystem Research. Sydney Levitus, Satoshi Sato, Catherine Maillard, Nick Mikhailov, Pat Cadwell, Harry Dooley, June 2005.**

NESDIS 118 **Simultaneous Nadir Overpasses for NOAA-6 to NOAA-17 Satellites from 1980 and 2003 for the Intersatellite Calibration of Radiometers. Changyong Cao, Pubu Ciren, August 2005.**

NESDIS 119 **Calibration and Validation of NOAA 18 Instruments. Fuzhong Weng and Tsan Mo, December 2005.**

NESDIS 120 **The NOAA/NESDIS/ORA Windsat Calibration/Validation Collocation Database. Laurence Connor, February 2006.**

NESDIS 121 **Calibration of the Advanced Microwave Sounding Unit-A Radiometer for METOP-A. Tsan Mo, August 2006.**

NESDIS 122 JCSDA Community Radiative Transfer Model (CRTM). Yong Han, Paul van Delst, Quanhua Liu, Fuzhong Weng, Banghua Yan, Russ Treadon, and John Derber, December 2005.

NESDIS 123 Comparing Two Sets of Noisy Measurements. Lawrence E. Flynn, April 2007.

NESDIS 124 Calibration of the Advanced Microwave Sounding Unit-A for NOAA-N'. Tsan Mo, September 2007.

NESDIS 125 The GOES-13 Science Test: Imager and Sounder Radiance and Product Validations. Donald W. Hillger, Timothy J. Schmit, September 2007.

NESDIS 126 A QA/QC Manual of the Cooperative Summary of the Day Processing System. William E. Angel, January 2008.

NESDIS 127 The Easter Freeze of April 2007: A Climatological Perspective and Assessment of Impacts and Services. Ray Wolf, Jay Lawrimore, April 2008.

NESDIS 128 Influence of the ozone and water vapor on the GOES Aerosol and Smoke Product (GASP) retrieval. Hai Zhang, Raymond Hoff, Kevin McCann, Pubu Ciren, Shobha Kondragunta, and Ana Prados, May 2008.

NESDIS 129 Calibration and Validation of NOAA-19 Instruments. Tsan Mo and Fuzhong Weng, editors, July 2009.

NESDIS 130 Calibration of the Advanced Microwave Sounding Unit-A Radiometer for METOP-B. Tsan Mo, August 2010.

NESDIS 131 The GOES-14 Science Test: Imager and Sounder Radiance and Product Validations. Donald W. Hillger and Timothy J. Schmit, August 2010.

NESDIS 132 Assessing Errors in Altimetric and Other Bathymetry Grids. Karen M. Marks and Walter H.F. Smith, January 2011.

NESDIS 133 The NOAA/NESDIS Near Real Time CrIS Channel Selection for Data Assimilation and Retrieval Purposes. Antonia Gambacorta, Chris Barnet, Walter Wolf, Thomas King, Eric Maddy, Murty Divakarla, Mitch Goldberg, April 2011.

NESDIS 134 Report from the Workshop on Continuity of Earth Radiation Budget (CERB) Observations: Post-CERES Requirements. John J. Bates and Xuepeng Zhao, May 2011.

NESDIS 135 Averaging along-track altimeter data between crossover points onto the midpoint gird: Analytic formulas to describe the resolution and aliasing of the filtered results. Chang-Kou Tai, August 2011.

NESDIS 136 Separating the Standing and Net Traveling Spectral Components in the Zonal-Wavenumber and Frequency Spectra to Better Describe Propagating Features in Satellite Altimetry. Chang-Kou Tai, August 2011.

NESDIS 137 Water Vapor Eye Temperature vs. Tropical Cyclone Intensity. Roger B. Weldon, August 2011.

NESDIS 138 Changes in Tropical Cyclone Behavior Related to Changes in the Upper Air Environment. Roger B. Weldon, August 2011.

NESDIS 139 Computing Applications for Satellite Temperature Datasets: A Performance Evaluation of Graphics Processing Units. Timothy F.R. Burgess and Scott F. Heron, December 2011.

NESDIS 140 Microburst Nowcasting Applications of GOES. Kenneth L. Pryor, September 2011.

NESDIS 141 The GOES-15 Science Test: Imager and Sounder Radiance and Product Validations. Donald W. Hillger and Timothy J. Schmit, November 2011.

NOAA SCIENTIFIC AND TECHNICAL PUBLICATIONS

The National Oceanic and Atmospheric Administration **was established as part of the Department of Commerce on October 3, 1970. The mission responsibilities of NOAA are to assess the socioeconomic impact of natural and technological changes in the environment and to monitor and predict the state of the solid Earth, the oceans and their living resources, the atmosphere, and the space environment of the Earth.**

The major components of NOAA regularly produce various types of scientific and technical information in the following types of publications

PROFESSIONAL PAPERS – Important definitive research results, major techniques, and special investigations.

CONTRACT AND GRANT REPORTS – Reports prepared by contractors or grantees under NOAA sponsorship.

ATLAS – Presentation of analyzed data generally in the form of maps showing distribution of rainfall, chemical and physical conditions of oceans and atmosphere, distribution of fishes and marine mammals, ionospheric conditions, etc.

TECHNICAL SERVICE PUBLICATIONS – Reports containing data, observations, instructions, etc. A partial listing includes data serials; prediction and outlook periodicals; technical manuals, training papers, planning reports, and information serials; and miscellaneous technical publications.

TECHNICAL REPORTS – Journal quality with extensive details, mathematical developments, or data listings.

TECHNICAL MEMORANDUMS – Reports of preliminary, partial, or negative research or technology results, interim instructions, and the like.

U.S. DEPARTMENT OF COMMERCE
National Oceanic and Atmospheric Administration
National Environmental Satellite, Data, and Information Service
Washington, D.C. 20233